# UNIVERSIDAD DE ANTIOQUIA

**Evaluation of the photodegradation of Bisphenol A and Triclosan, in the presence of 6- methoxyquinoline ligand coordination compounds as singlet oxygen photosensitizers, compared to the use of the persulfate ion**

Gloria Maria Doria Herrera

Tesis doctoral presentada para optar al título de Doctor en Ingeniería Ambiental

**Asesores**
Gustavo Peñuela Mesa, Doctor (PhD)
Gloria Cristina Valencia, Doctor (PhD)

Universidad de Antioquia
Facultad de Ingeniería
Doctorado en Ingenieria Ambiental
Medellín, Antioquia, Colombia
2021

| Cita | (Doria Herrera, 2021) |
|---|---|
| **Referencia**<br><br>**Estilo APA 7 (2020)** | Doria Herrera, G. (2021). Evaluation of the photodegradation of Bisphenol A and Triclosan, in the presence of 6-methoxyquinoline ligand coordination compounds as singlet oxygen photosensitizers, compared to the use of the persulfate ion [Tesis doctoral]. Universidad de Antioquia, Medellín, Colombia. |

Doctorado en Ingenieria Ambiental, Cohorte VII.

Grupo de Investigación Diagnóstico y Control de la Contaminación.



**Repositorio Institucional:** http://bibliotecadigital.udea.edu.co

Universidad de Antioquia - www.udea.edu.co

**Rector:** John Jairo Arboleda Céspedes

**Decano/Director:** Jesús Francisco Vargas Bonilla.

**Jefe departamento:** Julio Eduardo Cañón Barriga

El contenido de esta obra corresponde al derecho de expresión de los autores y no compromete el pensamiento institucional de la Universidad de Antioquia ni desata su responsabilidad frente a terceros. Los autores asumen la responsabilidad por los derechos de autor y conexos.

**acknowledgements**

Here I wish to thank my spiritual guides who have led me to have peace and discernment towards all the challenges that this process has brought to my life.

To my family, for being willing to live with me along the whole process unconditionally, and for always supporting me in fulfilling my dreams.

To Universidad de Antioquia and, especially, to the GDCON group since they supported me enormously with their knowledge, experience and willingness to serve. To the instrumental team, especially to Adrian for being with me in transcendent moments of my research.

To Universidad Nacional de Colombia, especially to the Chemistry College for always supporting me with all experimental needs. To the GIAFOT and SIRYTCOR group for having been colleagues and friends in these years of hard work.

To my thesis supervisors, doctors Gustavo Peñuela and Gloria Cristina Valencia for always being by my side, advising me on difficulties and accompanying me throughout the process.

To the Emerging Leaders of the Americas Program (ELAP) for the financial support, and to the University of Saskatchewan, particularly the Engineering College for providing the necessary infrastructure for this research. Thanks to the program COLCIENCIAS, with its call for entries No. 647 2015 for the appointment with the study in Colombia and the Foundation for the Promotion of Research and Technology, through project No. 3973, for the financial support of the project.

Finally, I give my thanks to my colleagues who have become friends, David, Santiago, Jhon Dario, Caro Velasquez, Andrés Merino, Isa, Joan, and some that I have forgotten to mention but who will always count on me.

# Table of Contents

# List of the figures

# Tables List

**Pag**

# Abbreviatures

ACN: Acetonitrile

BPA: Bisphenol A

DFIBF: 1,3-diphenylisobenzofuran

DMA: 9,10-dimethylanthracene

DMSO: Dimethyl sulfoxide

DRIFT: Diffuse Reflectance for Infrared Fourier Transform

DSC: Differential Scanning Calorimetry

EO: Eosin Y

HPLC: High Performance Liquid Chromatography

IR: Infrared

ISC: Intersystem Crossing

LMCT: Ligand-to-Metal Charge Transfer

LUMO: Lowest Unoccupied Molecular Orbital

MLCT: Metal Ligand for Charge Transfer

PNF: Perinaphtenone

STEM: Scanning transmission electron microscope (STEM)

TCS: Triclosan

TGA: Thermogravimetric Analysis

TOC: Total Organic Carbon

$^3O_2$: Triplet oxygen

$^1O_2$: Singlet oxygen

$\Phi_\Delta$: Quantum yield of singlet formation

$\Phi_T$ : Quantum yield of triplet formation

$\Phi_{en}$ : Efficiency of the transferred energy

$K_{en}$: Velocity constant of the transferred energy

$K_q$: Sum of the velocity constants

## 1. Description of the Problem

Emerging pollutants, by definition, are associated with substances whose risks to the health of animals and human population are not yet clear, many of them are part of commercial products that are used daily at the domestic and industrial level. In general, they are found in low concentrations in the environment, but despite this, they could cause damage to organisms, especially through contact or continuous consumption, as occurs with fish that live in polluted rivers. In addition, it has been previously reported that some emerging pollutants are persistent under normal conditions in the environment and are not removed by conventional wastewater treatment and water purification processes For the study, the photosensitizer to be synthesized will be used in the degradation of emerging pollutants Bisphenol A and Triclosan, which have been monitored and found by the GDCON group in raw waters and in purification plants(Zapata & Peñuela, 2012).

The Bisphenol A has been reported as an endocrine disruptor, with estrogenic activity, even at concentrations of $1mg/m^3$. The Bisphenol A is estrogenic compounds can have harmful effects on living organisms, as they can alter the natural hormonal balance in men and women (Careghini, et al. 2014). This compound, has been used abundantly in the manufacture of plastics for more than fifty years, which has produced a continuous dumping of water resources and therefore the exposure of animals and even human population to this toxic substance (Staples et al., 1998). On the other hand, the Triclosan is an antimicrobial agent widely used in many personal care products such as soaps, detergents, toothpastes, disinfectants, cosmetics, and pharmaceuticals. It has been proven to be an endocrine disruptor for aquatic organisms (Latch et al., 2003), and some recent findings even indicate that it blocks lipid biosynthesis in bacteria, specifically inhibiting the enzyme enol-acyl reductase (Ying & Kookana, 2007).

Progress has been made in the study of treatment systems to eliminate emerging pollutants, such as the use of membranes, reaching yields of 54% (Pal et al., 2010) for removals with activated carbon, activated sludge, coagulation and chlorination, with efficiencies ranging between 20% and 60%, in which pH plays an important role (Bolong et al., 2009).

In advanced oxidation processes, reactive species such as the hydroxyl free radical originate, are originated oxidizes refractory organic pollutants at high reaction rates (Andreozzi, 1999) (Gogate & Pandit, 2004) (De la Cruz et al., 2013). By combining advanced oxidation with biological processes such as those reported by (Oller et al., 2011), such as

the combination of ozone with native strains of microorganisms present in active sludge have achieved removals of emerging pollutants of 95%, however, Enzyme induction is highly sensitive to temperature, salinity, pH, oxygen concentration, redox potential, the concentration and nature of various substrates, nutrients, and the presence of toxic substances.

The GDCON group has used the ferric ion and humic substances as photosensitizers in the degradation of triclosan (Martínez-Zapata et al., 2013), as well as other treatment methods, such as membrane technology, Fenton and biological processes to the removal of emerging pollutants (Londoño & Peñuela, 2015)(Zúñiga et al., 2015).

The questions were, ¿Are 6-methoxyquinoline ligand coordination complexes good photosensitizers to degrade Bisphenol A and Triclosan, present in waters? In terms of efficiency, ¿is it comparable to other established chemical methods?

The above, taking into account that 6-methoxyquinoline is a good singlet oxygen photosensitizer, but easily oxidizable, so the use of metal complexes is presented as a strategy to improve its stability and preserve its photophysical properties (Villa-Pérez et al., 2015). The aim is then to synthesize new materials that, through the generation of singlet molecular oxygen, can be used to efficiently degrade emerging pollutants and this method is efficiency terms is a good option comparative with other methodologies.

## 2. Objectives

### 2.1 General Objective

To evaluate the photodegradation of Bisphenol A and Triclosan compounds using as a photosensitizer a product of the synthesis of the ligand 6-methoxyquinoline with transition metals, establishing its potential photosensitizing activity of singlet molecular oxygen in relation to the oxidant of the persulfate ion.

### 2.2 Specifics Objectives

- ✎ To synthesize and characterize the coordination compound of 6-metoxiquinoline ligand starting from transition salts, determining the structure, thermal stability, photophysical properties, and photosensitizing capacity.
- ✎ To evaluate the best degradation conditions for each pollutant, taking into account the initial concentration ratio of the pollutant, concentration of the 6-metoxiquinoline ligand coordination compound, pH and UV irradiation time in the photodegradation process.
- ✎ To determine the percentage of degradation and mineralization for each emerging contaminant using both the 6-metoxiquinoline ligand coordination compound and the persulfate.
- ✎ To identify some of the intermediates generated during photodegradation for each contaminant in the presence of the 6-metoxiquinoline ligand coordination compound and persulfate.

## 3. Chapter 1: Synthesis of Coordination Compounds Like $^1O_2$ Generators

## 3.1 Introduction for The Coordination Compounds

The organometallic compounds are generally defined as a compound having at least one metal- carbon bond. Usually, these compounds are generally prepared by two general methods: reactions using elemental metals and reactions of already formed chemical compounds(Komiya, 1997).

One the most characteristics of this kind of the compounds is the electronegativity and electronic structure, specifically in the transition metal organocompounds that are generally covalent and to be unstable because of the intrinsic instability of transition metal-carbon σ-bond; the apparent instability usually arises from low energy pathways for decomposition via β- hydrogen elimination, reductive elimination, oxidation, hydrolysis etc.

In this chapter, the synthesis reactions for the preparation of photosensitizers were carried out as part of the research objectives. For this, initially various experiments reported in the literature were carried out, which consequently led to the optimization of the reaction conditions of these compounds under environment conditions. Among the most significant characterization analyzes like as DRIFT, Raman, TGA, DSC, STEM, physical tests and some experiments that allowed to evaluate the bactericidal capacity of these obtained compounds stand out.

## 3.2 Conceptual Framework

### 3.2.1 Ruthenium synthesis mechanism

The first report on Ru-halide-DMSO compounds was prepared by James et al. (1971) which described the product $RuCl_2(DMSO)_4$ with geometry where chlorides located in position *trans*. Then, reactivity of this compound was included (Evans et al., 1973) and finally Mercer and Trotter (1975) reported for this compound results of single-crystal X-ray investigation (Alessio, 2004).

There are reports that suggested Ru (II)-Halide- sulfoxide precursor from hydrated $RuCl_3$ with hot DMSO (120 ºC-150 ºC) induce the reduction Ru (II) with formation of cis, fac-$RuCl_2(DMSO-S)_3(DMSO-O)$ in high yield, shown in the figure 1. The treatment of $RuCl_3$ in DMSO at 70 ºC yielded the kinetic isomer trans-$RuCl_2(DMSO-S)_4$ **and** its isomer. Finally, the treatment of $RuCl_3*nH_2O$ with DMSO at room temperature was found to be a less soluble isomer and an isomer to thermodynamic product in hot DMSO was obtained (Alessio, 2004).
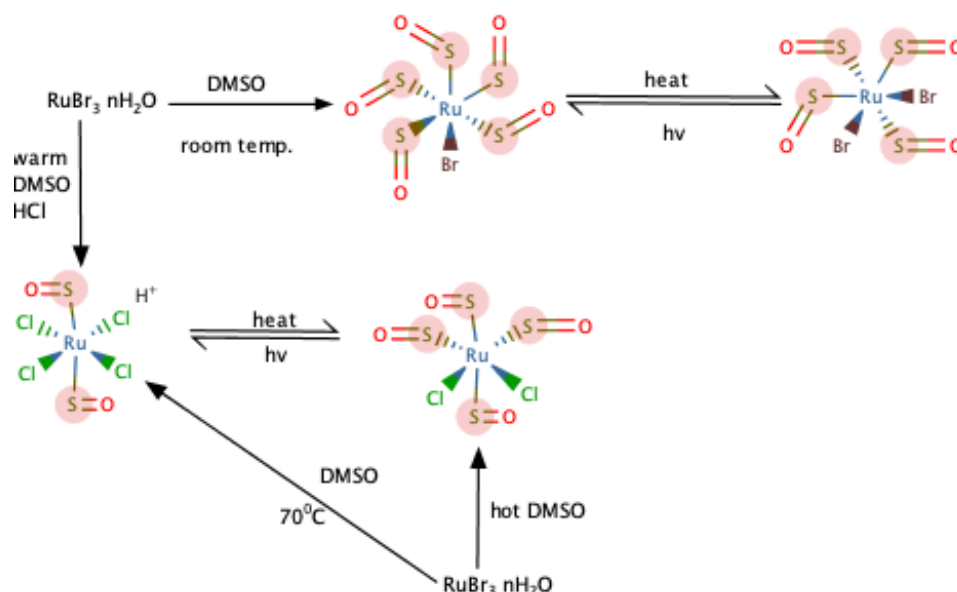
**Figure 1.** Mechanism of the Ru (II)-Halide- sulfoxide precursor (Alessio, 2004).

In some cases, these compounds act as precursors to synthesize new compounds, that is to say, these intermediate structures can be incorporated with Nitrogen ligands or Nitrogen heterocycles at room temperature(Gutierrez et al., 2003). In figure 2 (A), it is shown how the substitution reaction occurs, however, being in the middle of ethanol or methanol, they can be coordinated so that the central atom is Ruthenium and the location of the ligands is similar to a monomer as shown in figure 2(B).
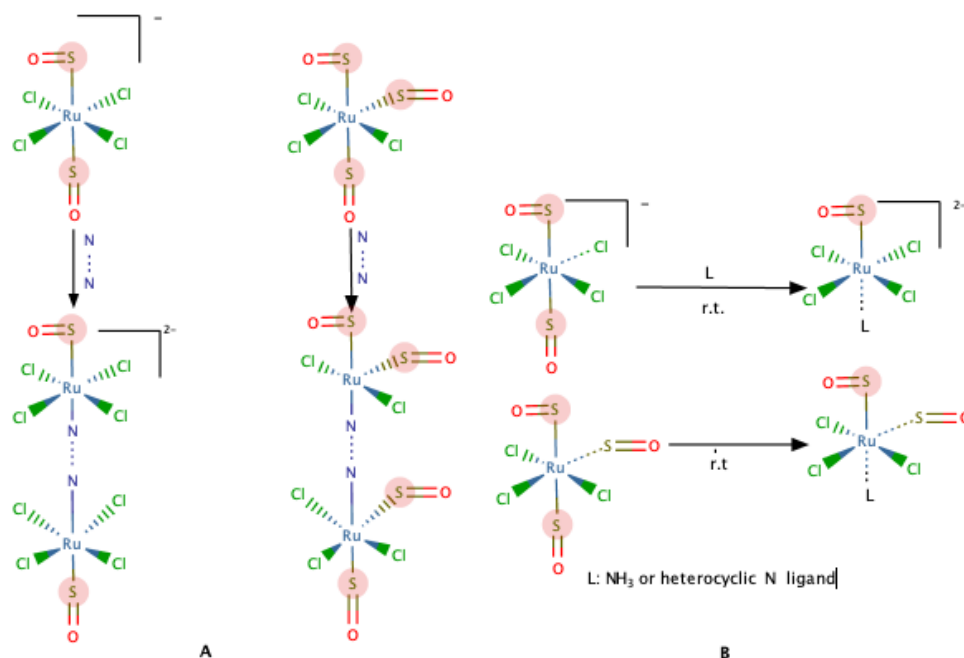


**Figure 2.** Mechanism of the synthesis of the Ru (II)-Halide- sulfoxide precursor with N-ligand. (Alessio, 2004)

There are several examples where this kind of compounds are synthesized for different applications such as catalytic application, for selective oxidative cleavage of olefins to aldehydes (Manikandan et al., 2016) or aldehyde to amide conversion for N-alkylation and transfer hydrogenation reactions (Prakash & Viswanathamurthi, 2014). Specifically, the ruthenium complexes are excellent representatives of transition metal complexes that strongly adsorb visible light, since they can also act as light sensitizers, and the records for the water oxidation performance has been set for this family of complexes (Xue et al., 2015) and it is possible to establish that these compounds form dimers that confer stability and better photochemical properties (Puntoriero et al., 2011).

### 3.2.2 The Zinc, Manganese and Gold synthesis mechanisms

The manganese compounds with the oxidation state ranging from -3 to 7 are known to be the most stable, specifically those of Mn (II). Specifically, for the coordination chemistry, there are Manganese (II) complexes bonded with Nitrogen, an example is 1,3,5-triaza-7-phosphadamantane (PTA) in which the metal coordinates (Mn) to a Nitrogen. The most interesting is the requirements for nitrogen versus phosphorous coordination, because the hard-soft acid base (HSAB) theory said that there is preference for phosphorous center but in this case, was possible stablished that preferred coordinate with the Nitrogen atom, in the figure 3, shown the mechanism (Frost et al., 2006; Karlsson et al., 2011).
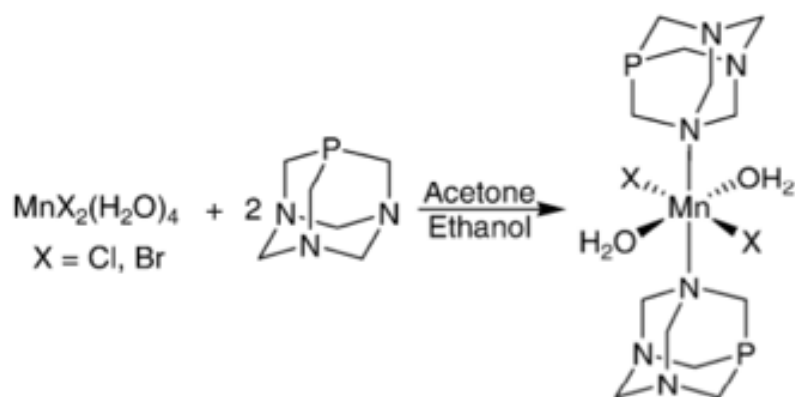


**Figure 3.** Synthesis of $Mn(OH_2)_2PTA_2X_2$, Where X: Cl or Br.(Karlsson et al., 2011)

The zinc complex has been limited for its low reactivity as compared to the other organometallic compound and generally employed in organic synthesis without isolation (Komiya, 1997). However, the organozinc complex has a significant importance as photosensitizer, an example of this are the zinc phthalocyanine complexes because their appreciably long triplet lifetimes constitute a great advantage for the number of diffusional

encounters between the triplet excited state and ground state molecular oxygen increases with the lifetime of the excited state (Gürol et al., 2007).

In the case of the gold complex, found as inorganic salts such as AuCl and $AuCl_3$, are of great importance because of its participation in the synthesis coordination compounds and because it provides excellent proprieties such as reactivity, stability, and, more recently, selectivity. The actual catalytic species is the putative cationic gold (I) complex $[Au(L)]^+$ (where L is a phosphorus-based species or N-heterocyclic carbene, NHC). The early gold systems bear phosphine and phosphite ligands. More recently, the use of NHC as ligands for gold has rapidly gained popularity, because, these two-electron donor ligands combine strong σ-donating properties with a steric profile that allows for both stabilization of the metal center and enhancement of its catalytic activity (De Frémont et al., 2005).

An example of this kind reaction is the proposal for (Nolan, 2011), where a series of [Au(NHC)Cl] complexes was initially synthesized under the silver oxide route developed to generate [Ag(NHC)Cl] complexes which that are used as NHC transfer agents when reacted with the [Au(DMS)Cl] precursor (DMS = dimethyl sulfide) of the free NHC in a simple ligand substitution reaction. Other route is possible with silver, this reaction happens in situ by combining a [Au(L)Cl] (L=phosphine or NHC) complex with a silver additive which acts as a halide abstractor, the mechanism is shown in the figure 4.
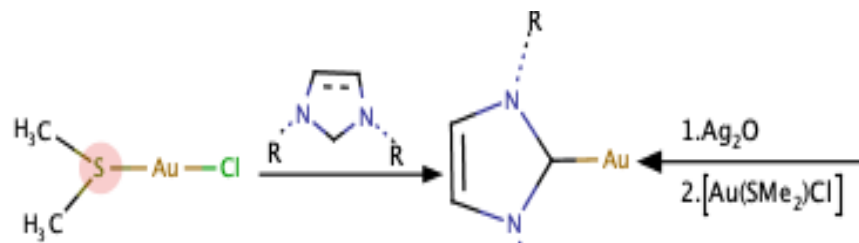


**Figure 4.** General reaction with N-heterocyclic carbene.(De Frémont et al., 2005)

### 3.2.3 Characterization Techniques for The Synthesis Products

To establish its thermal stability, **the thermogravimetric analysis (TGA)** technique was used, which allows to know the thermal stability of the synthesized compounds, it is worth remembering that this is a measure that relates the loss of mass as a function of temperature, therefore, it is important to know until the temperature range the structure does not present mass losses and consequently it is not altered in composition. Similarly, **the differential scanning calorimetry (DSC)** analysis was performed for the morphological analysis of the samples, in order to analyze the **glass transition temperature ($T_g$)** that

occurs in vitreous materials, polymers and other amorphous inorganic materials was performed, this state is considered as the intermediate state between the molten and rigid state of the material. When being observed, this last parameter can be established if the material has amorphousness. On the other hand, when establishing the way in which the peak is projected in the thermogram, it is possible to propose the potential transformations and, consequently, the types of transition that occur in the sample, in the Figure 8 below proposed by (Granados Cristancho, 2015) showing some of these transformation processes.

The analysis of **IR and RAMAN spectroscopy**, the capacity of certain molecules is used at certain frequencies to generate movements of vibrational character, in the case of the average IR, which is of special interest for organic molecules generate signals at frequencies ranging from 4000-400 cm$^{-1}$ In the case of the analysis by RAMAN, its principle is related to the irradiation of a sample with a monochromatic light laser. During the irradiation, a spectrum of the scattered radiation is generated with an angle of 90 degrees. In the majority of organic compounds including organometallics do not show a substantial difference in the IR and RAMAN, however, some signals generated in the fingerprint region that are neither visible in the IR, nor in the analysis by RAMAN, can be determined with greater clarity being these signals part of the elucidation of the new compounds (Douglas et al., 2001).

Finally, for the morphological determination and composition, **Transmission Electron Microscopy (TEM)** analysis was performed, in which there is an incidence of an electron beam, which crosses the sample (by adsorption of energy), forming the image by contrast in size and volume. For this analysis, an additional attachment of the technique called **Scanning Transmission Electron Microscopy (STEM)** was used. In this case, the sample is scanned and the transmitted/scattered electrons give information on the volume and morphology of the material (Shibata et al., 2010).

The TEM technique, explained in Figure 5, provides additional information about the crystalline structure of the sample which may be nanometric or powder; one of the best-known strategies to establish the shape of a polycrystal at random. It is done by rotating the axes producing a set of nested spheres which, when intersected, are compared to the Ewald Sphere. These will be reflected in the rings that are engraved and keep a common pattern between them. It should be remembered that the distance of the electron beam to each of the patterns is inversely proportional to the crystalline space. In the case of amorphous solids, forming an image will show a spot of white dots against a dark background (Williams

& Carter, 2013). It is important to shown that TEM is an excellent technical to find nanoparticles, this aspect is of critical importance for these compounds and their applications.
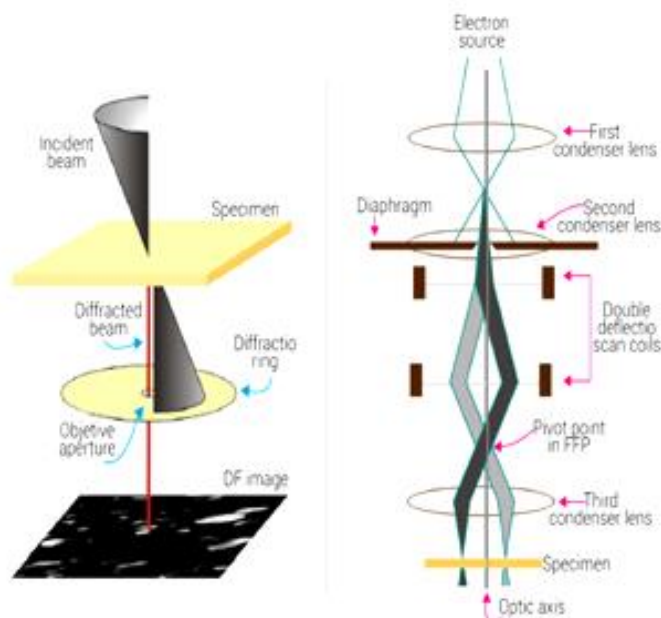


**Figure 5.** On the left, the Ray diagram showing hollow-cone illumination conditions, the angle are always scattered on axis for the formation the image. On the right, the explanation of the scanning of the convergent probe for STEM image formation using two pairs of scan coils between the C2 lens (usually switched off) and the upper-objective polepiece(Williams & Carter, 2013).

## 3.3 Materials and methods

### 3.3.1 Reagents and Equipment

For carrying out the synthesis of the compounds, in the case of the ruthenium compound, $RuCl_3.3H_2O$ (Merck brand at 68%) and the $(CH_3)_2SO$ (Dimethyl sulfoxide-DMSO sigma Aldrich brand at 99%). In the case of the manganese complexes, $MnCl_2$ (Sigma Aldrich at ≥99%) and in the case of the gold complex AuCl (Alfa Aesar at 99 %). In all case, the ligand used was the 6-methoxyquinoline (Alfa Aesar at 98 %). The solvent used was ethanol HPLC/spectrophotometric grade (Merck ≥99.5%).

In the case of the equipment used for the characterization of synthetizing compounds, for the IR analysis Perkin Elmer Spectrum Two FT-IR ATR was used; and for the RAMAN analysis spectrometer Horman Jobin Yvon confocal, Model Labram HR was used, in both cases, for looking the functional groups and the changes of the synthesis reaction. Then, for the characterization of the new compounds, the solubility test was analyzed, and for the morphological characterization the scanning transmission electron microscope (STEM) was used in the equipment of Transmission Electronic Microscope TMP Tecnai F20 Super Twin.

For the thermogravimetric characterization, Thermogravimetric Analysis (TGA) was performed with Marca T. An Instruments, TGA Q500 model and Differential Scanning Calorimeter (DSC) TA Instruments, Q100 model. The **SpectraGryph 1.2** software® was used in order to translate the signals obtained for the analysis.

### 3.3.2 Synthesis of organometallic compounds

### 3.3.2.1 Synthesis of the ruthenium complex with 6-methoxyquinoline

For the preparation of the intermediate complex $RuCl_2(DMSO)_4$, 2.00 g $RuCl_3 \cdot 3H_2O$ in 12.5 mL of ethanol were used in refluxed for 5 hours at 78 ºC Then, filtered and rotary evaporator (Evans et al., 1973; Alessio et al., 1988; Alessio et al., 1991). Then, 1.5mL of Dimethyl sulfoxide (DMSO) were added at 140 ºC for 6 hours in reflux. After cooling to room temperature, the formation of the microcrystals is increased. It was washed with 15 mL of acetone cold four times (Brastos et al., 2010), put the solid previously washed and dried in a desiccator for seven days in the dark, the summary procedure is shown in Figure 6. The expected reaction for the formation of the intermediary is shown in Figure 7.



**Figure 6.** Summary procedure for the synthesis of the Ruthenium complex with 6-methoxyquinoline.
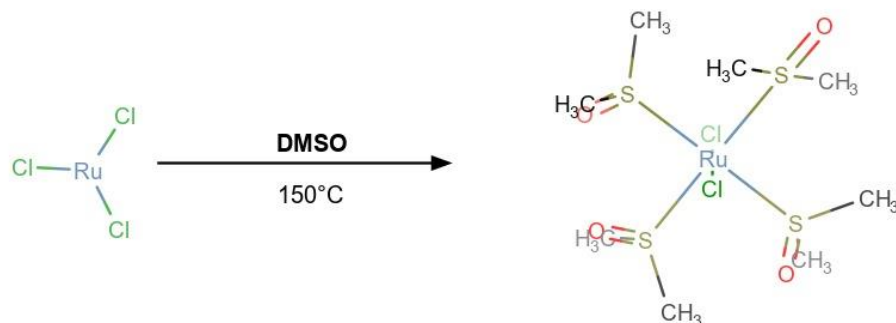
**Figure 7.** Intermediary coordination compounds (Alessio et al., 1988).

For the preparation of the intermediate complex with 6-methoxyquinoline, 99.5 mg of $RuCl_2(DMSO)_4$ were dissolved in 10 mL of ethanol for 2 hours in reflux at 78 ºC. Then, 60µL of the 6-metoxyquinoline were added, and the reflux continued for 1 hour at 78 ºC. When this step was finished, the product was put in a cold bath for 40 minutes and finally washed with 15 mL of cold acetone for four times. the proposed mechanism of the synthesis reaction is shown in Figure 8.
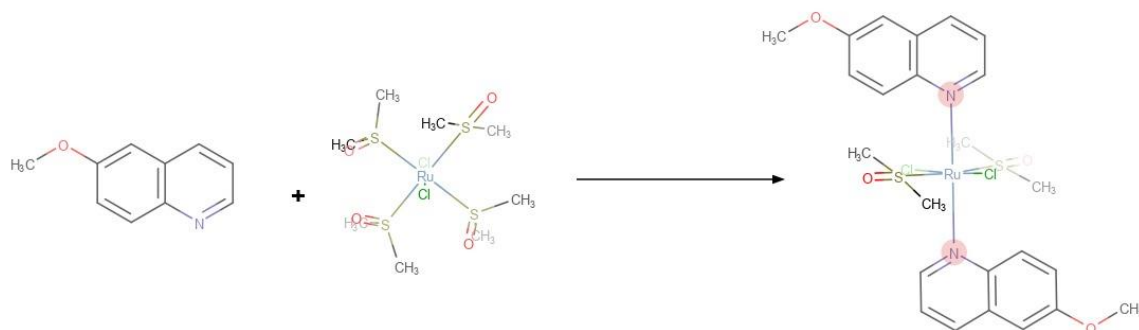


**Figure 8.** Reaction of the intermediate coordination compound with 6-methoxyquinoline (proposed by the author)

### 3.3.2.2 Synthesis of The Manganese And Gold Complex With 6-Methoxyquinoline

For the manganese reaction in solid phase, 0.0178 g of $MnCl_2$ and 50 $\mu$L of 6-methoxyquinoline were added; then, in an agate mortar, the mixture was made homogeneous, after that it was placed in the vacuum desiccator for 3 days, until the mixture was completely dry. After that, the sample was scraped and rinsed with benzene to clean the obtained solid. In the case of the liquid mixture, the same amount of salt was weighed, and 10 mL of HPLC grade ethanol was added and shaking by sonication to favor the dissolution; later, 50 $\mu$L of 6-methoxyquinoline was added and mixed for 30 minutes; after this time, the solution was left at rest for 8 days (this is the time needed for the formation of the crystals); then, it was rinsed with benzene and dried at room temperature for 8 days. In

the figure 9 the summary procedure for the synthesis of manganese chloride with 6-methoxyquinoline is shown, and the Figure 10 shows that the proposed chemical structure has 2 molecules ligands, and the metal is the central atom.
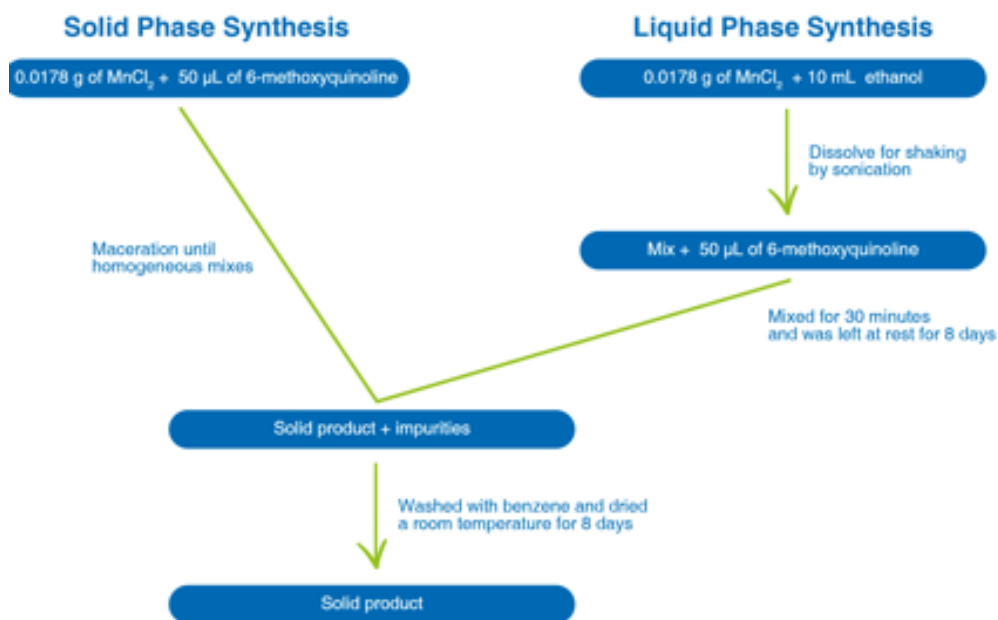


**Figure 9.** Summary procedure for the synthesis of manganese chloride with 6-methoxyquinoline.
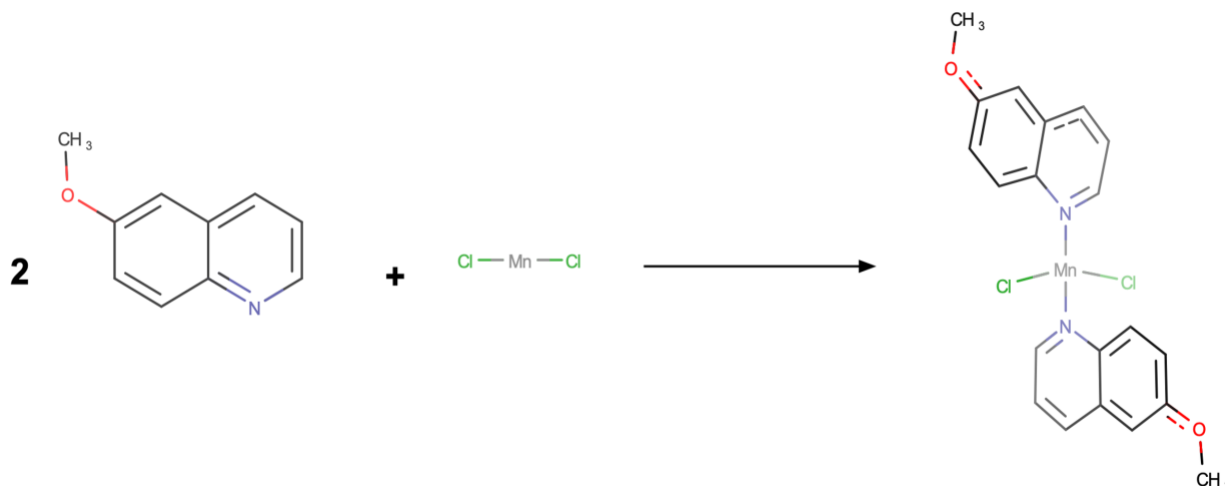


**Figure 10.** Reaction of the formation coordination compounds between manganese chloride with 6-methoxyquinoline. (proposed by the author)

On the other hand, the gold reaction in solid phase, was weighed 0.0178 mg of the AuCl and 25 µL of 6-methoxyquinoline was added; then, in an agate mortar the mixture was made homogeneous; after that, it was placed in the vacuum desiccator by 8 days, until the mixture was completely dry. After that, the sample was scraped and washed with benzene to clean

the obtained solid. In the case of the liquid mixture, the same amount of salt was weighed, and 10 mL of HPLC grade ethanol was added and shook by sonication to favor the dissolution; then, 25 µL of 6-methoxyquinoline was added and mixed for 2 minutes; after this time, the solution was left at rest for 15 days (this is the time needed for the formation of the crystals); then, it was rinsed with benzene and dried at room temperature for 8 days. In the figure 11 the summary procedure for the synthesis between gold chloride and 6-methoxyquinole is shown, and in the figure 12 it is shown the proposed chemical structure of 2 molecule ligands and the metal is the central atom.
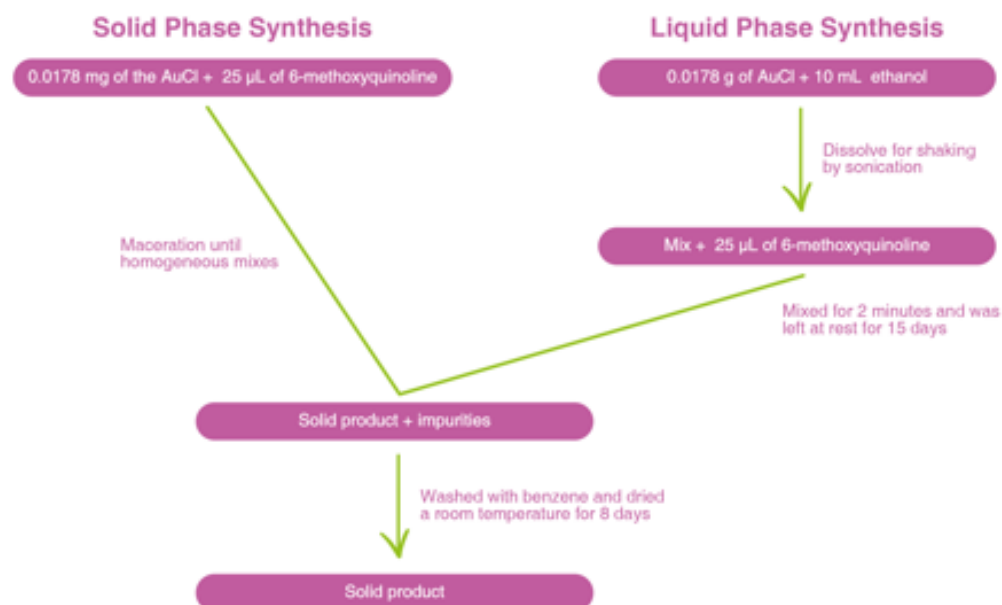


**Figure 11.** Summary procedure for the synthesis of gold chloride with 6-methoxyquinoline
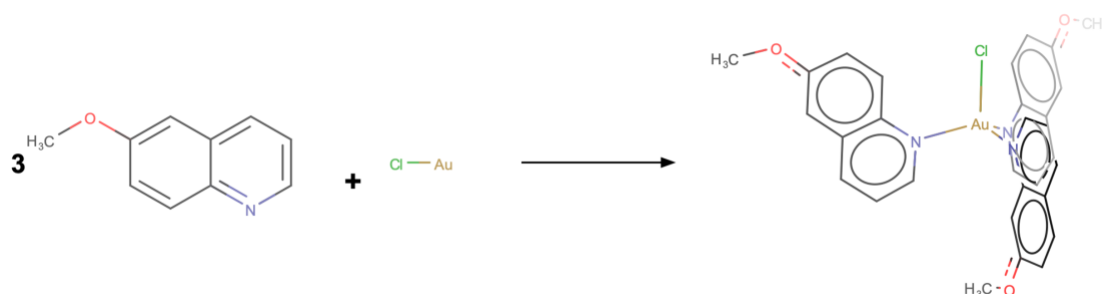


**Figure 12.** Reaction of the formation coordination compounds between gold chloride with 6-methoxyquinoline. (proposed by the author)

### 3.3.2.3 Antibacterial activity tests

A sterile swab was soaked in the previously prepared bacterial solution. Sowing was carried out in grass on the surface of the Petri dish with Mueller Hinton agar culture medium in order to achieve a homogeneous growth of bacteria. Subsequently, 20 µL of each of the crude

extracts were deposited on 6 mm diameter MN 827 ATD discs, which were placed on the bacteria lawn. In order to allow diffusion into the agar before bacterial growth, the boxes were stored inverted at 4 °C for 2 hours and then incubated at 36 °C, between 18 and 24 hours. Tetracycline was used as a positive control at a concentration of 2 mg/disk. Inhibition values will be reported as total diameter (disc diameter + inhibition diameter).

## 3. 4 Results and analysis

### 3.4.1 Synthesis and Characterization Synthesis Product

It is important to note that the times in this optimization were longer than proposed by the methodology reported by (Alessio et al., 1988), because factors such as environmental conditions may modify the times to which all the allusive modifies the evidence of the existence of a reaction. After obtaining the green sample with an oily appearance, dimethyl sulfoxide (DMSO) is added; the smallest amount possible of this reagent should be added in stoichiometric terms because, when there is an excess, it was experimentally noted that it did not allow the precipitation of the formed complex.

For the development of phase II of the reaction, there were some complications because this ligand choice is less reactive for the Nitrogen position in comparison with other ligands (De Frémont et al., 2005); for this reason, the synthesis product was delayed for its obtention. However, the order in which the reactive was included in the reaction affected the results, for example, for the 6-metoxiquinoline, it was necessary to add it drop by drop for 20 minutes, at this moment the color changed from yellow to orange. The formation of the new compound is evidenced in Figure 13.



**Figure 13.** Reaction step of $RuCl_2(DMSO)_2(6\text{-}OMeQ)_2$. Source: the author

For the preparation of the manganese and gold complexes, two methods were applied: Solid and liquid phase shown in the Figure 14 and 15. In the first methodology, the salt was mashed then input the 6-metoxyquinoline and continued mashed. With this methodology,

the changes happen depending on the strength applied during the process of maceration. At this moment, there is no literature that shows this methodology; in the second method, 10 mL of ethanol were used, the salts were dissolved and the reaction happened; in both reactions, the physical characteristics were the same.



**Figure 14 .** Synthesis of the manganese with 6-methoxyquinoline (complex) by maceration. Source: Author.
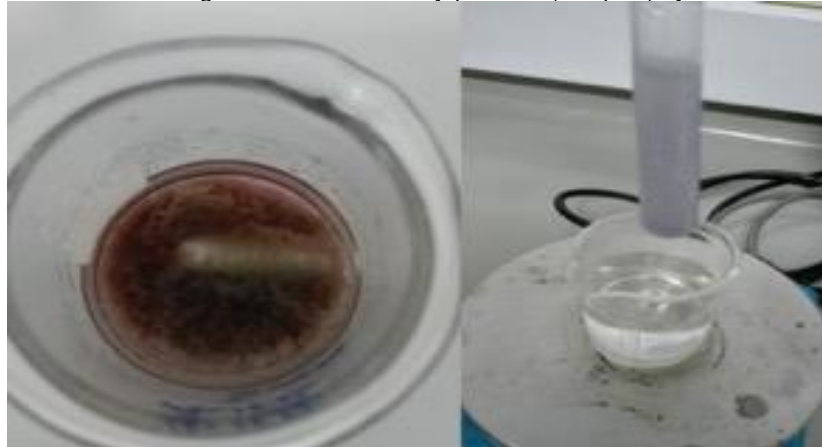


**Figure 15.** Synthesis of the gold with 6-methoxyquinoline (complex) by liquid mechanism. Source: Author

### 3.4.2 Characterization of the organometallic compounds obtained

Initially, all the analysis was for the characterization of materials for its application, however, all the results were focused at analysis of bulk and are not specifically for the specifically chemistry structure, our priority is to ensure that the compounds were obtained.

First, tests of solubility were carried out and it was found that the compounds have particular characteristics. In the case of $RuCl_2(DMSO)_2(6OMeQ)_2$, it is soluble in ethanol/dimethyl sulfoxide, moderately soluble in hot water but insoluble in benzene, acetone, hexane and acetonitrile; in the case $MnCl_2(6OMeQ)_2$, it is soluble in ethanol and hot water but insoluble in benzene, acetone, hexane and acetonitrile. Finally, $AuCl(6OMeQ)_3$, was moderately soluble in hot water and ethanol and insoluble in benzene, acetone, hexane and acetonitrile. Some results about the test, conducted in the laboratory are shown in Figure 16, the

solubility in water prevent these compounds to be fixed in polymeric materials such as silicones.
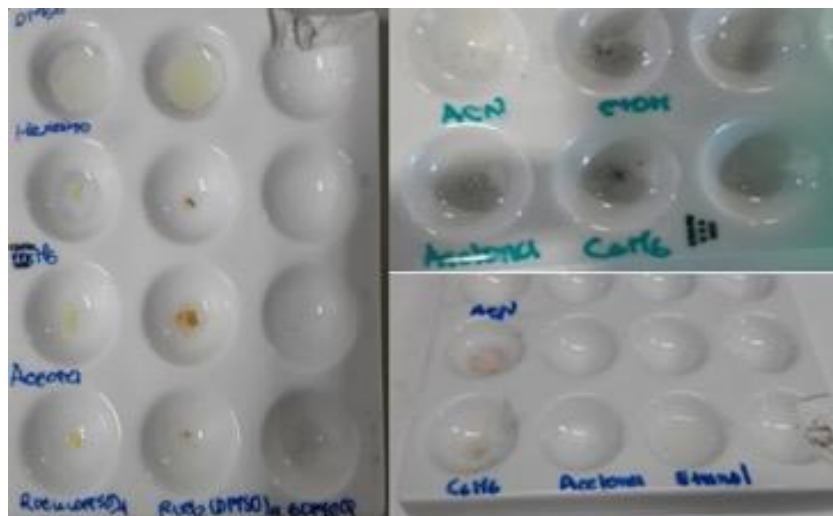


**Figure 16.** Solubility test for the synthetized compounds**.** Source: Author

In the case of the analysis of functional groups that are associated with the explanation of changes between reactants and products. Two analyzes were performed on the IR and RAMAN analysis as a complementary technique. As shown in Figure 17, the IR analysis took both the precursors (the salts and the ligand) as well as the reaction products. In the latter, it is perceived the appearance of characteristic signals of the ligand, 6-methoxyquinoline. For the ruthenium complex, the findings (Allan & Dahyrnple, 1991) are taken as reference. The signal around spectrum bands due to the aliphatic and aromatic C–H groups is observed in the 3100–2800 $cm^{-1}$ region and signal between 1340-1260 $cm^{-1}$ associated to aromatic amines in double bond of C-N, characteristic signals of 6-methoxyquinoline (6-OMeQ). Then, the signals like ring vibrations (1623, 1572 and 1500 $cm^{-1}$) were shifted to a higher wavenumber in the complex spectrum, indicating the binding of the gold and manganese to the nitrogen atom of the quinolinic ring (Villa-Pérez et al., 2015). In the case of the ruthenium complex, in 1575 $cm^{-1}$ and 1502 $cm^{-1}$ associated with the vibration of the ring. In the case of the strong signal, 1230 $cm^{-1}$ is associated to the signal of the C=O present in the structure, these signals were evident within the spectrum of the IR shown; however, when analyzing the band that is at 1596 $cm^{-1}$, it showed a tendency to disappear both in the solution before and after filtering, so the formation of the new

compound is affirmed. However, it is proposed to explore in the 200 cm$^{-1}$ region to confirm what was stated by (Allan & Dahyrnple, 1991) in their investigation.
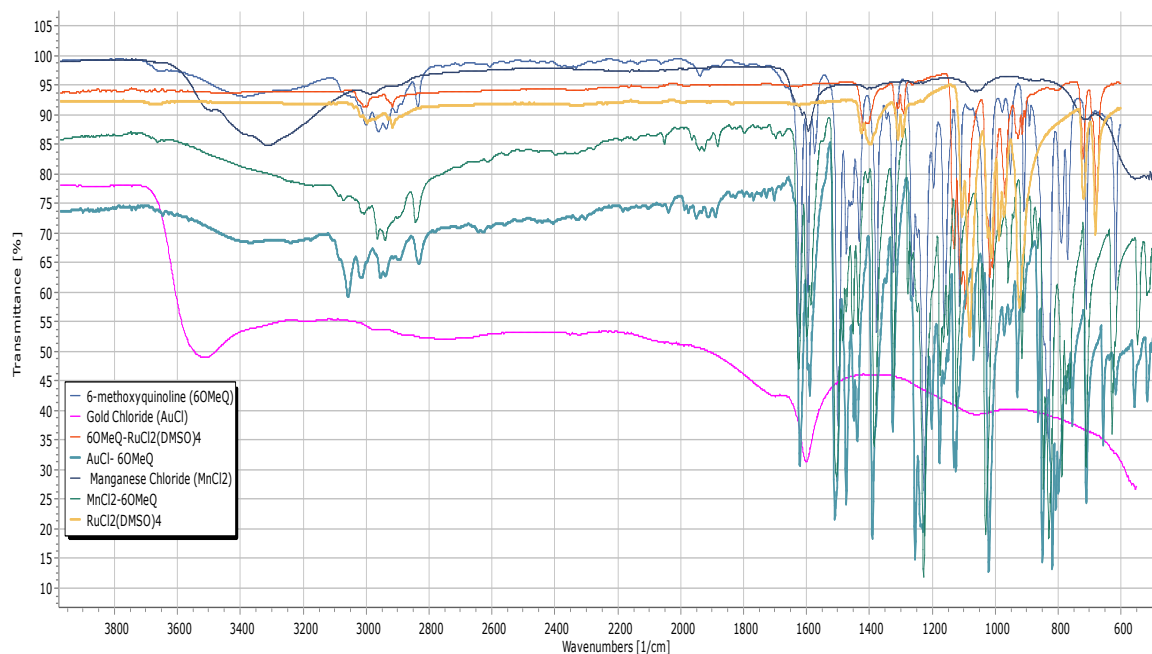


**Figure 17.** IR Spectrum of the reactants and product of the synthesis reactions

For the analysis of RAMAN shown in the Figure 18, the signals (1623, 1572 and around 1500 cm$^{-1}$) were shifted to a higher wavelength after complexation according to the N-donor coordination with the metal center in the formation of the new complex of AuCl(6-OMeQ)$_3$ according to the 6-methoxyquinoline spectrum. The signals relationship in 271 and 260 cm$^{-1}$ were assigned to the symmetric modes Au-Cl and their interaction. Another signal is at 113 cm$^{-1}$ could be associated the Au–N bond (Villa-Pérez et al., 2015).

Other results were associated with the signals from $v$(XY) to 347 cm$^{-1}$ and the signal $v$(XY2) is 171 cm$^{-1}$ (Nakamoto, 2006). In the case of the manganese complex shown in the figure 19, no result is evident, because the laser used to obtain the RAMAN analysis deteriorates the sample, so this result corroborates those obtained in thermal stability. Then, In the case of Ruthenium complex shown in the figure 20, the signal around 221 cm$^{-1}$ is assigned at N-Ru-N bending. Another signal is around 277 cm$^{-1}$ is related to Ru-N stretching, which demonstrates that the complex was formed (Chiu et al., 2014).
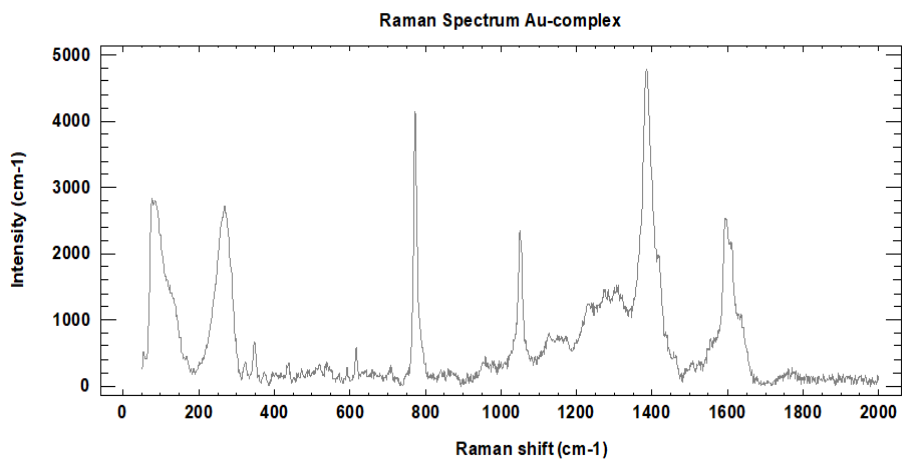
**Figure 18.** RAMAN Spectrum of AuCl(6-OMeQ)$_3$
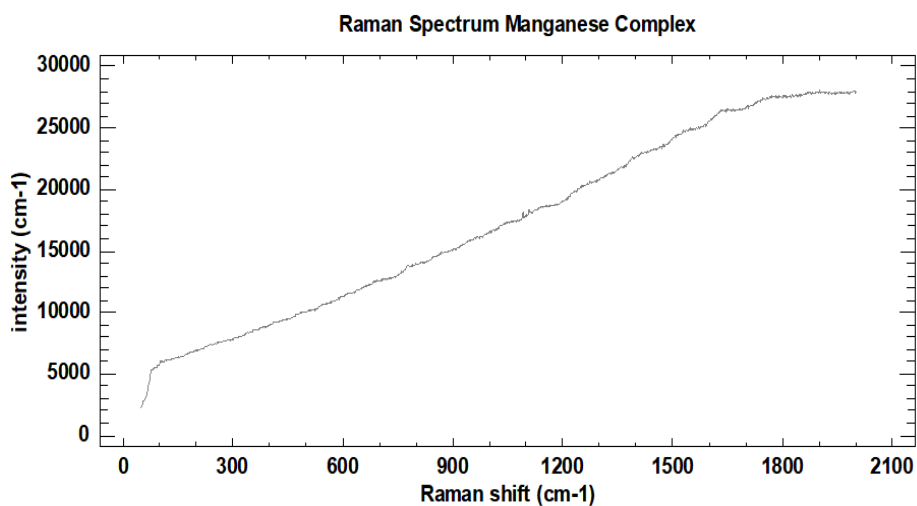


**Figure 19.** RAMAN Spectrum of MnCl$_2$(6-OMeQ)$_2$
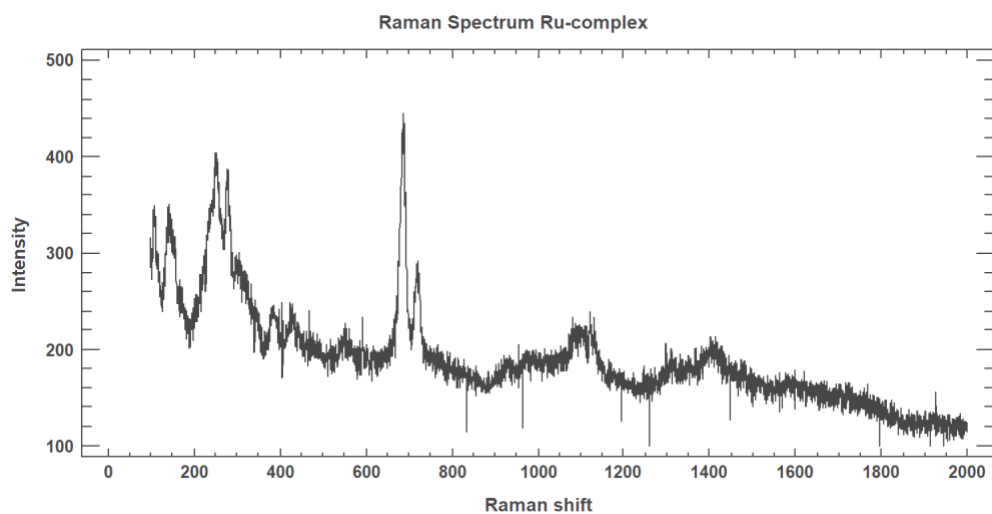


**Figure 20.** RAMAN Spectrum of RuCl$_2$(6-OMeQ)$_2$

In the thermogravimetric analysis for AuCl(6-OMeQ)$_3$, shown in figure 21, it was observed that in the first loss observed was (6.53 % at 187.67°C) is associated with the loss of mass by presence organic solvent traces such as benzene, ethanol, acetone or mixes of them. The second mass loss (14.83 % at 208.74 °C) is possibly associated with the loss of the 6-metoxyquinoline ligands (Villa-Pérez et al., 2018a). Finally, the remaining AuCl decomposes above 245-300°C to produce Au(0), the results shown was 5.10% at 265.13% (Otto et al., 2014).

In the case of the MnCl$_2$(6-OMeQ)$_2$ complex, shown in figure 22, the first loss of 1.76% at 110.06 °C is possibility associated with the presence traces of water and traces of the benzene that may remain in the sample (Smith & Matheson, 1938); then, the next loss of (19.99% at 149.69 °C) is associated with the loss of mass by presence organic solvent traces such as benzene, ethanol, acetone or mixes of them. Other loss mass on the thermogram (41.87 % at 283.29 °C) is possible presence remaining of MnCl$_2$ (Abdelrazek et al., 2012). Finally, the next mass loss (around 592 °C) is related to the melting temperature of the manganese salt and its decomposition.
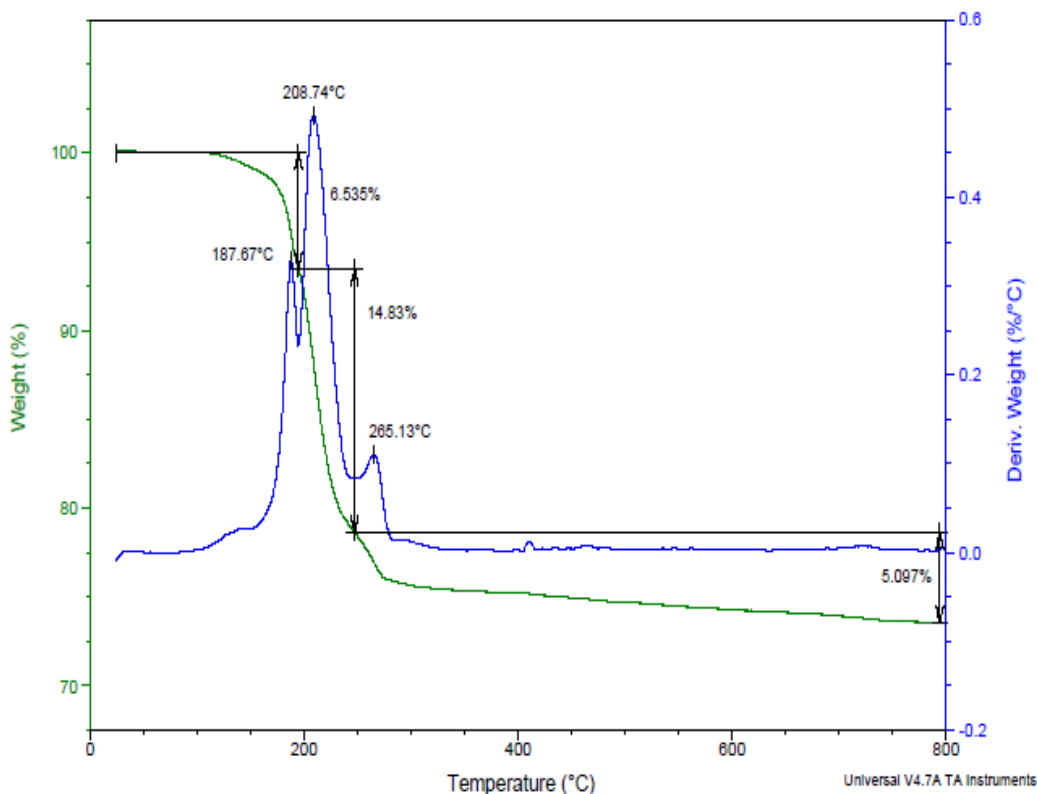


**Figure 21.** Thermogram TGA of the AuCl(6-OMeQ)$_3$ complex.
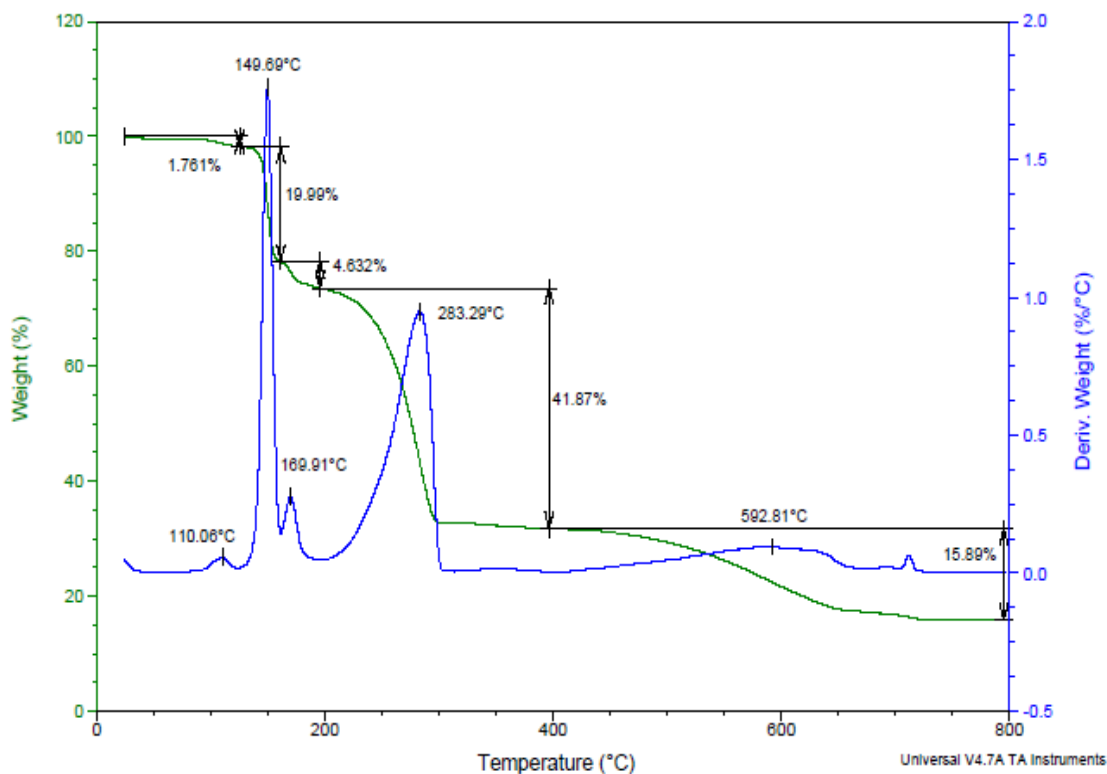
**Figure 22.** Thermogram TGA of the MnCl$_2$(6-OMeQ)$_2$ complex.

Particularly, in the analysis of the AuCl(6-OMeQ)$_3$ complex proposed in Figure 23, the formation of crystalline phases is evidenced: Exothermic peaks in 192.45 °C (with an enthalpy of decomposition of 28.24 J/g) related to water vaporization (Ferreira et al., 2019). For the MnCl$_2$(6-OMeQ)$_2$ complex shown in Figure 24, a glass transition at 115.09 °C is evidenced, so it is presumed immediately that it does not have a crystalline phase. Then, the next transition temperature was of 153.76 °C (with an enthalpy of 52.11 J/g), by the shape of the observed peak, crystallization is evidenced in isothermal conditions, that is why it is related to the findings of the TGA, and very related to the presence of the salt of the decomposition reaction and, consequently, the salt present in the sample.
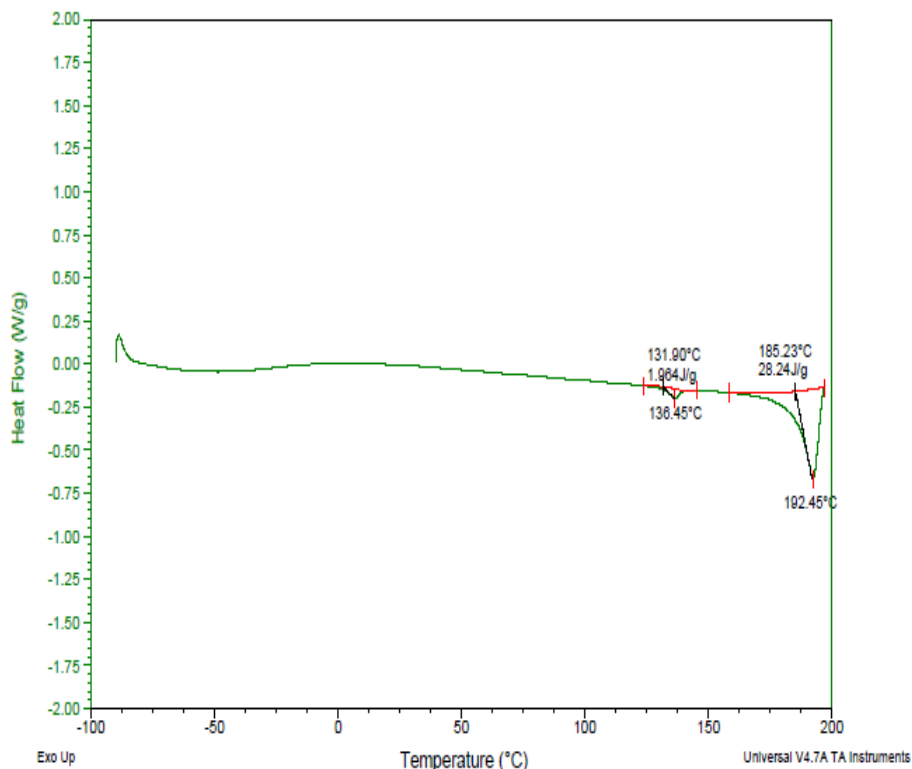
**Figure 23.** Thermogram DSC of the AuCl(6-OMeQ)$_3$ complex.
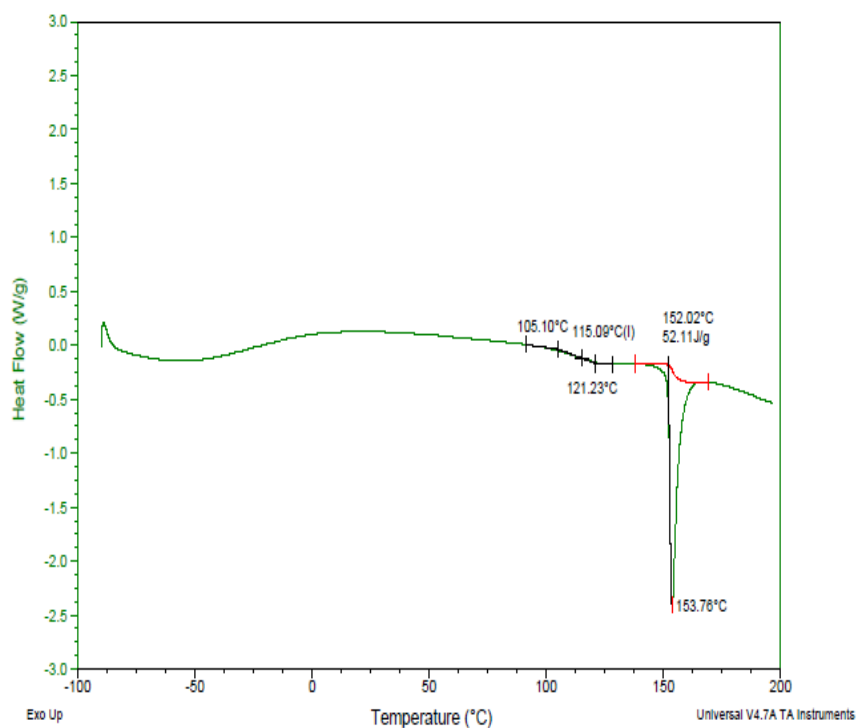


**Figure 24.** Thermogram DSC of the MnCl$_2$(6-OMeQ)$_2$ complex.

For the morphological analysis, it is evident in the micrograph of AuCl (6-OMeQ)$_3$ that the formation of the new compound occurs through the formation of polycrystals (marked with a size of 54.37 nm), and the generation of byproducts of the reaction (13.49 nm), which are considered gold nanoparticles, as a consequence of the excess salt present in the development of the reaction aspect that is visible in the agglomerate, shown in Figure 25. The formation of polycrystalline phases is also evident based on the diffraction analysis, because of the poor definition of the rings; however, the information that is available is not enough to determine the structure required for analysis computations that allow establishing clearly the crystal structure.

In Figure 26, the complex MnCl$_2$ (6-OMeQ)$_2$ showed an opaque imaging in this micrograph; the micrographic for the MnCl$_2$ appears to be globular, resembling agglomerates of fibrous, thinner particles (Varin et al., 2017). However, compared to the result of this complex, it has a different structure; in this micrographic it is shown whether this complex is amorphous thanks to its presence because MnCl$_2$ segregated into interlamellar or intercrystalline regions reduces the degree of crystallinity (Abdelrazek et al., 2012).
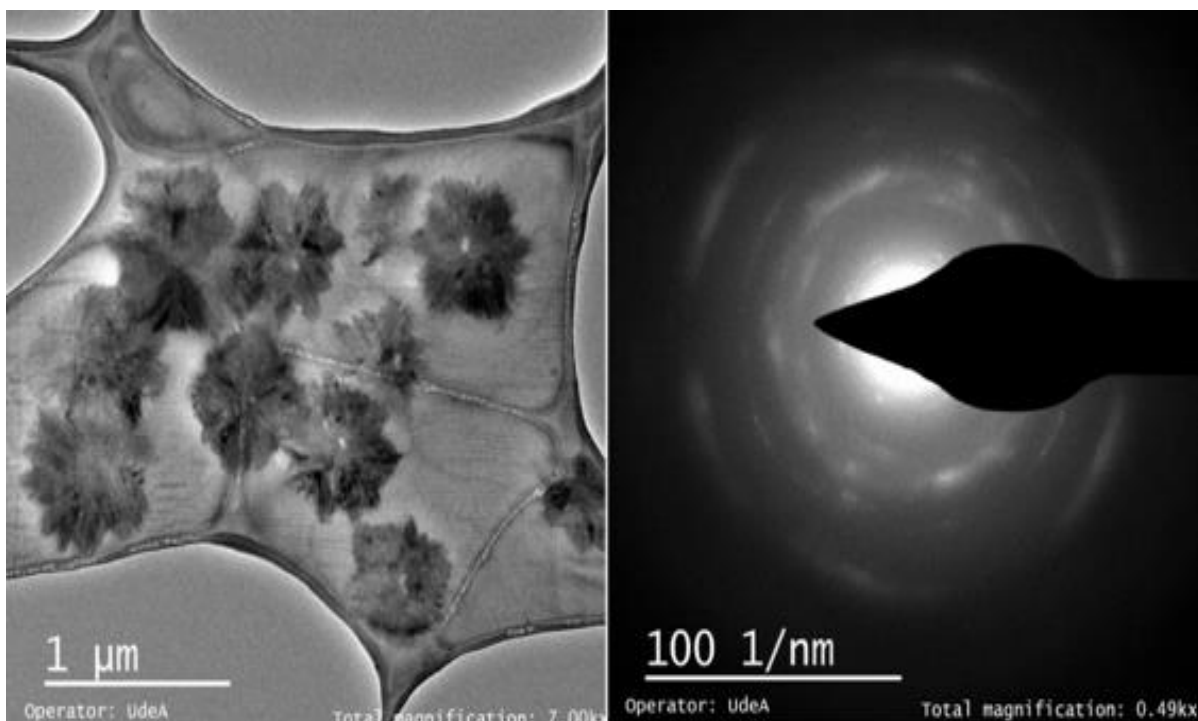


**Figure 25.** Micrographs of the AuCl(6-OMeQ)$_3$. On the right the agglomerate formed as a product of the reaction is observed, the formation of gold nanoparticles is evidenced as a by-product of the reaction. On the left, the formation of a polycrystalline phase is preliminarily evidenced.
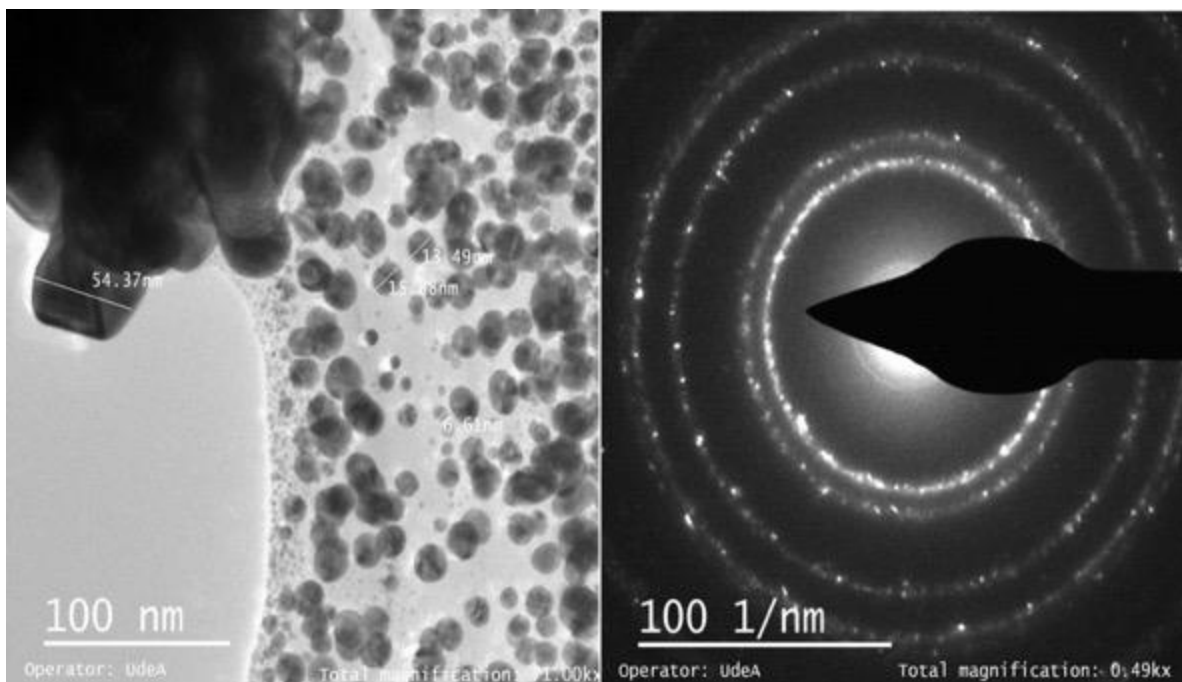
**Figure 26.** Micrographs of the $MnCl_2(6\text{-OMeQ})_2$. On the left showed particles like stars of size micrometer. On the right, shown the Rx Analysis, the complex is amorphous because the ring showed low definition and opaque.

Finally, the antibacterial test results obtained are shown in Figure 27. In a clockwise direction, AuCl is found first, then 6-OMeQ and finally the complex formed by both AuCl (6-OMeQ)$_3$. There is no antimicrobial activity for either AuCl or 6-OMeQ; likewise, no effect is shown on the *B. Cereus* strain; however, in *E. Coli*, a very sharp small halo (~ 9 mm) can be observed, accounting for the activity of the complex on this strain. Given that gram-negative bacteria, such as *E. Coli*, have a double cell membrane (one external and the other cytoplasmic), it could be concluded that the synthesized AuCl(6-OMeQ)$_3$ complex has a potential antimicrobial effect and, if a higher concentration is achieved in the solution, one could speak of a greater bactericidal activity. For the other compounds no antibacterial activity was found.



*E. Coli*
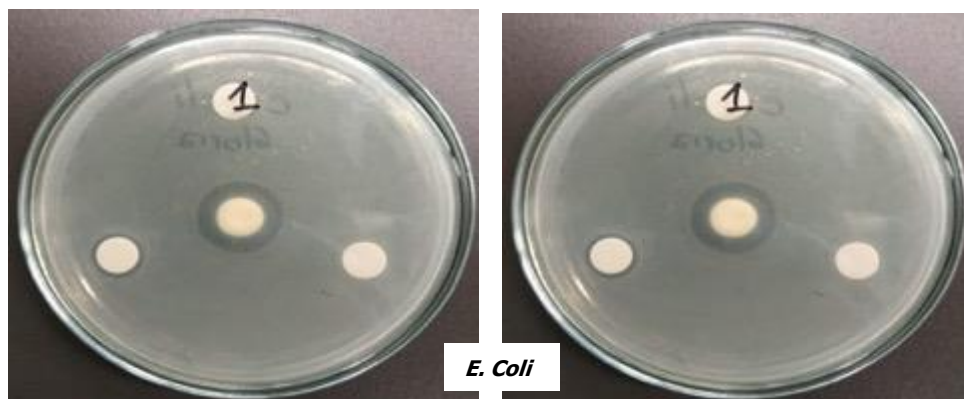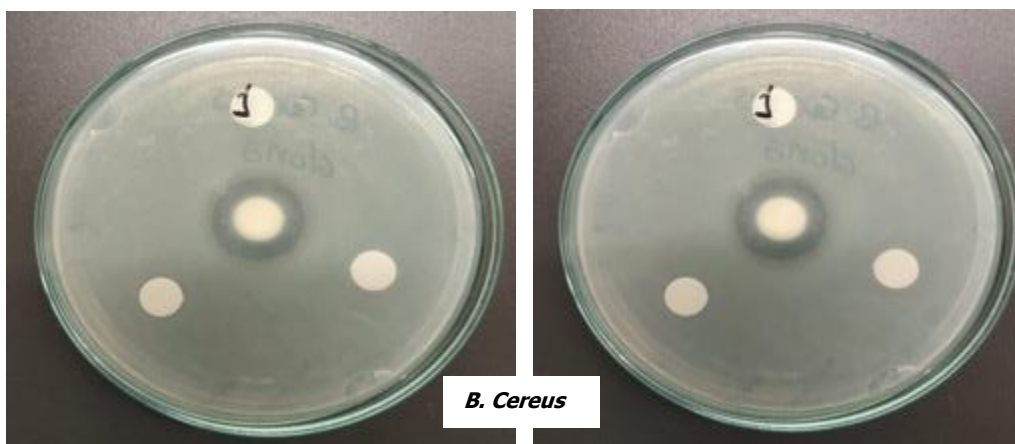
**Figure 27.** Antibacterial susceptibility tests for AuCl (6-OMeQ)$_3$ complex.

## 4. Chapter 2: Photosensitization Process

## 4.1 Introduction the Photosensitization Process

The photochemical reactions occur thanks to the presence of photons energy, which should be enough to break a specific chemical bond or otherwise induce a reaction. With the increase of light intensity, the reaction rate increases, that is, it requires energy to trigger a reaction, this energy is greater than the energy per photon of light of a certain wavelength (Lu & Ogilby, 1987) (DeRosa & Crutchley, 2002).

Specifically, singlet molecular oxygen is considered a powerful electrophile agent that can react with a pair of electrons of an electron-rich heteroatom (Pospíšil et al., 2008) . A clear example of this type of compounds are those that contain nitrogen in their structure or in effect coordination compounds that have this type of ligands, and that contain transition metals at the ligand for the transfer by transfer of electrons from the molecular orbital with metal character to those with ligand character for charge transfer (MLCT) (Seneviratne et al., 2002) or vice versa Ligand-to-Metal Charge Transfer (LMCT) (Gross & Kaim, 1987) both are able to react favorably for the formation of singlet oxygen, a species of great interest for this research.

Particularly, the singlet molecular oxygen ($^1O_2$) is a reactive oxygen species which is considered as the lowest electronically excited state of molecular oxygen (LUMO) and is generated exclusively by photosensitization. This deficient species of electrons (electrophile), with diamagnetic character (singlet multiplicity) and with an excess of energy of 22.5 Kcal/mol$^{-1}$ (94.2 KJ/mol$^{-1}$) with respect to its basal state, can participate in chemical reactions that, for the molecular oxygen in the triplet basal state, are forbidden by the spin(DeRosa & Crutchley, 2002). The average life of the species depends on factors such as viscosity this may be due to the inhibition for the collision deactivation of singlet oxygen in highly viscous solvents; the polarity, temperature and even the mole fraction of water present in the solution (Miyoshi et al., 1982), and the reactions with $^1O_2$ are given by charge transfer or energy transfer (DeRosa & Crutchley, 2002)(Payán Aristizábal, 2015).

## 4.2 Conceptual Framework

As shown in Figure 28, the pair of electrons that enter the orbital $\pi^*$ occupy two different antibonding orbitals two excited: the first excited state $^1O_2$ ($^1\Delta_g$) and second excited state $^1O_2(^1\Sigma_g)$, which differ according to the anti-binding $\pi$, giving it a paramagnetic character. By applying energy in the form of radiation they can pair, thus moving to a first excited level for which 22 Kcal/mol is required and if more energy is applied (37 Kcal/mol) can go to a second

level of excitation, if no reaction occurs it is possible that it undergoes a decay and the oxygen passes to its state of triplet that is more stable, generating with it a band of emission of luminous energy (1260 and 760 nm)(DeRosa & Crutchley, 2002).



**Figure 28.** States orbital assignment of singlet orbital

Within the processes of photosensitization carried out at laboratory scale are by continuous irradiation and by pulsed excitation. However, this research has a special interest in photosensitization reactions, which require oxygen, radiation of an adequate wavelength that is capable of transferring energy to a photosensitizing material, and by intersystem crossing (ISC) it manages to transfer the energy to the oxygen present in triplet state (basal) and take it to the singlet state. The half-life of the triplet state is greater than the singlet state´s one and this excited state can react in one or two mechanisms; this is  shown in the figure 29:
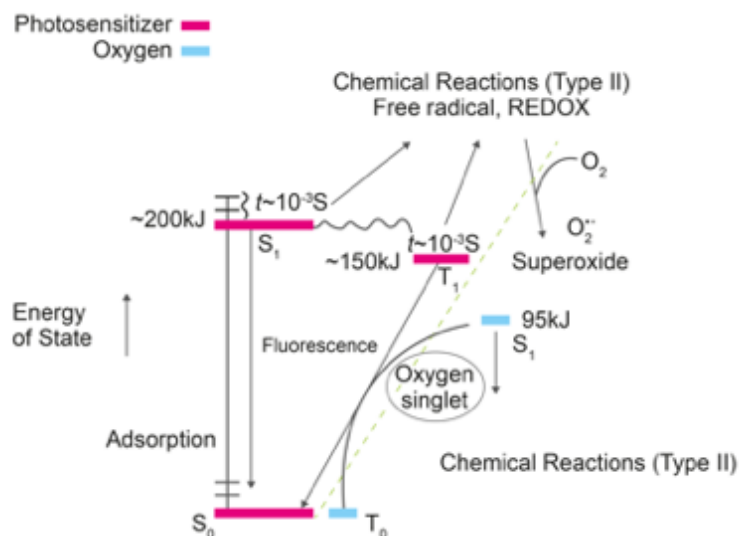


**Figure 29.** Excited states of oxygen.(DeRosa & Crutchley, 2002)

**Type I:** the mechanism that involves the abstraction of a hydrogen atom or transfer of electrons between the excited sensitizer and the substrate, the generation of free radicals. These radicals can react with oxygen to form a kind of active oxygen such as the superoxide anion radical, as evidenced by the following shown in the Eq. 1:

$$P(S_0) \xrightarrow{h\upsilon} P(S_1) \xrightarrow{K_{ISC}} P(T_1) \quad \textbf{Eq. 1}$$
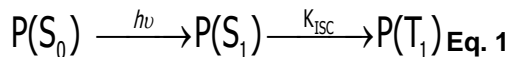
**Type II:** in this case, the singlet oxygen is generated by the energy transfer during the collision of the excited triplet sensitizer with oxygen, as shown in the Eq. 2:

$$P(T_1) + {}^3O_2 \xrightarrow{K_{en}} P(S_0) + {}^1O_2 \quad \textbf{Eq 2}$$
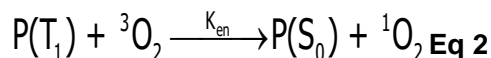
Where P is the photosensitizer, ground state $S_0$, $S_1$ excited first singlet state, $T_1$ first excited triplet state, constant $K_{ISC}$ rate associated with the crossing between systems and $K_{en}$ is the velocity constant for energy transfer, ${}^3O_2$ and ${}^1O_2$. Competing with the reactions shown in equations 1 and 2 are radiative and non-radiative mononuclear processes and the equation 3 at 6 shown the quantum yield of ${}^1O_2$ production $(\phi_\Delta)$ is defined as

$$P(T_1) \xrightarrow{K_T} P(S_0) + h\nu'' \quad \textbf{Eq 3}$$

$$P(T_1) \xrightarrow{k_{nr}} P(S_0) \quad \textbf{Eq 4}$$

$$P(T_1) + O_2 \xrightarrow{k_{dO_2}} P(S_0) + O_2 \quad \textbf{Eq 5}$$

$$P(T_1) + O_2 \xrightarrow{k_{et}} P^+ + O_2^{\bullet-} \quad \textbf{Eq 6}$$
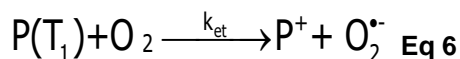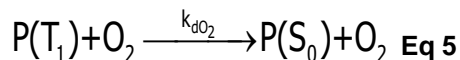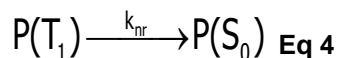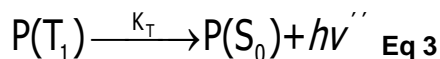
The way in which every proton fraction adsorbs a photosensitizer at a wavelength is called quantum yield (Werner et al., 1984). Which is defined by (DeRosa & Crutchley, 2002) and shown in the equation 7:

$$\Phi_\Delta = \Phi_T \Phi_{en} = \Phi_T \left( \frac{k_{en}[O_2]}{k_r + k_{nr} + k_q[O_2]} \right) \quad \textbf{Eq 7}$$

Where,
$\Phi_\Delta$: Quantum yield of singlet formation
$\Phi_T$ : Quantum yield of triplet formation

$\Phi_{en}$ : Efficiency of the transferred energy
$K_{en}$: Velocity constant of the transferred energy

$K_q$: Sum of the velocity constants from the P (T1) of the Oxygen $K_{en} + K_{dO_2} + K_{et}$

For the determination of quantum yields Wilkinson et al., (1993) mention in their research the use of techniques such as luminescence, calorimetric technical irradiation, loss of absorbance or fluorescence; however, the commonly known technique is the determination using a tracer and a reference photosensitizer.

There are structural factors affecting $^1O_2$ generation, for example, effects of halogenated substituents. These results demonstrating that increasing the atomic mass of the halogen induced a decrease of the quantum yield as well as the rate of fluorescence, whereas internal conversion was enhanced. Other reason explained by the authors, is the effect of radical substituent increase; in the triplet quantum yield, the lifetimes were long enough to facilitate $T_1$ to $^3O_2$ energy transfer (Jeong & Choi, 2016). Moreover, the singlet oxygen molecular can be detected directly, by measuring typical singlet oxygen phosphorescence at 1270 nm; in such case, EPR spectroscopy can be used when singlet oxygen is trapped by a species able to generate a stable radical; or indirectly, using chemical probes that react with singlet oxygen producing compounds that are the detected species (Pibiri et al., 2018). Another option is the commercial Singlet Oxygen Sensor Green (SOSG), the principle is the presence of singlet oxygen, SOSG produces an endoperoxide (SOSG-EP) and green emission from the fluorescein moiety is turned on; nevertheless, the first inconvenient is the production of triplet excited states, thus affecting the measurement (Pedersen et al., 2014).

### 4.2.1 Photosensitizers

According to (García-Fresnadillo, 2001), the concept of the photosensitizer is associated with a molecule or group of compounds that have specific characteristics, which are related to:

1. Intense absorption of UV-VIS light (preferably in the visible region between 400 and 750 nm) with molar absorption coefficients ($\varepsilon$) greater than $10^4$ $M^{-1}$ $cm^{-1}$.

2.High efficiency or quantum yield  in the inter-system crossing ($\Phi_{ISC}$), step from the excited state singlet ($S_1$) to excited state triplet ($T_1$), proximity to 100 %, and an energy gap between $S_1$ and $T_1$ of the photosensitizer higher than the energy difference between the excited and basal singlet states in molecular oxygen (> 95 $KJmol^{-1}$), so that there is an efficient energy transfer from the photosensitizer to the oxygen.

3. Long lifetimes of the excited state ($\tau$), in the order of μs or higher, in order to allow enough time for the collision between the photosensitizer molecules and the oxygen molecules present in the medium.

4. The high quantum yield of singlet oxygen production ($\Phi_\Delta$) in different condition. The number of events that occur from singlet oxygen production divided by the number of photons absorbed by the photosensitizer and per unit of time should be as high as possible. In general, good photosensitizers have ($\Phi_\Delta$) values close to unity.

5. Thermal and photochemical stability. In order to avoid the decomposition of the photosensitizer molecules, even by the photogenerated singlet oxygen itself.

6. Ability to be immobilized in polymeric supports in an affordable way, in order to facilitate the development of applications.

### 4.2.1.1 Organic Photosensitizers

These compounds have been widely used for photodynamic therapy against cancer and since its inception they emerged as its main application(Fernandez et al.,1997). The anthraquinones was studied as photosensitizers for antiparasitic photodynamic inactivation shown the lowest toxic activity against fibroblasts(Dimmer et al., 2019).

At a general level, the organic photosensitizers are compounds which main characteristic is being donors or electron-rich structures which are visualized. The main advantage of photooxidation with dye sensitizers is the use of two resources: Solar photons in the visible range for photoexcitation of the dye and oxygen in the air. For this reason, photosensitizing oxidation occurs in nature, participating to some extent in the restoration of equilibrium in the destroyed environment (Gryglik et al., 2007). Due to this the range of dyes applied in the processes of photosensitization remains in continuous search for the wide application of the same, within the most applied dyes are Rose Bengal, phenalenone and methylene blue (García-Fresnadillo, 2002).

Within the visible examples of dye in environmental applications, was reported by Gryglik et al. (2007) uses  Bengal Rose (RB) as a photosensitizer in a homogeneous aqueous solution and with a sensitizer immobilized in non-soluble carrier water for the removal of 2-chlorophenol compounds that are widely used in industry and daily life, and have caused considerable damage and threat to ecosystems, which, at the end of the publication, showed that the contaminant was adsorbed on the material that was fixed in a polymer.

Other application was shown (Piwowar et al., 2015) on five selected amine-derivatives of phenothiazine were electropolymerized on an ITO/glass substrate and then used in the daylight-activated process to produce in situ singlet oxygen which degrades phenol in a solution. The phenothiazines were immobilized in a simple electrochemical procedure in an

acidic solution which led to the formation of an ultrathin transparent polymeric film, all films obtained on the ITO substrate including azure A (AA), azure C (AC), methylene blue (MB), toluidine blue (TBO), and thionine (Th). The results shown that e highest efficiency at a level of 51.4% and 45.4% was found for the AC/ITO and MB/ITO layers.

Finally, other dyes in the Eosin Y which has stood out for being with laser applications, fluorescent tags for use in molecular biology  and for potential photosensitizing biological activity and photosensitizer (Meallier et al., 1999). In the actually, was developed to immobilize ecofriendly dye inside a porous metal−organic framework (MOF) built from Eosin Y with $[Cd_2(COO)_2(\mu_2-H_2O)]$ secondary building units for the first time. The MOF exhibited efficient photocatalytic activity for $H_2$ evolution under visible-light irradiation which was approximately 31 times the photocatalytic efficiency of Eosin Y(J. Wang et al., 2018).

### 4.2.1.2 Inorganic Photosensitizers

In this family of compounds, inorganic photosensitizers have been considered at some metal oxides by photocatalytic activation of dissolved oxygen, and it is possible to generate $^1O_2$. A clear example is a research of Buchalska et al. (2010) where the photoactivity in the suntan lotions was evaluated,  providing evidence on generated species reactive of oxygen, specifically, radical hydroxyl and singlet molecular oxygen, which can be produced quite efficiently. For example, there are others studies reported using Zinc oxide (Wang et al., 2004), Bi(V)/Bi(III) composites for the degradation of Bisphenol A (Zhang et al., 2015) and some reactive chemistry such as potassium perchromate (Peters et al., 1976) among other things.

### 4.2.1.3 Organometallic photosensitizers

Among the multiple applications of these compounds, which stand out as catalysts in chemical reactions (Cho et al., 2002) (Martínez et al., 2005) (Rigo et al., 2014), their capacity has also been demonstrated for photosensitizer applications in water treatment, whereby the photosensitive material is fixed on a polymer surface in solid phase, studies reveal that using polymers such as silicone preserve the fluorescence signals so it is very convenient to fix it on these materials (Iu & Ogilby, 1987).

There are studies that assure that the coordination compounds with transition metals, as described by Allan & Dahyrnple (1991); however, the type of compounds of greatest environmental interest are the Ruthenium compounds which are able to take advantage of

the visible part of the solar spectrum. Due to their ability to be, as strongly adsorbed visible light (Fuller et al., 2003), very characteristic of complexes with transition metals, they can also act as photosensitizers generating interaction with ruthenium production of oxidation reactions with water. As stated by these authors, there are three key components in water oxidation: light absorption unit-photosensitizer, water oxidation catalyst and a sacrificed electron acceptor (Xue et al., 2015).

Several compounds that may have photosensitizing capacity have been proposed, so the possibility of including metals which demonstrate that they can generate singlet oxygen has been studied. Within the range of compounds synthesized with this property stand out the coordination compounds with ruthenium (which is characterized by complexes that are stable, inert, soluble in water, and have long luminescence lifetimes) are extremely valuable as optical sensors and luminescent probes for the investigation of heterogeneous microsystems, or as probes for biological systems (García-Fresnadillo et al., 1996) (Yin et al., 2017) (Kitajima et al., 2018)(Teixeira et al., 2020). In the patent presented by Orellana Moraleda et al. (2006) it is shown Ruthenium complexes based photosensitizers and their efficiency in water disinfection (Villén et al., 2006).

Díez-Mato et al. (2014) show the results for the removal of three pollutants: Ibuprofen, paracetamol and bisphenol A using a photosensitizing material consisting of tris(4,7-diphenyl-1,10-phenanthroline)ruthenium(II) chloride, immobilized in a porous poly (dimethylsiloxane) inert support using ultra-pure water and river water at different conditions; in this case the removal range for ibuprofen was (40%-100%); for Bisphenol A it was (70%-80%); and finally, for paracetamol was (20%-35%). The difference in the results depends of the matrix composition.

### 4.2.2 Singlet molecular oxygen in the environment

Naturally, the oxygen is detected in the basal state as a triplet stated, considered at lowest state of energy, but it needs to gain energy for the change at the excited state (exactly 94 KJ/mol). The singlet state can be generated in solution directly or by energy transfer from excited photosensitizers. The characteristic of the singlet state is that it has a $E^0$ ($^1O_2/O_2^{\bullet-}$) versus Normal Hydrogen Electrode (NHE) at pH 7.0 of 0.65 V (Koppenol & Butler, 1985); the steady-state concentration in sunlit natural waters is of $10^{-12}$ to $10^{-13}$ M; and a lifetime in pure water (pH 7.0) is around of 4 µs (Burns et al., 2012). It is possible to obtain the species, but it depends on the photosensitizer and the proper lighting.

In the atmosphere it is possible to find the singlet oxygen for the reaction between ozone, and it does absorb some near-surface solar UV at wavelengths < 320 nm showed in the equation 8 (Larson & Marley, 1999). The other source of tropospheric energy transfers from other electronically excited molecules to ground-state oxygen; this is explained in the equation 9 (Zafiriou et al.,1984).

$$O_3 + h\nu \rightarrow {}^1O_2 + O \quad \textbf{Eq 8}$$

$$^*NO_2 + {}^3O_2 \rightarrow NO_2 + {}^1O_2 \quad \textbf{Eq 9}$$
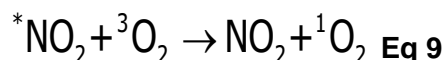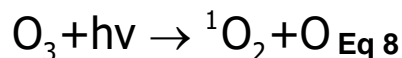
The $^1O_2$ exists in lakes, oceans and other phases such as ice (Momzikoff et al.,1983; Bower & Anastasio, 2013); but specifically, in natural waters its lifetime may be shorter due to the presence of additional quenchers, such as dissolved organic matter (DOM), that can be produced and scavenged continually by the small quantity of DOM present in the medium: Triplet-state excited organic matter ($^3OM^*$), singlet oxygen $^1O_2$ and radical hydroxyl ($OH^•$) (Zepp et al., 1977);(Paul et al., 2004);(Bodhipaksha et al., 2015) and (Porras et al., 2016). The reaction involving single oxygen is too quick to be significant in natural waters; for this reason, the best way to understand the consumption of oxygen is to use quenching processes, such is the case of the study reported by Wolff et al. (1981), where it is mentioned that the formation of singlet oxygen in natural waters by the presence of humic and fulvic acids generates a photochemical excitation that leads to a transfer of energy to triplet oxygen. In this investigation, the authors used the 2,5-dimethyl furan, which confirms the formation of by-products; in this case, a direct relation of the Total Organic Carbon with the singlet oxygen formed was demonstrated.

Other studies reported by Werner R. Haag et al. (1984) and (W R Haag & Hoigne, 1986) shows the use of furfuryl alcohol as a singlet oxygen quencher, evidencing that it is a chemical type quencher with proven high efficiency for the entrapment of singlet oxygen, however, the action of UV light is effective for the treatment of humic acids in natural waters.

In fact, there are some research papers that indicate that there is an accelerating effect on the rate of decomposition caused by the humic substances. This effect was associated with the photosensitized capacity of humic substances to facilitate energy transfer from an excited humic state to the ground state of the pollutant (Porras et al., 2016).

## 4.3 Materials and Methods

### 4.3.1 Reagents and Equipment

For the preparation the calibration curves were used Bisphenol A brand sigma Aldrich 100% purity, Triclosan Carlo Erba 100% purity; 9,10-dimethylanthracene sigma Aldrich 99%; eosin Y sigma Aldrich at ~99% purity; Perinaphthenone Sigma Aldrich at 97% purity and 1,3-Diphenylisobenzofuran Sigma Aldrich at 97% purity.

For the construction of the calibration curve of Bisphenol A was taking a stock solution of 1003 mg/L, the Triclosan was 1050 mg/L; for the eosin Y the stock solution of 540mg /L, for the Perinaphthenone was 1.3mg/L; for the 1,3-Diphenylisobenzofuran was 0.59mg/L and 9,10-dimethylanthracene was 210 mg/L. The solvent used was ethanol HPLC/spectrophotometric grade (Merck ≥99.5%).

The equipment used was the spectrophotometer Perkin Elmer Lambda 35. The lamps used in the experiments had different wavelengths: UV lamp, halogen and LED lamp that covered the UV/VISIBLE range, important for this research. For the execution of the experiments, the samples were taken at 2 mL in cell quartz with a capacity of 3 mL, disposed inside the compartment using a laboratory-made metallic support equipped with a water inlet and outlet that generated a controlled temperature inside the compartment. Every sample was situated in front of the lamp and were shook the whole duration, to ensure that the light interacted with the analyte for the irradiation times. All of the experiments were carried out at a distance of 7 cm with a height of 21.5 cm, as shown in Figure 30.
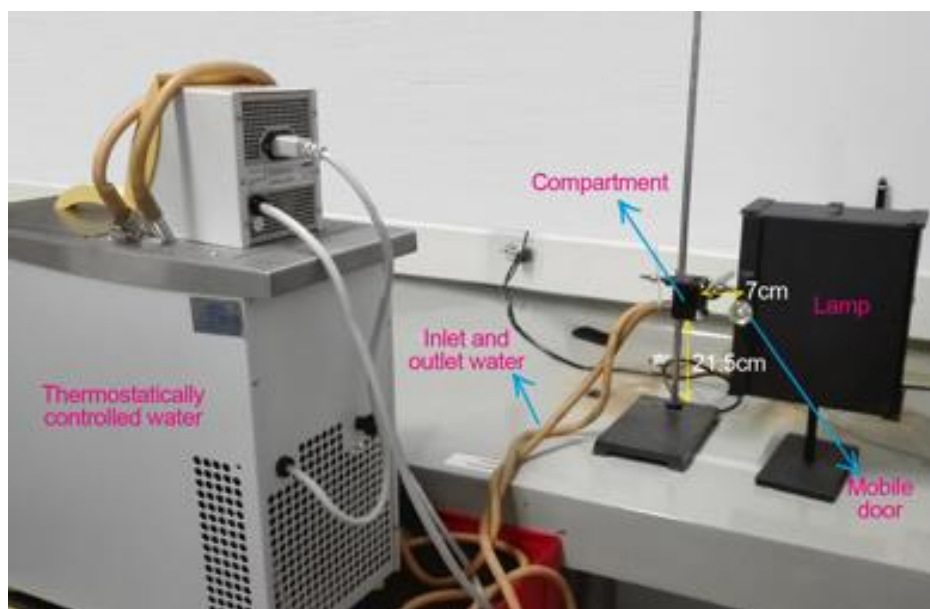


**Figure 30.** Experimental assembly for irradiations. Source:Author

### 4.3.2 Determination of Calibration Curves

For the preparation of the calibration curves, a spectral scan was initially made to establish the maximum wavelength of each of the reagents to be used. Then, to establish the linear range of the study, the criterion was not to exceed 1.5 absorbances, according to the Beer-Lambert law; this principle was applied for all pollutants, photosensitizers and trappers.

### 4.3.3 Determination of The Quantum Yields for The Synthetized Photosensitizer

The evaluation of the synthesized complexes was performed by stationary deactivation, using a reference photosensitizer, which in this case at Eosin Y (EO)  0.42 as reported in the literature(Wilkinson et al., 1993). The actinometer used is 9,10-dimethylanthracene (DMA). The kinetic measures of the actinometer consumption were compared in the presence of the reference photosensitizer and the coordination compound formed, such as explained in the equation 10:

$$\frac{(\phi_\Delta)_{complex}}{(\phi_\Delta)_{EO}} = \frac{k_{\exp complex}}{k_{\exp EO}} \textbf{ Eq 10}$$

In the development of the experiment, both photosensitizers must have a common absorbance zone. In the case of the targets, it was possible to evaluate that there are no interferences for the components of the mixtures which developed the photosensitizer-deactivator and coordination-deactivator compound.

### 4.3.4 Determination of complex formation and kinetics parameters

For the determination the Benesi-Hildebrand equation (Benesi & Hildebrand, 1949), which assumes that having high concentrations of one of the components of the binary mixture tends to predominate those species, dissolving the complex formed.

To demonstrate the possibility of quantifying with the formation of the mixture, the spectral scanning was initially performed in the range UV/VISIBLE. Later, binary mixtures were prepared with the pollutant (acting as scavenger), particularly Bisphenol A and Triclosan and the photosensitizer at fixed concentration (around 0.4 Absorbances), specifically eosin Y. However, with these values, it was possible to obtain $\Delta\varepsilon$, whichrepresents the change in value between $\varepsilon^{HG}$, and $\varepsilon^{G}$ can be derived from the intercept while a complexing constant ($K_a$) that can be calculated from the slope.

Finally, for the determination of the kinetic parameters, an analysis of the decay curves was carried out as the fixed concentration of the photosensitizer, actinometer and the contaminant. In the case of BPA, a system with DFBF/PNF and TCS the system was

DMA/EO, which were previously analyzed individually and mixed, the principle of analysis was that they did not exceed 0.4 Abs.

## 4.4 Result and Discussion

### 4.4.1 Calibration curves

For the analysis of quantum yields and photosensitizing properties of the complexes obtained, it is necessary to corroborate the molar extinction coefficients of all the components involved in the photosensitization reactions. The importance of using ethanol as a reference solvent is that, in this solvent, the half-life of the species is greater, so it is useful to perform the base trials using this solvent as a reference. In Figure 31 and 32 the linear range and the molar extinction coefficient of both pollutants is shown. Bisphenol A (BPA) has a reported molar extinction coefficient of 3.213 L cm$^{-1}$mol$^{-1}$(Maroto et al., 2011) and Triclosan (TCS) 4.700 L cm$^{-1}$mol$^{-1}$ (X. Yang et al., 2016). On the other hand, the standard photosensitizers that were Eosin Y (EO) $\varepsilon \sim 10^5$ (Kira et al., 2006)$^,$ shown in Figure 33. Perinaphtenone (PNF), shown in Figure 34; the trapped 1,3-diphenylisobenzofuran (DFIBF) 24.320 L cm$^{-1}$mol$^{-1}$, shown in Figure 35 (X. F. Zhang & Li, 2011) and 9,10-dimethylanthracene (DMA), shown in Figure 36 were finally checked.
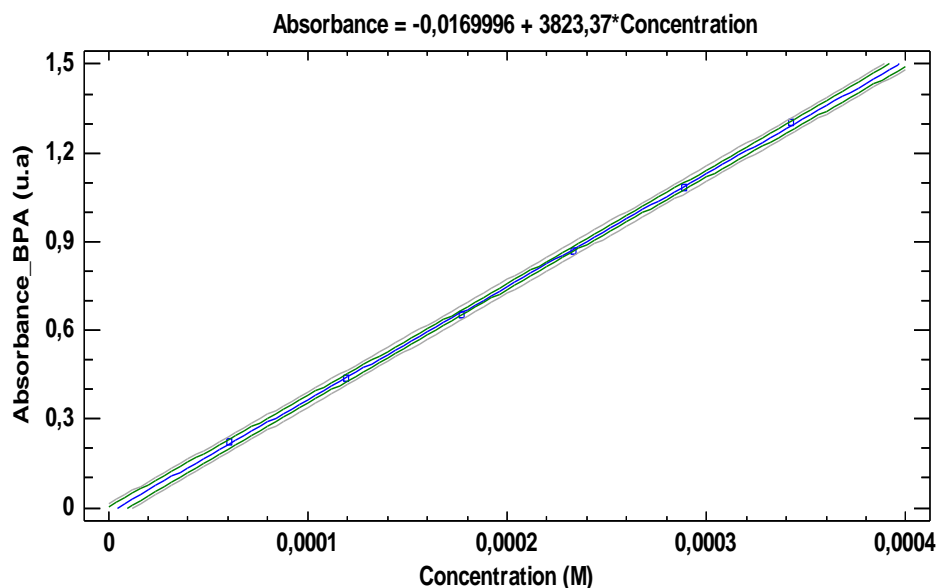


**Figure 31.** BPA calibration curve in UV-VIS Spectrophotometer. Taking a stock solution of [1003 mg/L]. Additions of 30 µL of the stock solution, working solvent: Ethanol.

**Absorbance2 = 0,0407097 + 4013,63*Concentration2**
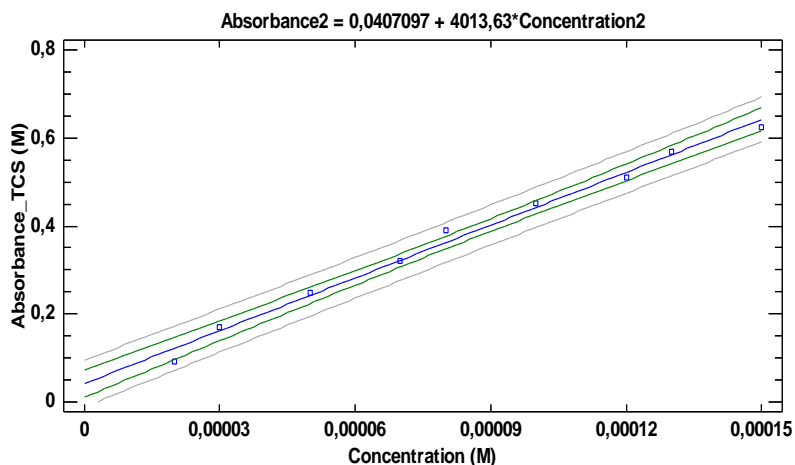


**Figure 32.** TCS calibration curve in UV-VIS Spectrophotometer. Taking a stock solution of [1050 mg/L]. Additions of 30 µL of the stock solution, working solvent: Ethanol.

**Absorbance EO = 0,0020789 + 110262*Concentration EO**
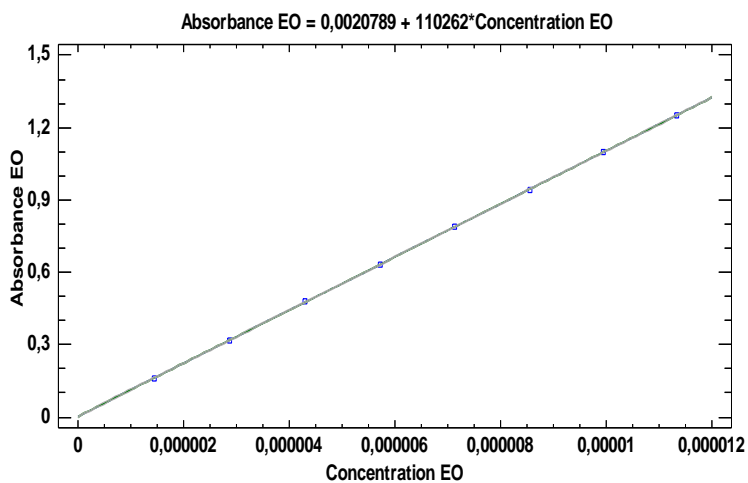


**Figure 33.** EO calibration curve in UV-VIS Spectrophotometer. Taking a stock solution of [540mg /L]. Additions of 5 µL of the stock solution, working solvent: Ethanol.

**Absorbance_PNF = -0,0000448509 + 14169,9*Concentration_PNF (M)**
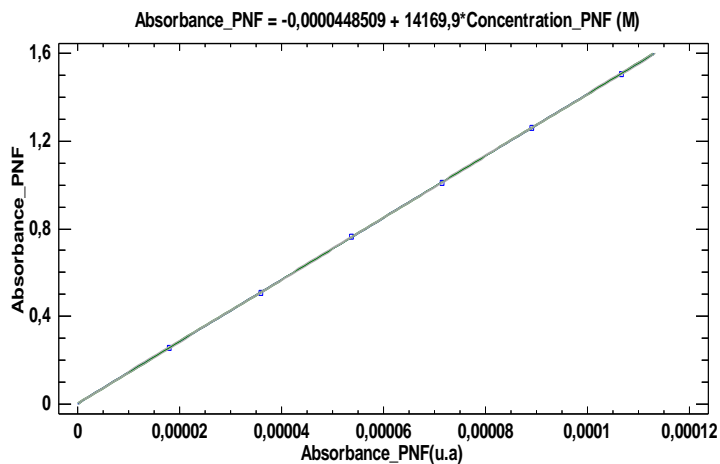


**Figure 34.** PNF calibration curve in UV-VIS spectrophotometer. Taking a stock solution of [1.3mg/L]. Additions of 5 µL of the stock solution, working solvent: Ethanol.

**Absorbance_DFIBF = -0,00234862 + 12945,5\*Concentration_DFIBF**
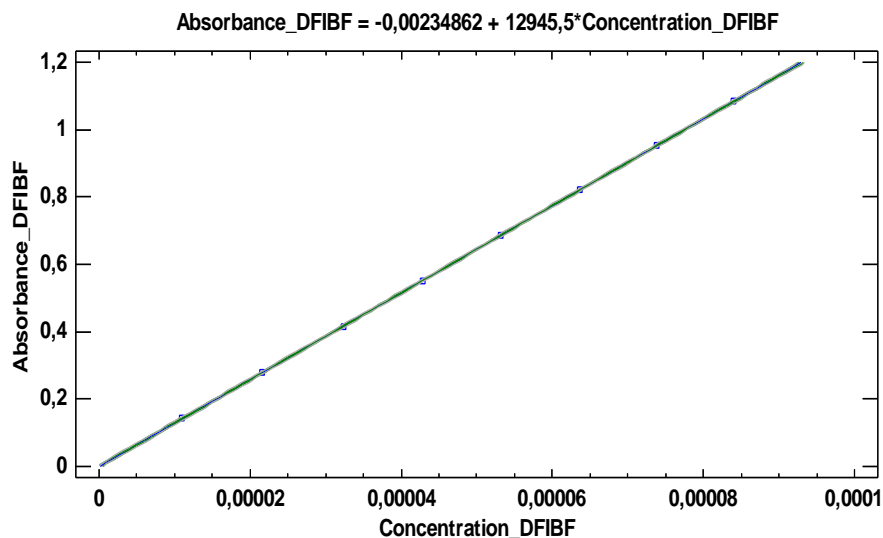
**Figure 35.** DFIBF calibration curve in UV-VIS Spectrophotometer. Taking a stock solution of [0.59mg/L]. Additions of 10 µL of the stock solution, working solvent: Ethanol.

**Absorbance_DMA = -0,00141983 + 12755\*Concentration_DMA**
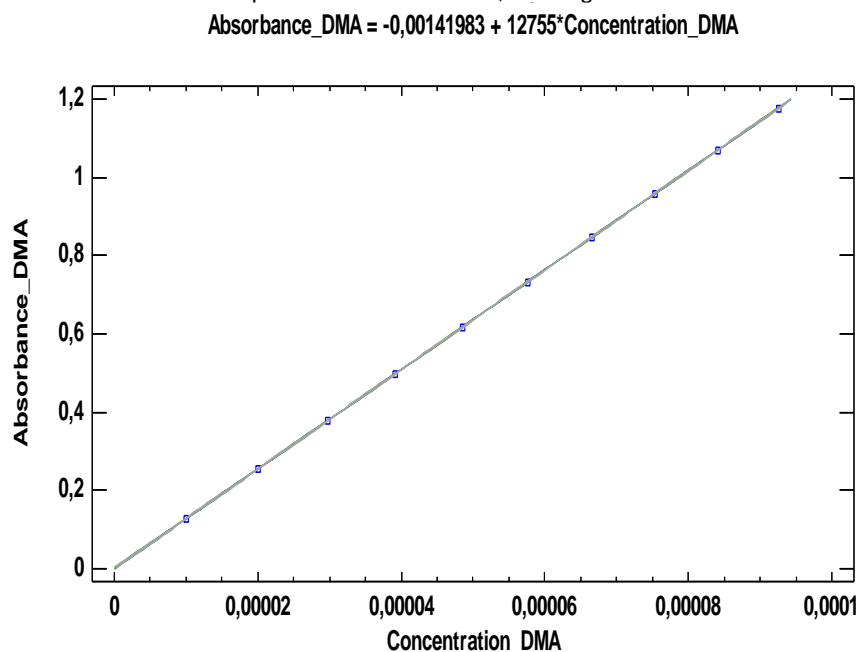
**Figure 36.** DMA calibration curve in UV-VIS Spectrophotometer. Taking a stock solution of [210 mg / L]. Additions of 10 µL of the stock solution, working solvent: Ethanol.

## 4.4.2 Complex Formation

Spectral scanning of the components was carried out individually using the working solvent, as shown in the Figure 37, with the purpose of knowing the range in which it is possible to check the actinometer without effects on the mixture, thus establishing where they absorb the compounds of interest (contaminant). In this analysis it was possible to determine that the BPA and the TCS absorb in the region that is between 270-280 nm; so, through this

technique it is required to make individual analyzes; in the case of PNF, it absorbs in the region of 360 nm; however, it has a small portion that adsorbs in the region of the pollutants; and for EO, which has a maximum wavelength at 527 nm, it presents a similar portion where adsorb the other photosensitizer. In addition, the DFIBF has appropriate characteristics as an actinometer, since when the species is present, their consumption predominates over other possible reactive oxygen species that are present in the reaction; however, it also has signals that may be overlapping with the rest of the compounds present in reaction, so it is decided to monitor the reactions in the region of ~ 420 nm to ensure that there is no interference with the rest of the signals associated with the presence of other compounds.

In addition, it is evident that there is formation of complexes in the region that ranges from 320-220 nm, since in that region EO has an absorption peak that is mixed with the maximum wavelength band of BPA, and the result shown in the Figure 38 and 39 in mixed with EO like standard photosensitizer, in this case, is not necessary to calculate the $K_a$ because the contribution is the smallest.
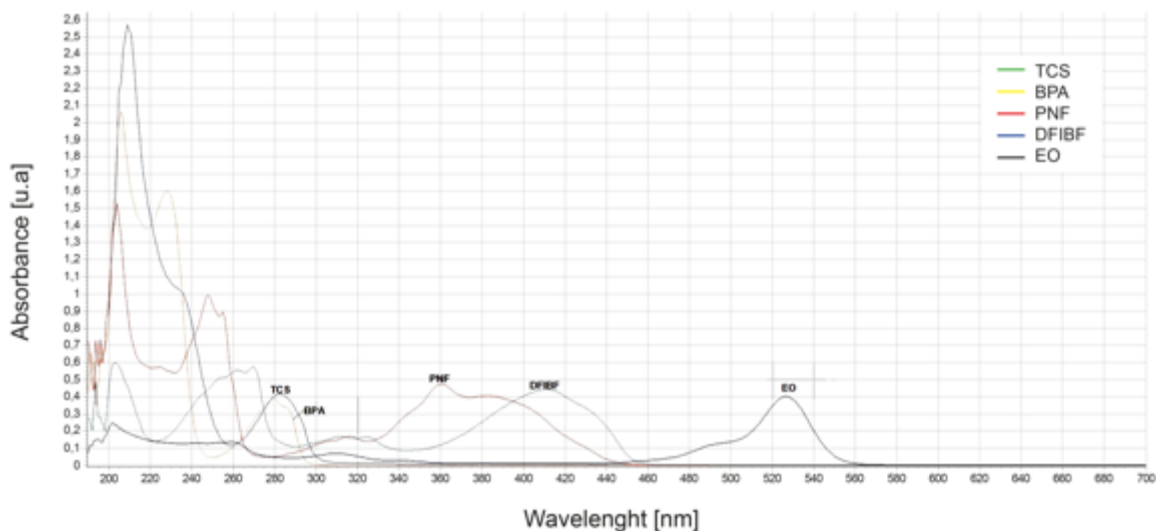


**Figure 37.** Spectral scanning of Bisphenol A (BPA), Triclosan (TCS), Eosin Y (EO), Phenalenone (PNF), 1,3-diphenyl isobenzofuran (DFIBF) ~ 0.4 Abs. Ethanol working solvent
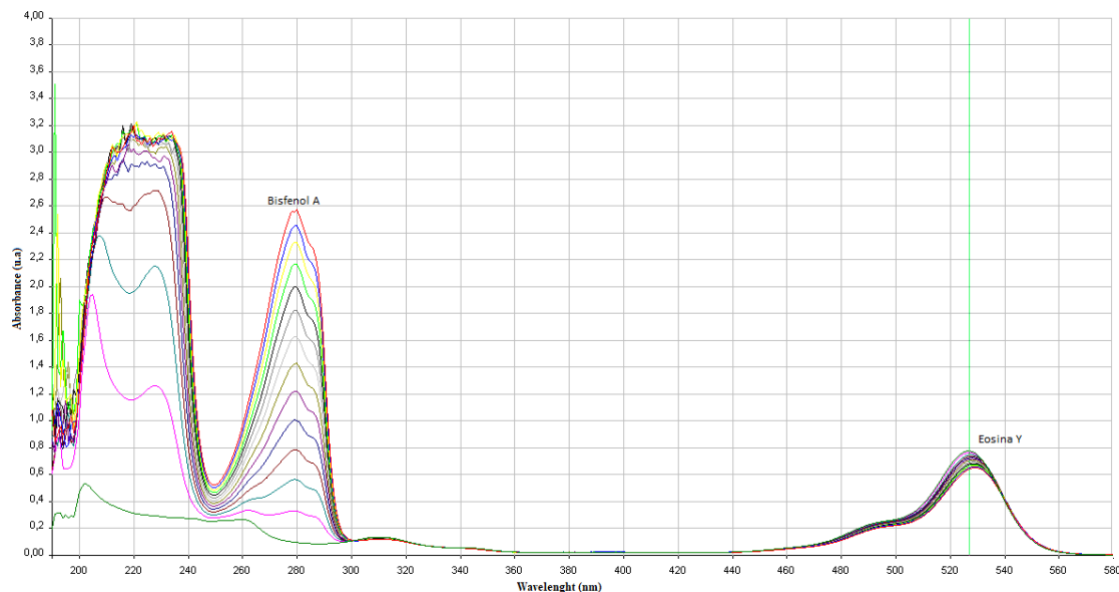
**Figure 38.** Complex formation between EO + BPA. Additions of BPA were 30µL of the stock solution of 1003ppm. Ethanol working solvent
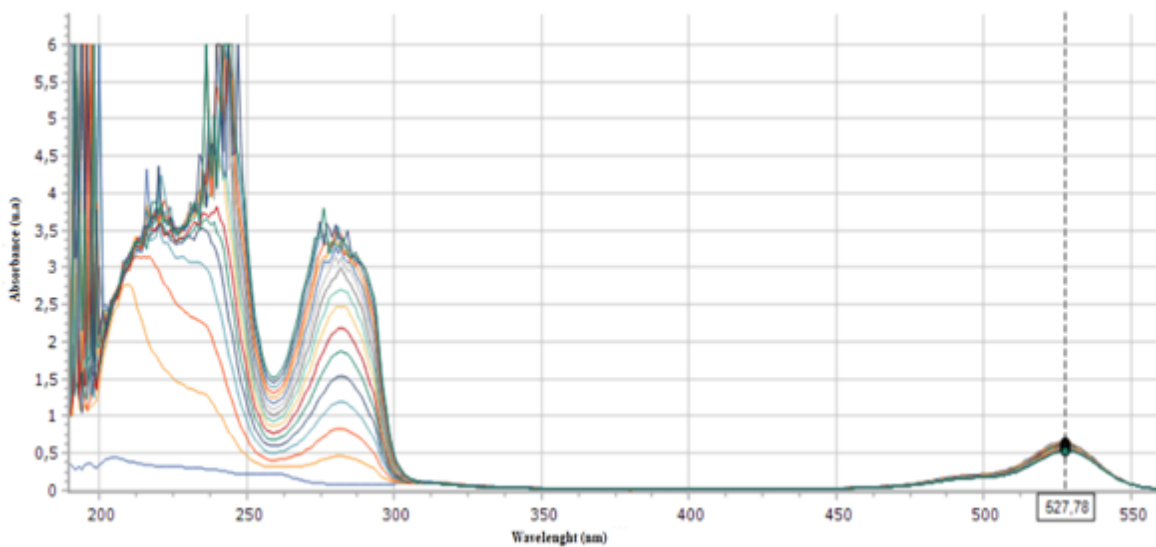


**Figure 39.** Complex formation between EO + TCS. The TCS additions were 30µL of the 1050ppm stock solution. Ethanol working solvent.

### 4.4.3 kinetics Parameters

For photodegradation experiments, the UV-Visible spectrophotometry technique was used, since it is the most versatile and economic photochemical reaction monitoring technique, and since the purpose of this first stage was to know some photosensitizing properties, such as the measure the concentration of the half-life of the species; for this, the behavior of the contaminants must be analyzed directly and with photosensitizers/standard actinometers that ensure a correct measurement and its effects.

In table 1, the direct consumption of every component that participates in the reaction in 10 minutes using UV Lamp with concentration between 0.4-0.6 Abs is shown. These results demonstrate that, for the BPA, TCS and PNF are not affected by the light. In the case of DFBF, it had a consumption of 9.4%, for this reason the suggested work times is less 10 minutes.

**Table 1.** Direct consumption of the components directly for the UV lamp

| Reactive | % consumption |
|---|---|
| BPA | 0.0 |
| TCS | 0.0 |
| DFIBF | 9.4 |
| DMA | 1.5 |
| PNF | 0.0 |
| EO | 2.1 |

Source: the author

Particularly, the DFIBF, even though it is not an actinometer exclusive to the specie however it has been widely used in the analysis of singlet molecular oxygen. In the Figure 40 and the Figure 41, shown the consumption of the actinometer with photosensitizer (blank) and the effect of the pollutant at different concentrations is shown.
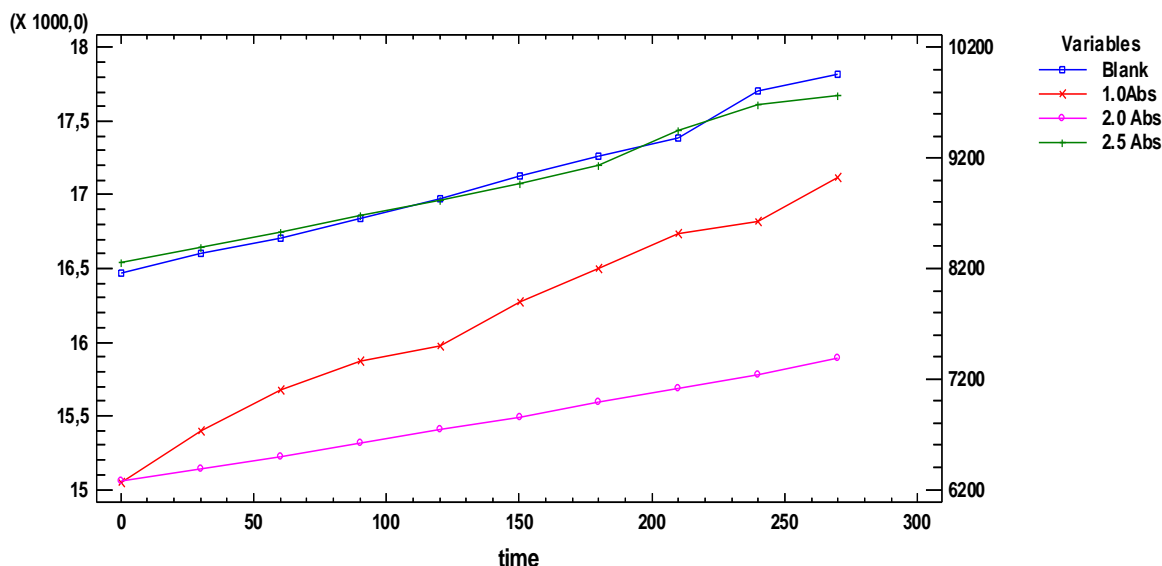


**Figure 40.** Curve the second order for BPA. Photosensitizer: PNF actinometer: DFIBF.
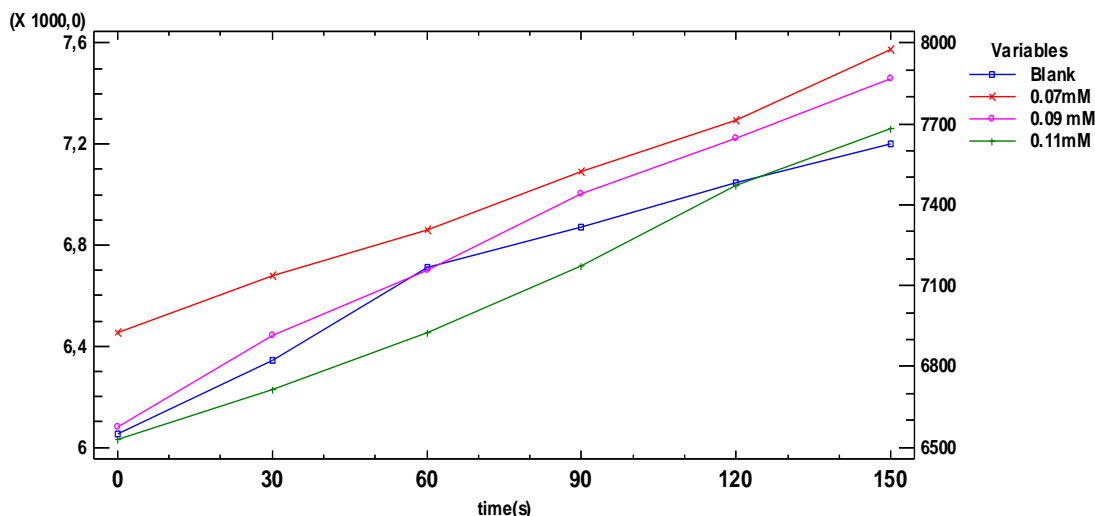
**Figure 41.** Curve the second order for TCS. Photosensitizer: EO actinometer: DMA.

The $R^2$ for all decay curves were between 0.9846 – 0.9907 for the BPA and in the case for the TCS this value is around 0.9906, which demonstrate that to be bimolecular reaction, the order in the second.

### 4.4.4 Quantum Yield of Synthesized Complexes

The selected monitoring zone was at 397 nm, the area where the DMA is absorbed (showed in Figure 42), the lamp used for the analysis was the Rayonet lamp with $U_{340}$ filter at distance of 2 cm in ethanol. The determinations were made in the Perkin Elmer lambda 35 spectrophotometer. The results obtained for the $MnCl_2\,(6OMeQ)_2$ complex were 0.672, which is consistent with other complexes synthesized with the same ligand which was 0.595 (Payán, 2015).
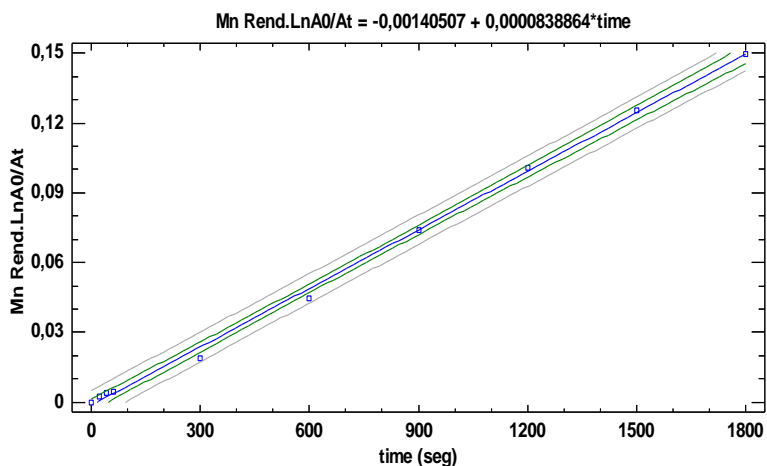


**Figure 42.** Ln Ao/A vs time (min) of DMA consumption, in the presence of the photosensitizer $MnCl_2\,(6OMeQ)_2$

In the case of the result obtained for the AuCl (6OMeQ)$_3$, acetonitrile was used (the reported quantum yield is 0.57) (Figure 43), due to the poor solubility of the complex arising from the presence of nanoparticles of gold, by-product of the synthesis reaction. It was carried out under the same conditions mentioned above, the Rayonet lamp with U$_{340}$ filter at distance of 2 cm, the result was 0.6 for the quantum field, if is probable that this result has an incongruence value, due to its poor solubility.

**Au Rend.LnA0/At = 0,0117415 + 0,000746723*Au Rend.time**
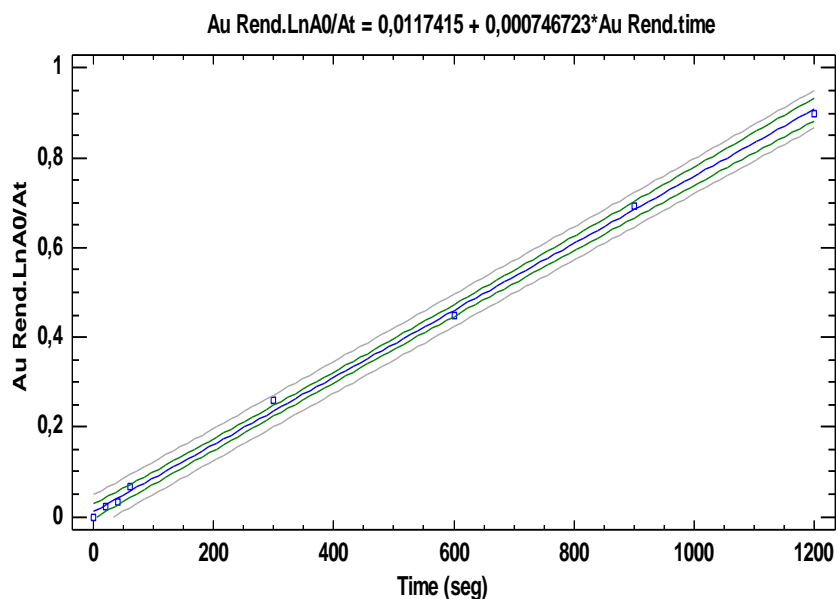


**Figure 43.** Ln Ao/A vs time (min) of DMA consumption, in the presence of the photosensitizer AuCl (6OMeQ)$_3$

## 5. Chapter 3: Parameters that Affecting the Photodegradation

### 5.1 Introduction for the Photodegradation

The emerging pollutant are defined as synthetic or natural chemical substances that are not commonly monitored in the environment but have the potential to enter the environment and cause known or suspected adverse effects for the environment and/or human health (Geissen et al., 2015). In some cases, the release of emerging contaminants to the environment that has been occurring for a long time may have not been identified until new detection methods were developed. In other cases, the synthesis of new chemicals or changes in the use and disposal of existing chemicals can create new sources of emerging pollutants.

There are different ways to classify the emerging compounds, among which the most prominent is associated with its relation with the application and with a possible emission source (Gil et al., 2012), among which pharmaceutical products for personal care, industrial additives, food additives and flame retardants stand out, among others.

In other studies, such as that presented by (Noguera-Oviedo & Aga, 2016), an association between emerging pollutants with wastes of anthropogenic and natural chemical products such as pharmaceutical products and personal care products and their metabolites, illicit drugs, the artificial nanomaterials, and antibiotic resistance genes is evidenced. Although there is a rapid progress in the instruments for its determination and quantification, there is a concern about the toxicity of these compounds, which includes its presence in the environment and the need to assess its ecological risks along with its original compounds. This leads to the need to innovate with new treatment methodologies in order not to favor degradation by-products, and instead, the total mineralization of these compounds.

This chapter deals with some general aspects about the study pollutants, subject to the study, experimental design, factorial design with points at the center, in order to establish the best operating conditions, at laboratory scale, for the photosensitized degradation of bisphenol A (BPA) and triclosan (TCS), for both photosensitizers: EO (standard) and $ZnCl_2(6OMeQ)_2$ (synthesized photosensitizer), the variables taken for the experimental design were chosen based on previous studies and supporting literature.

Later, for the optimization studies it was established that, at pH 5 and at 0.00104 mM photosensitizer concentration equivalents at 0.7Abs, 20% removals were obtained in the case of EO with BPA. Then, using the same photosensitizer, but with Triclosan, it was possible to establish photodegradation up to 56% at the same pH but at a temperature of $50^0C$, associating this result with the increase in temperature generated, and an increase in speed being reflected in the results obtained. Later, when analyzing the contaminants using the coordinated compound, BPA, a removal was obtained at pH 5.0, and at 0.00119 mM photosensitizer concentration, a 26.7 % photodegradation was obtained and, finally, at a temperature $50^0C$ and a pH 6, yielding a photodegradation percentage of 52.3%. It was not possible to establish mineralization through the methodology due to the complexity of the matrix having all the components of the reaction in a homogeneous system.

## 5.2. Conceptual Framework

### 5.2.1 Physicochemical properties of Bisphenol A and Triclosan

For BPA, the chemical name is 4,4-dihydroxy-2,2-diphenylpropane (Figure 44), it is widely used in the industry as an intermediate of polycarbonate and epoxy resins, flame retardants and, within its application as an end product, it is used in electrostatic paint, protective coatings, automotive lenses, GBZ protective window, compact discs, optical lenses and electronic parts encapsulation, among others (Staples et al., 1998).
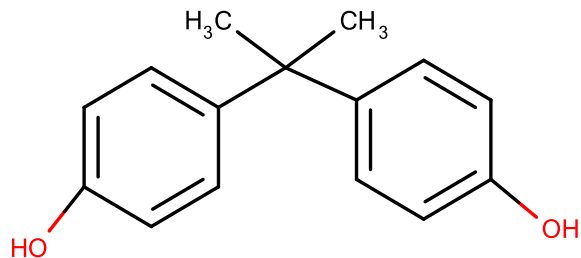
**Figure 44.** Chemical structure of BPA

Some properties are molar mass 228.291 g/mol, its formula is $C_{15}H_{16}O_2$, its composition is C (78.92%), H (7.06%), O (14.02%), its solubility in water is 0.150 mg/mL in any pH, the pKa is 9.78 and Polarizability 26.59 Å.

On the other hand, for the Triclosan, its chemical name is 5-chloro-2-(2,4-dichlorophenoxy) phenol (Figure 45), it is widely used as an antimicrobial agent, antibacterial agent, bactericide, disinfectant and fungicide, and it is found in hand soap, dish-washing products, laundry detergents and softeners, plastics (e.g., toys, cutting boards), toothpaste, pesticides (as an inert ingredient) among others (Hughes & Denver, 2006). Its molar mass is 289.54 g/mol, its composition is C (49.78%), H (2.44%), Cl (36.73%), O (11.05%), it has a low solubility in water (in pH between 1-10, it is zero) and its pKa is 7.68.
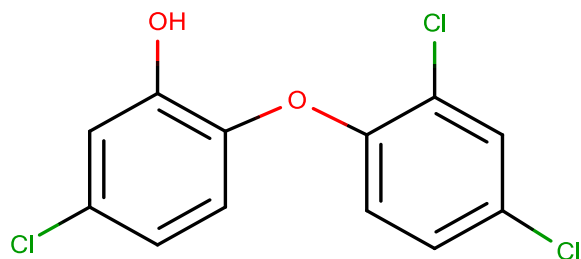


**Figure 45.** Chemical structure of triclosan

## 5.2.2 Bisphenol A and Triclosan behavior in the environment

There are several sources of entry of BPA into the environment, however, the most common way of entry are discharges such as surface waters and atmosphere, this situation probably occurs during the processing and handling of BPA during its manufacture and is shown in the Figure 46 (Michałowicz, 2014), in which the several inputs of this pollutant in the environment are explained. Another option is from the products that contain small amounts of unreacted BPA or that are converted to BPA under specific conditions (Staples et al., 1998); however, the degradation half-life of BPA in soils ranges from 1 to 10 days depending

on soil composition and temperature. For this reason, it is not considered a Persistent Organic Pollutant (POP), but its presence in sediments and urban ecosystems underlines the necessity to decrease both plastic pollution and BPA production consecutively (Legeay & Faure, 2017), the reason is because of their physicochemical properties and its capacity to adsorb into sediments and to accumulate in tissues subject to rapid metabolism (D. Chen et al., 2016); nevertheless, the BPA also shows estrogenicity and this situation is the most significant environmental problem. It has been mention in several research papers that the Bisphenol A has a weak toxicity to aquatic biota, for example, the $LC_{50}$ values are 1.1 mg/L for shrimp and 1.0 ± 3.1 mg/l for green algae (Yamamoto et al., 2001); however, the main problem is the effect in the environment, as small quantities may cause widespread effects.

In addition, when the triclosan is released into the environment, the compound may undergo photodegradation or biodegradation such as methyl triclosan (methylation), dioxins, chloroform, and other chlorinated compounds which are potentially more toxic. Recently, the methyl triclosan has been found in wastewater treatment and its lipophilicity increases, meaning that it will be more likely to bioaccumulate in fatty tissue and it is not likely to photodegrade (Hughes & Denver, 2006).



**Figure 46.** Environmental exposure of BPA. Source: Author

### 5.2.3 Toxicity of Bisphenol A and Triclosan in Living Beings

The concept **"endocrine disruptor"** was mentioned in the 1990s and is associated with the change in organs, reproductive toxicology, and the ecosystem (Colborn et al., 1993). Endocrine disrupting chemicals (EDCs) are defined as the natural and/or synthetic compounds that may affect endocrine systems of fishes and other aquatic animals. These compounds can generate a variety of adverse effects of EDCs on the endocrine systems. These effects may be cumulative, they may only appear in subsequent generations, and then the resulting effects may be irreversible. Mostly, the EDCs are some synthetic organic chemicals being introduced to the environment by anthropogenic activities, but they can also be naturally generated estrogenic hormones and therefore are ubiquitous in aquatic environments receiving wastewater effluents (Jiang et al., 2013).

According to previous studies, in the presence of BPA, the affections that are caused when encountering living beings become estrogenic, carcinogenic and anti-androgenic causing feminization of men as part of the side effects and it was also identified as an obesogenic alongside pesticides, heavy metals and polychlorinated biphenyl (PCBs) (Legeay & Faure, 2017). In the animals, BPA is transformed in vertebrates during oxidation (including hydroxylation) reactions. Those reactions are catalyzed by microsomal enzymes (monooxygenases) at presence of cytochrome $P_{450}$ (Michałowicz, 2014); lignolitic fungi have shown capability to degrade because they effectively utilize aromatic substrates of natural origin (including lignin and phenolics) (Loffredo et al.,2012). In the figure 47, postulated metabolic pathways leading to the production of a variety of metabolites from the transformation of the BPA is shown; however, if the substituent is salt or glucuronide, the possible by product will not have any problem, but in another situation, when the BPA suffers an oxidation or other carbon group is added, the estrogenic power increases (D. Chen et al., 2016).
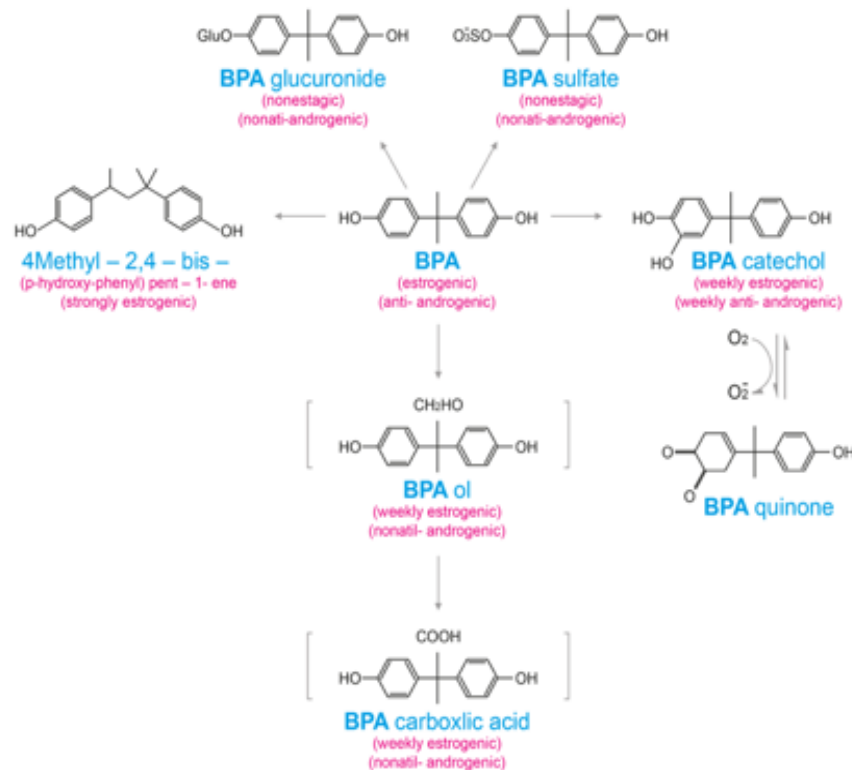
**Figure 47.** Postulated metabolic pathways leading to the production of a variety of metabolites in the BPA degradation. Source: (D. Chen et al., 2016)

On the other hand, the triclosan is highly toxic to some aquatic organisms, especially fish, and can bioaccumulate (Martínez-Zapata et al., 2013). In both cases, they are considered endocrine disruptors because of the damage they cause to living beings when they come into contact; they are also considered chemosensitizers, antineoplastic drugs, similar to the problems that organochlorine compounds show when entering into the environment (Daughton & Ternes, 1999)(Moldovan, 2006).

**5.2.4 Advanced Oxidation Processes (AOP) applied to the photodegradation of bisphenol A**

The Advanced oxidation processes-AOPs is based on the *in-situ* generation of strong oxidants for the oxidation of organic compounds. This includes processes based on hydroxyl radicals (•OH), which constitute the majority of available AOPs; but also, processes based on other oxidizing species. In advanced oxidation processes, reactive species such as the hydroxyl free radical, which oxidizes refractory organic pollutants at high reaction rates (Andreozzi, 1999). The combined processes of advanced oxidation with biological are reported as the combination of ozone with native strains of microorganisms present in active sludge have reached removals of 95 % emerging contaminants (Oller et al., 2011); however,

enzymatic induction is very sensitive to temperature, salinity, pH, oxygen concentration, redox potential, the concentration and nature of various substrates, nutrients and the presence of toxic substances.

Within the different studies carried out for its elimination, the ozonation method has been reported (Garoma & Matsumoto, 2009) (Deborde et al., 2008) although they present positive results, the issue of the formation of byproducts derived from degradation remains a subject of revision.

Research has also been conducted with Fenton (Poerschmann et al, 2010) and Photo Fenton (Katsumata, 2004),(Rodríguez et al., 2010), and it has reported a comparative study with the Fenton reagent and the $TiO_2$ doped with Fe (III), the latter showing the better performance. However, in some treatments, organic byproducts are produced. More sophisticated processes such as sonochemistry through ultrasound have been used, showing positive results in the degradation of BPA (Torres et al., 2007). Other studies have shown that the degradation efficiency of BPA using $\delta$- and $\alpha$-$MnO_2$ PHMSs was more than 90 % in the presence of ozone within 30 min reaction time. The probe tests for reactive oxidative species (ROSs) displayed that BPA degradation by catalytic ozonation is dominated by $^{\bullet}O_2^-$ and $^{\bullet}OH$ in our present study (Tan et al., 2017); it was also found that the BPA was mineralized within 60 min with a removal 97.6 % process under optimal conditions (Moussavi et al., 2018) and finally, the use of other products such as $\alpha$-$Fe_2O_3$ material it could be demonstrated that this material is efficient for the photocatalytic degradation of BPA with 91 % of BPA (30 mg/L) was degraded by using 1 g/L $\alpha$-$Fe_2O_3$ within 6 h under the simulated sunlight irradiation (Ye et al., 2019). The research evidences the relationship with the photodegradation using singlet molecular oxygen combination with solar energy employing a photosensitizing material consisting of tris(4,7-diphenyl-1,10-phenanthroline) ruthenium (II) chloride, immobilized in a porously (dimethyl siloxane) inert support. The results showed that, for the BPA, a conversion percentage of 80 % was presented in ultra-pure water (Díez-Mato et al., 2014), this result showed that technology is a proper strategy for the removal of this kind of pollutant.

### 5.2.5 Advanced Oxidation Processes (AOP) applied to the photodegradation of Triclosan

The triclosan degradation using photolysis has been reported in periods of 4 to 8 days, demonstrating that degradation is possible (Aranami & Readman, 2007); however, it has

also been demonstrated that photolysis degradation products are obtained with greater recalcitrance than triclosan, since cyclization occurs that produces greater stability (Latch et al.,2003). In the study reported by (Ying & Kookana, 2007), it was shown that, from active sludge, the degradation of triclosan is possible, obtaining removal percentages between 72% and 93%, however, and also the adsorption of these showed compounds in the sewage.  The batch experiments conducted on ultrapure and natural water showed that the TCS had a fast-paced oxidization (>90 % at ~5 min) (Rozas et al., 2017).

Finally, some studies have proven that the TCS is photodegraded for the singlet molecular oxygen, using Bismuth oxyhalides an outstanding visible-light driven semiconductor photocatalyst, the results showed that the singlet oxygen played critical part in the TCS degradation (Chang et al., 2019).

## 5.2.6 Persulfate like advances oxidation process

In the early 1940s, Lawrence J. Heidt conducted studies on the behavior of work and the effect of contact with light, this research with persulfate photolysis, where photochemical efficiency is presented at a wavelength of 254 nm, the six-dimensional formation of a mole of persulfate by Einstein absorbed, suggesting that the formation of the persulfate species is possible if it is irradiated at said wavelength (Heidt, 1942).

Subsequently, evidence was shown that potassium persulfate decomposes thermally in aqueous solutions by two reactions: asymmetrical rupture of the O-O bond to form two sulfate free radicals which disappear by reaction with water to liberate oxygen and an acid-catalyzed reaction involving the unsymmetrical rupture of the O-O bond of the $HS_2O_8^-$ ion to form sulfur tetroxide (Kolthoff & Miller, 1951).

The Peroxydisulfate or called persulfate has been subject to research for its ability to degrade recalcitrant organics compounds, its activation is possible by heat, transition metals, ultraviolet (UV) light at 254 nm forming the highly reactive sulfate radical with a potential redox ($E^o$= 2.60 V) and nonselective specie, a great reason for its use in an environmental remediation (Matzek & Carter, 2016).

There is some research that carried out on the removal of the BPA (at concentration of 0.22 mM) with ''electro/$Fe^{3+}$/peroxydisulfate'' process, wherein the effects of initial pH, electrolyte concentration, $Fe^{3+}$ concentration, peroxydisulfate (PDS) concentration and current density were studied. The significant finding was almost completely removed after 60 min reaction and a TOC removal efficiency of 94.3% was achieved when the reaction

time was extended to 120 min (Lin et al., 2013). Other study reported that it was generated by the activation of persulfate with ferrous ion for the removal of BPA (88µM) (X. Jiang et al., 2013), the important conclusion is the addition of $Fe^{2+}$ had a significant impact on BPA, a removal of 97% and the highest removal rate of TOC (85%) at 2 h. Finally, the thermally activated persulfate oxidation process to treat aqueous BPA solution was subject to research (Olmez-Hanci et al.,2013). The effect of temperature (40–70∘C), initial pH (3.0-11.0) and persulfate concentration (0–20 mM) at initial concentration of BPA (88 µM), the results were reflected in the acute toxicity with *Vibrio Fischer,* and indicated the inhibitory effect of 88 µM BPA solution originally, then the results showed 58 % removal, which increased to 84% after 30 min and decreased to 22% after 90 min hot persulfate treatment that could be attributed to the formation and subsequent disappearance of oxidation products.

On the other hand, the persulfate as oxidant has been used for the degradation of the triclosan. A research was conducted in which generating persulfate (PS) activated by transition metals ($Fe^{2+}$, $Co^{2+}$, $Cu^{2+}$ and $Ag^+$) was evaluated to destroy TCS, the results showed that the oxidants by themselves did not show any decomposition of TCS, while the reactivity of sulfate radicals generated from the oxidant/metal conjugations were highly effective in oxidizing and mineralizing TCS (Nfodzo & Choi, 2011). In their research, Gao et al. (2016) shown the TCS degradation to be pH dependent, in acidic conditions was beneficial but the performance was found under neutral condition (around pH 7); moreover, the initial concentration for both reactants was of 0.155 mM $K_2S_2O_8$ and TCS 0.031 mM with a molar ratio of 1:0.5 (TCS:PS), this relationship was obtained from the previous experiments where the initial concentration of TCS was considered a relevant variable. Other variables generated effects in the degradation process by temperature (40°C –70°C), using the initial concentration of TCS (50 ppm), the results shown an increase in the degradation when the PS doses increased (18.8 mM). Other finding was that at less than 20 °C, degradation of TCS (around 8%) was present in the following 360 minutes, and then, the reaction started (L. Chen et al., 2019).

## 5.3. Materials and Methods

### 5.3.1 Reagents and Equipment Used for Monitoring and Quantifying Emerging Contaminants

The reagents used for the execution of this objective were: BPA brand sigma Aldrich at 100% purity, triclosan Carlo Erba 100% purity. For the preparation of the buffer solutions,

the $NaH_2PO_4$ salts of the Sigma Aldrich brand were used at 99% purity, Sigma Aldrich $Na_2HPO_4$ at 99% purity; $Na_2CO_3$ Sigma Aldrich at 99% purity, $NaHCO_3$ Sigma Aldrich at 99% purity and KCl Sigma Aldrich at 99 % purity. Finally, for the persulfate test, $K_2S_2O_8$ salt was used at 99 % purity brand Sigma Aldrich.

In the case of the equipment used in the development of contaminant monitoring, the Perkin Elmer UV-Visible Spectrophotometry Lambda 35. Then, for the optimization results, an Agilent Technology HPLC high efficiency chromatography equipment was used by means of a gradient method using ACN: $H_2O$ at minute 0, 70:30; minute 1, 50:50; minute 2, 40:60; minute 4, 20:80; minute 8, 40:60; minute 9, 50:50; and minute 11-12, 70:30. The column used was a $C_{18}$ Zorbax 4.6 × 150 mm 35-micron column.

## 5.3.2 Experimental Design for Determination of Parameters for Singlet Molecular Oxygen ($^1O_2$) for Bisphenol A and Triclosan.

The initial concentration of the study pollutants and the reaction time were proposed as a constant (0.15 mM), since, in initial experiments, the effect of the initial concentration of the contaminant was no significant incidence (these conclusions derived of the parameters kinetics studied in the chapter 2). Another constant parameter is the time, because in the preliminary kinetics were demonstrated that at 14 minutes was enough time for the complete reaction.

For the screening a $2^k$ factorial design with two points in the center was used and all the experiments were by triplicate. In the table 2 shown in the studied range for the preliminary factors, with this range did the experimental design, is shown in table 2. For the response variable is called the percentage of photodegradation and it is expressed as:

$$\% \text{ Photodegradation:} \frac{C_i - C_f}{C_f} \times 100\% \quad \textbf{Eq 11}$$

Where $C_i$ is the initial concentration and $C_f$ is the final concentration. Subsequently, the results of the screening analysis evidenced that the levels of improvement were not sufficient, therefore, the optimization was required through the **Response Surface Method (RSM)** (H. Gutierrez & De la vara, 2012); The experimental design was developed using the statistical tools of **Statgraphics®** software. For the experiments, for the temperature was used the thermostatics bath with temperature control and the pH were prepared buffer acetate and phosphate respectively. The experimental assembly for irradiations is shown in the figure 28.

For the experiments with the standard photosensitizer was used the halogen lamp; in the case with the complex photosensitizer was used the UV Lamp, in both case without filter maintaining the same distance and height.

**Table 2.** Experimental design screened for the initial experiments

| Factors | Low level | High Level |
|---|---|---|
| Eosin Y concentration - standard photosensitizer (mM) | 0.0036(0.4 Abs) | 0.0054(0.6 Abs) |
| $ZnCl_2(6OMeQ)_2$ complex photosensitizer (mM) | 0.00059(0.4 Abs) | 0.00089(0.6 Abs) |
| Temperature (°C) | 25 | 40 |
| pH | 6 | 9 |

The working concentrations for the photosensitizers were different since it depended on the solubility in the solvent and that it was in a concentration range that was between 0.4-0.6 absorbance unity.

### 5.3.3 Experimental design of parameters for triclosan and bisphenol A persulfate A

For the experimental design of persulfate, it was assumed that the initial concentration was not a significant variable in the process, for this reason, it was used as comparation method and did not depend on the initial concentration(0,15mM) at the same time frame (14 minutes). The rest of the factors were selected for the several researches reported (Olmez-Hanci et al., 2013) (Matzek & Carter, 2016). In the Table 3 shows the study ranges for the three variables of interest, the pH values will be controlled with buffer solutions, lamp was germicidal.

For the screening a $2^k$ factorial design with two points in the center was used and all the experiments were by triplicate.

**Table 3.** Experimental design screened for the initial experiments

| Factors | Low level | High Level |
|---|---|---|
| Concentration $K_2S_2O_8$ (mM) | 5 | 20 |
| Temperature (°C) | 25 | 40 |
| pH | 6 | 9 |

### 5.3.4 Determination of Intermediate Products and Mineralization Of Bisphenol A and Triclosan

For the analysis of the BPA, SPE cartridges were used (Oasis HLB, 6 mL, 250 mg) pre-conditioned with 3 mL of methanol, 5 mL of ultrapure water and 2 mL of 0.1 N hydrochloric acid. Then, the sample was passed through the SPE cartridges at a flow rate of 5 mL/min. The elution of oxidation intermediates trapped in the SPE cartridges carried out twice with 2.5 mL acetonitrile. After pre-conditioning and before elution, the SPE cartridges were dried under vacuum for 15 min to ensure the total vaporization of water. The pH for the extraction

was set close to 2.0 to ensure that acidic intermediates were uncharged, and therefore could easily be absorbed on the material of SPE cartridges (Molkenthin et al., 2013).

For the triclosan, 100 mL of reaction suspensions were used. Then, the samples were adjusted to a pH value of about 2 with 1 M HCl and saturated with NaCl. Intermediate products were extracted by vigorous shaking with 3 × 10 mL dichloromethane. Each extract was passed through an anhydrous $Na_2SO_4$ column to remove water. The extract was concentrated under a gentle nitrogen stream and re-dissolved in 1 mL methanol. Each final extract was then filtered through a 0.22 μm nylon syringe filter, into a 2 mL amber glass vial which was kept at −20 °C until analysis (B. Yang et al., 2011). Finally, the GC chromatography was used for the analysis of these compounds.

For the analysis of TOC of the sample solution, it was measured with Teledyne tekmar Apollo 9000 with nondispersive infrared detector (NDIR). The detection limit of the instrument and the quantification limit is 1,0 mg C/L. These sample were analyzed in the GDCON Laboratory.

## 5.3. Results and Analysis

### 5.3.1 Experimental Design and Optimization for the Bisphenol A and Eosin Y

The following combination of experiments executed in the stipulated order were yielded, together with the results obtained in each combination of experiments, which are reported in Table 4, being the better results at pH 6, temperature 25°C and a photosensitizer concentration of 0.0036 mM (0.4 Abs).

**Table 4.** Screening design for eosin Y and BPA

| pH | mM Photosensitizers | Temperature (°C) | Phot. (%) | pH | mM Photosensitizers | Temperature (°C) | Phot. (%) |
|---|---|---|---|---|---|---|---|
| 9.0 | 0.4 | 40.0 | 0.0000 | 6.0 | 0.6 | 25.0 | 0.0000 |
| 6.0 | 0.4 | 25.0 | 3.2464 | 9.0 | 0.6 | 40.0 | 0.0000 |
| 6.0 | 0.4 | 40.0 | 0.0000 | 7.5 | 0.5 | 32.5 | 0.0000 |
| 9.0 | 0.4 | 25.0 | 0.0000 | 7.5 | 0.5 | 32.5 | 0.0000 |
| 9.0 | 0.6 | 25.0 | 3.0230 | 6.0 | 0.6 | 40.0 | 0.0000 |
| 6.0 | 0.6 | 25.0 | 0.0000 | 9.0 | 0.4 | 40.0 | 0.0000 |
| 9.0 | 0.6 | 40.0 | 0.0000 | 6.0 | 0.4 | 25.0 | 3.4131 |
| 7.5 | 0.5 | 32.5 | 0.0000 | 6.0 | 0.4 | 40.0 | 0.0000 |
| 7.5 | 0.5 | 32.5 | 0.0000 | 9.0 | 0.4 | 25.0 | 0.0000 |
| 6.0 | 0.6 | 40.0 | 0.0000 | 9.0 | 0.6 | 25.0 | 3.0549 |
| 9.0 | 0.4 | 40.0 | 0.0000 | 6.0 | 0.6 | 25.0 | 0.0000 |
| 6.0 | 0.4 | 25.0 | 3.9970 | 9.0 | 0.6 | 40.0 | 0.0000 |
| 6.0 | 0.4 | 40.0 | 0.0000 | 7.5 | 0.5 | 32.5 | 0.0000 |
| 9.0 | 0.4 | 25.0 | 3.2464 | 7.5 | 0.5 | 32.5 | 0.0000 |
| 9.0 | 0.6 | 25.0 | 0.0000 | 6.0 | 0.6 | 40.0 | 0.0000 |

**Constants:** irradiation time 840 sec; Initial concentration of the contaminant: 0.15mM. The pH values will be controlled with buffer solutions; Lamps: halogen

Later, in order to verify the statements made in the preliminary analysis claiming that the data had a normality and independence in the errors; that, in addition, the factorial model is suitable for the experiment; and also, to demonstrate that the variances are homogeneous with each other, the analysis was carried out of variance (ANOVA) supported by the statistical coefficient of determination ($R^2$), which are reported in table 6. The objective of this analysis is to compare the treatments in terms of their population means and their variances with respect at the equality of the treatments, therefore the fundamental hypothesis are shown in the equation 12 and equation 13 is to test when the $k$ treatments are compared:

$$H_0: \tau_1 = \tau_2 = \cdots = \tau_k = 0 \ \textbf{Eq 12}$$

$$H_A: \tau_i \neq 0 \text{ for some } i \ \textbf{Eq 13}$$

Where $\tau_i$ is the treatment effect $i$ on the response variable, If $H_0$ is accepted, it is confirmed that the effects on the response of the $k$ treatments are statistically null (equal to zero) and if $H_0$ is rejected, it is concluded that at least one effect is different from zero. Specifically, in the table 6 shown information about the effect of this experiment, for example, in the column of source is related with the factors that participated in the experiment: pH, temperature, photosensitizer concentration and its interactions, block indicate the error between the repetitions and finally, the errors are related with the effect the errors in the measurements.

Then, in the next column called **sum of squares**, which is a measurement of the total variability existent in the observations (sum of treatments squares + sum of error squares) that's mean measurements the difference between treatments. If there is a lot of variation between the observations of each treatment, then the sum of squares will tend to be large, in the specific case of table 6 and its results, the values are very small, except for the temperature and the interaction between the concentration of the photosensitizer and the pH.

Subsequently, it analyzed the **means square,** it is an estimate of the source of variability, in which the mean square of treatments and the mean square of the error are related. Specifically, in this value it is appreciated, that if $H_0$ is true, both values that make up the mean squares estimate the variance, these values should be in coherence with the sum of squares. Based on these results obtained where it is known that the sum of squares of the error and the sum of squares of the treatment are independent variables, the $F_0$ statistic is constructed following an F distribution; if the $F_0$ is small, $H_0$ is accepted, thus for a level 95%

significance. Table 5 shows the result in the p-value where $p(F > F_0)$, as the significance value is less than 0.05, $H_0$ is rejected for the temperature variables and the relationship between the concentration of the photosensitizer (p-value: 0.0002), and the temperature (p-value: 0.0002), so it is accepted that at least for these mentioned variables participate in the photodegradation process. In the case of the statistics, it is evidenced that the $R^2$ was 62.18%, which suggests the need to perform a second optimization phase.

**Table 5.** ANOVA of design for Eosin Y and BPA

| Source | sum of squares | DF | mean square | F-reason | p-value |
|---|---|---|---|---|---|
| A: pH | 0.0555 | 1 | 0.0555 | 0.06 | 0.8061 |
| B: temperature | 16.9317 | 1 | 16.9317 | 18.79 | 0.0002 |
| C: Photosensitizer | 0.0555 | 1 | 0.0555 | 0.06 | 0.8061 |
| AB | 0.0555 | 1 | 0.0555 | 0.06 | 0.8061 |
| AC | 16.9317 | 1 | 16.9317 | 18.79 | 0.0002 |
| BC | 0.0555 | 1 | 0.0555 | 0.06 | 0.8061 |
| block | 20.7281 | 1 | 0.9012 | | |
| Total error | 54.8137 | 23 | | | |
| Total (corr.) | 0.0555 | 29 | | | |

**R-square** = 62.18 percent

In chemical terms, it is possible that the temperature effect is due to the photobleaching of eosin Y (from 36 ⁰C) and this directly affects the efficiency of the reaction (Herculano et al., 2013). Other effect is between pH and concentration of the photosensitizer, which is positive for this kind of reactions, because initially, in acidic pH, the photosensitizer maintains the same microspecies in an environment rich in the radical species it favors the photosensitized reaction. This result is consistent with In the Pareto diagram and analysis of main effects shown in the figure 48 and 49.
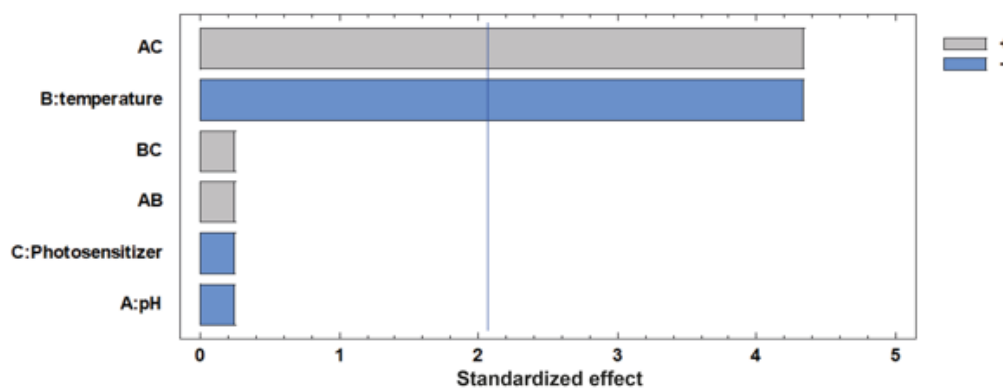


**Figure 48.** Pareto diagram of the process of photodegradation of BPA with Eosin Y photosensitizer
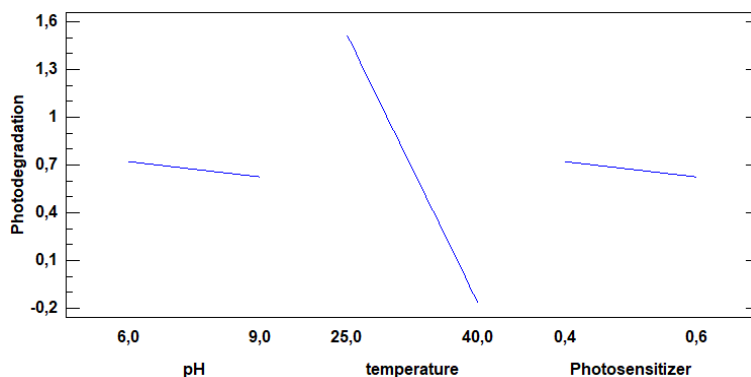
**Figure 49.** Graph of main effects in the process of photodegradation of BPA with Eosin Y as a Photosensitizer

Specifically, the optimization Response Surface Method (RSM) was used to find the combination of levels in the factors that show the optimum value on the response or the optimum direction of the movement in that is possible to experiment in the future. If the model does not explain the 70% minimal of the behavior of the model us not correct the optimization(Gutierrez & De la vara, 2012). The proposal of this research is to explore treatments may be localized over direction to maximum response from the initial design.

Then, based on the screening results as a reference, the decision was made to decrease by establishing for the pH range to (5 –6) in order to be consistent with natural water conditions. In the case of the concentration of the photosensitizer, a new range of concentration was established that maintained linear behavior 0.6-0.8 Abs equivalents (0.0054mM-0.0072mM) at constant temperature (25°C). In the table 6 shown the optimization result for the Eosin Y and Bisphenol A is shown.

**Table 6.** Response Surface Method (RSM) for Eosin Y and BPA

| pH | Abs Photosensitizers | (%) Phot. | pH | Abs Photosensitizers | (%) Phot. |
|---|---|---|---|---|---|
| 5.0 | 0.8 | 20.6392 | 5.5 | 0.8 | 15.0059 |
| 6.0 | 0.7 | 13.0493 | 5.0 | 0.6 | 17.0172 |
| 5.5 | 0.7 | 9.4816 | 6.0 | 0.6 | 15.5365 |
| 5.5 | 0.7 | 9.5264 | 5.0 | 0.7 | 20.5420 |
| 5.5 | 0.6 | 17.1983 | 6.0 | 0.6 | 15.1378 |
| 5.5 | 0.7 | 9.5128 | 5.5 | 0.7 | 9.9587 |
| 5.0 | 0.8 | 19.3827 | 5.5 | 0.8 | 15.8305 |
| 5.0 | 0.7 | 20.3510 | 6.0 | 0.7 | 13.6547 |

Lamp: halogen, distance 7 cm height 21.5 cm, fixed variable: 0.6 ppm BPA and temp: 25°C as constant

**Table 7.** ANOVA of Optimization design for Eosin Y and BPA

| Source | sum of squares | DF | mean square | F-reason | P- value |
|---|---|---|---|---|---|
| A: pH | 30.6097 | 1 | 30.6097 | 4.76 | 0.0569 |
| B: photosensitizer | 7.82449 | 1 | 7.82449 | 1.22 | 0.2984 |
| AA | 92.3998 | 1 | 92.3998 | 14.38 | 0.0043 |
| AB | 3.4416 | 1 | 3.4416 | 0.54 | 0.4829 |
| BB | 46.3638 | 1 | 46.3638 | 7.22 | 0.0249 |

| | | | | | |
|---|---|---|---|---|---|
| block | 1.39249 | 1 | 1.39249 | 0.22 | 0.6526 |
| Total error | 57.8246 | 9 | 6.42496 | | |
| Total (corr.) | 241.4280 | 15 | | | |

**R-square** = 76.05 percent

Statistically, the ANOVA shown in the table 7 was carried out, and based on the results, the variability in the photodegradation process could be established. After reviewing the result of the $R^2$ is 76.05%, it is concluded that the optimization can be considered better explaining the process of the photodegradation. It's possible to obtained better removal with pHs lower but the majorly the natural water doesn't have a pH so low. However, the R-Square is better than the screening experiments ($R^2$: 62%). In addition, chemically, the photodegradation process are better at more acidic pH the chemistry structure having two OH groups (conferring greater acidity) and being protonated are more susceptible to being oxidized(Alnaizy & Akgerman, 2000).Other potential reason was explained with the high concentration about of an environment rich in the radical species which favors the photosensitized reaction.

The Eq 14 that explains the optimization of the model is: $Removal_{279}$= 866.791 – 235.285*pH – 577.277*Photosensitizer + 19.9358*pH^2 + 17.4232*pH*Photosensitizer + 351.193*Photosensitizer^2. This result was shown in the figure 50.



**Figure 50.** Response surface estimated of the optimized model of Eosin Y – BPA

## 5.3.2 Experimental design and optimization for the Triclosan and Eosin Y

For the screening experiments for the triclosan and Eosin Y were used the same variables which in the methodology were used. The results were shown in the table 8. Initially, at pH 6

and 25°C, a degradation percentage of around 8.6% was obtained, preliminary, and judging by the results obtained, it could be evidenced that the concentration of photosensitizer is not a significant variable in the process, since the same results were obtained at both high and low concentrations of photosensitizer.

**Table 8.** screening design for Eosin Y and Triclosan

| pH | Abs Photosensitizers | (°C) Temperature | (%) Phot. | pH | Abs Photosensitizers | (°C) Temperature | (%) Phot. |
|---|---|---|---|---|---|---|---|
| 9.0 | 0.4 | 40.0 | 0.0000 | 6.0 | 0.6 | 25.0 | 8,6706 |
| 6.0 | 0.4 | 25.0 | 8.4214 | 9.0 | 0.6 | 40.0 | 0.0000 |
| 6.0 | 0.4 | 40.0 | 0.0000 | 7.5 | 0.5 | 32.5 | 0.0000 |
| 9.0 | 0.4 | 25.0 | 0.0000 | 7.5 | 0.5 | 32.5 | 0.0000 |
| 9.0 | 0.6 | 25.0 | 0.0000 | 6.0 | 0.6 | 40.0 | 0.0000 |
| 6.0 | 0.6 | 25.0 | 8.5341 | 9.0 | 0.4 | 40.0 | 0.0000 |
| 9.0 | 0.6 | 40.0 | 0.0000 | 6.0 | 0.4 | 25.0 | 8,5803 |
| 7.5 | 0.5 | 32.5 | 0.0000 | 6.0 | 0.4 | 40.0 | 0.0000 |
| 7.5 | 0.5 | 32.5 | 0.0000 | 9.0 | 0.4 | 25.0 | 0.0000 |
| 6.0 | 0.6 | 40.0 | 0.0000 | 9.0 | 0.6 | 25.0 | 0.0000 |
| 9.0 | 0.4 | 40.0 | 0.0000 | 6.0 | 0.6 | 25.0 | 8,6409 |
| 6.0 | 0.4 | 25.0 | 8.6880 | 9.0 | 0.6 | 40.0 | 0.0000 |
| 6.0 | 0.4 | 40.0 | 0.1907 | 7.5 | 0.5 | 32.5 | 0.0000 |
| 9.0 | 0.4 | 25.0 | 0.0000 | 7.5 | 0.5 | 32.5 | 0.0000 |
| 9.0 | 0.6 | 25.0 | 0.0000 | 6.0 | 0.6 | 40.0 | 0.0000 |

**Constants:** irradiation time 840 sec; Initial concentration of the contaminant: 0.15mM. The pH values will be controlled with buffer solutions; Lamps: halogen

**Table 9.** ANOVA of design for Eosin Y and Triclosan

| Source | sum of squares | DF | mean square | F-reason | P- value |
|---|---|---|---|---|---|
| A: pH | 111.4820 | 1 | 111.4820 | 104.73 | 0.0000 |
| B: Photosensitizer | 0.0000 | 1 | 0.0000 | 0.00 | 0.9946 |
| C: temperature | 109.8440 | 1 | 109.844 | 103.19 | 0.0000 |
| AB | 0.0000 | 1 | 0.0000 | 0.00 | 0.9946 |
| AC | 109.8440 | 1 | 109.844 | 103.19 | 0.0000 |
| BC | 0.0050 | 1 | 0.0050 | 0.00 | 0.9460 |
| block | 0.0176 | 2 | 0.0089 | 0.01 | 0.9917 |
| Total error | 22.3543 | 21 | 1.0644 | | |
| Total (corr.) | 353.5480 | 29 | | | |

R-square = 93.68 percent
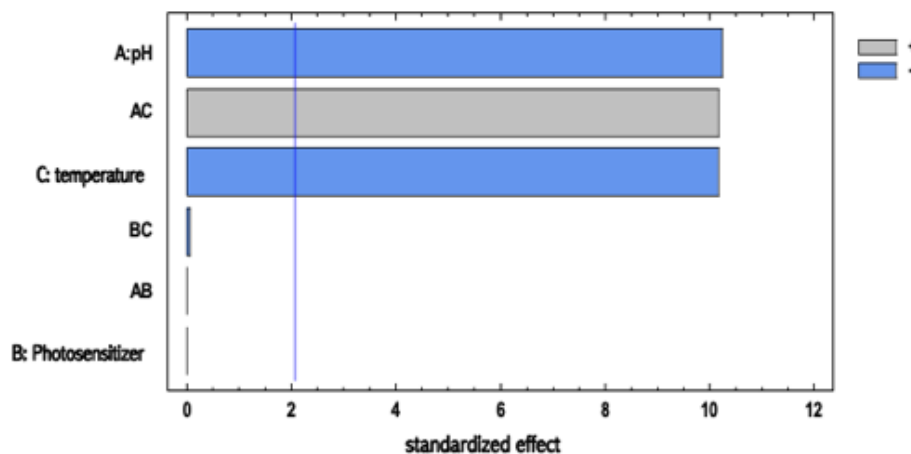
**Figure 51.** Pareto diagram of the photodegradation process of Triclosan with Eosin Y as a photosensitizer
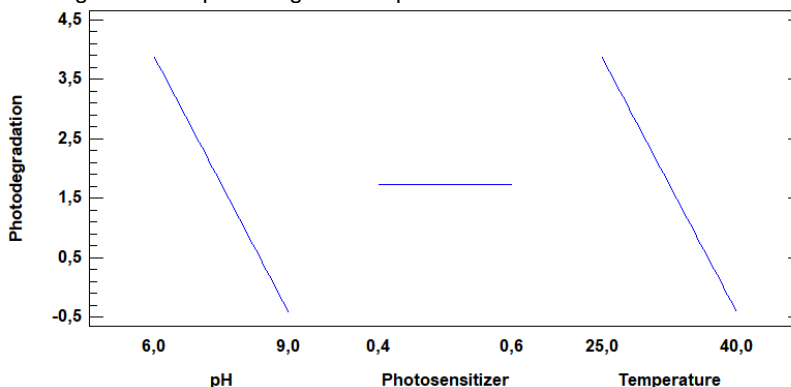


**Figure 52.** Graph of main effects in the photodegradation process of Triclosan with Eosin Y as a Photosensitizer

In the case of the analysis for triclosan with Eosin Y in the photodegradation process, the pH and temperature variables had a negative effect, but their interaction was positive for the experiments, this result indicated that modifying these variables may yield better results, which is shown in Figures 51 and 52.

From the chemical point of view, the chemistry structure has only one OH group and one chloride group, which provides acidity; therefore, the acidic medium allows the subsequent reactions and, with respect to the temperature, it promotes the OH-initiated transformation of TCS. However, this slight increase in the temperature constant rate implies that the reaction was actually dependent on diffusion-controlled processes and independent of chemical reaction-controlled processes (Y. Gao et al., 2014). Also, the statistics of the test were of 93.68% of the variability, with 95% reliability, shown in Table 9. This result does explain the photodegradation.

Although it is possible to think that the best option for the optimization is the decrease of temperature, the interaction of both variables has a major influence. So, in this research the increase of temperature and decrease of pH was proposed as a strategy to know the characteristics of the reaction that occurred. Table 11 shows the results about the photodegradation.

For this reason, a new range of pH and temperature values was taken, considering the bibliographic references (Gallard & von Gunten, 2002; Rule et al., 2005), in the case of the pH of 5 to 6 and a temperature between 40 ºC-50 ºC; in the case of the photosensitizer, the concentration was constant, because in the screening it could be established that it was not significant in the experiment.

The results of the photodegradation process are shown in Table 10, in which it was found that at pH 5 and a temperature of 50°C, it was possible to degrade up to 56%, which is an excellent result considering that, when developing experiments in homogeneous systems, photobleaching is a significant (Herculano et al., 2013).However, it is important to note that the high percentages are not necessarily associated with the oxidation of triclosan, these high temperatures may have favored other reaction routes, and consequently the degradation percentages are higher.

**Table 10.** Response Surface Method (RSM) design for Eosin Y and Triclosan

| pH | Temperature (°C) | (%) Phot. | pH | Temperature (°C) | (%) Phot. |
|----|------------------|-----------|----|------------------|-----------|
| 5.5 | 45.00 | 20.6674 | 5.5 | 50.00 | 24.9648 |
| 5.5 | 45.00 | 20.2213 | 5.0 | 50.00 | 56.9027 |
| 5.5 | 45.00 | 20.8917 | 6.0 | 40.00 | 0.0000 |
| 6.0 | 50.00 | 17.6039 | 5.0 | 40.00 | 16.5709 |
| 5.0 | 45.00 | 34.3153 | 6.0 | 40.00 | 0.0000 |
| 5.5 | 40.00 | 0.0000 | 5.0 | 50.00 | 56.9320 |
| 5.0 | 40.00 | 16.1376 | 6.0 | 50.00 | 9.1968 |
| 6.0 | 45.00 | 9.1819 | 5.0 | 45.00 | 20.1871 |

Lamp: halogen, distance 7 cm  height 21.5 cm, constant:0.6 ppm TCS Photosensitizer conc.  ~ 0.0054 mM

**Table 11.** ANOVA of Optimization design for Eosin Y and Triclosan

| Source | sum of squares | DF | mean square | F-reason | P- value |
|--------|----------------|----|-------------|----------|----------|
| A: pH | 1690.03 | 1 | 1690.03 | 31.06 | 0.0003 |
| B: temperature | 1746.28 | 1 | 1746.28 | 32.09 | 0.0003 |
| AA | 3.06672 | 1 | 93.074 | 0.06 | 0.8177 |
| AB | 269.323 | 1 | 223.65 | 4.95 | 0.0532 |
| BB | 34.421 | 1 | 26.3071 | 0.63 | 0.4469 |
| block | 2.11503 | 1 | 2.34507 | 0.04 | 0.8481 |
| Total error | 489.755 | 9 | 7.48386 | | |
| Total (corr.) | 4305.99 | 15 | | | |

R-square = 88.63 percent

According to the ANOVA of the optimization process reported in Table 11, it is evident that the two variables taken in the optimization were highly significant the pH and temperature, with $R^2$ of 88.63% in comparation with the screening results, this vale is lower. Therefore, as a recommendation for other investigations, it is suggested to lower the pH values even more in order to obtain a higher value in the percentage of photodegradation.

The surface design obtained is shown in Figure 53 which is explained with the Eq 15: $Removal_{283} = 145.961 + 35.7465*pH + 3.4238*temperature + 3.9493*pH^2 - 2.3209*pH*temperature + 0.1323*temperature^2$.
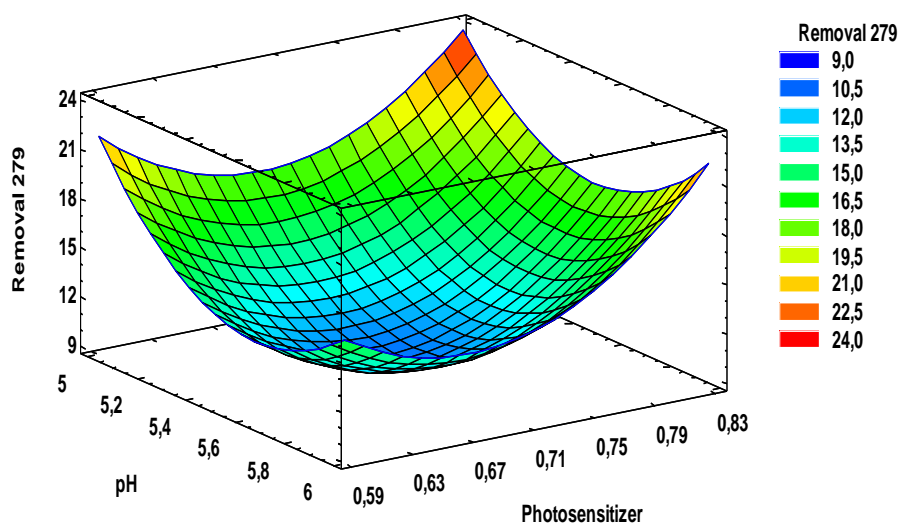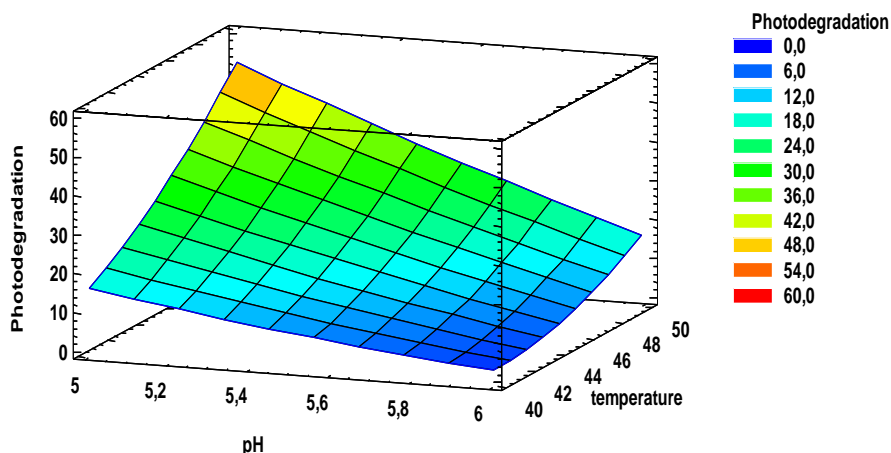
**Figure 53.** Response surface estimated of the optimized model of Eosin Y – Triclosan

### 5.3.3 Experimental Design and Optimization for the Bisphenol A and ZnCl$_2$(6OMeQ)$_2$

For the photodegradation process using coordination compounds, it was not possible to use the synthetized compounds because the synthetized reaction, its optimization and subsequent characterization were very late experimentally. This situation could be delaying the results of the research. Thus, a complex characterization by the GIAFOT group was performed and chosen, which is known for its crystalline structure and great benefits in terms of quantum yield and low costs for obtaining it, specifically the complex of Zinc (ZnC$_{20}$Cl$_2$N$_2$O$_2$H$_{18}$) and from now on ZnCl$_2$(6OMeQ)$_2$ will be noted (Villa-Pérez et al., 2018b). However, this compound was synthetized based on the reported methodology for the research papers.

The parameters of analysis were reported in the methodology, in the table 12 shown the results for all screening experiments, it is evidenced that at higher temperatures ($\sim$40°C) and at a high concentration of the photosensitizer was 0.0089mM (0.6 Abs).

**Table 12.** Screening design for ZnCl$_2$(6OMeQ)$_2$ and BPA

| pH | mM Photosensitizers | (°C) Temperature | Phot. (%) | pH | mM Photosensitizers | (°C) Temperature | (%) Phot. |
|-----|-----|------|--------|-----|-----|------|---------|
| 9.0 | 0.4 | 40.0 | 0.0000 | 6.0 | 0.6 | 25.0 | 0.0000 |
| 6.0 | 0.4 | 25.0 | 0.0000 | 9.0 | 0.6 | 40.0 | 0.0000 |
| 6.0 | 0.4 | 40.0 | 0.0000 | 7.5 | 0.5 | 32.5 | 0.0000 |
| 9.0 | 0.4 | 25.0 | 3.2005 | 7.5 | 0.5 | 32.5 | 0.0000 |
| 9.0 | 0.6 | 25.0 | 0.0000 | 6.0 | 0.6 | 40.0 | 15.1808 |
| 6.0 | 0.6 | 25.0 | 0.0000 | 9.0 | 0.4 | 40.0 | 0.0000 |
| 9.0 | 0.6 | 40.0 | 0.0000 | 6.0 | 0.4 | 25.0 | 0.0000 |
| 7.5 | 0.5 | 32.5 | 0.0000 | 6.0 | 0.4 | 40.0 | 0.0000 |
| 7.5 | 0.5 | 32.5 | 0.0000 | 9.0 | 0.4 | 25.0 | 3.1956 |
| 6.0 | 0.6 | 40.0 | 15.5775 | 9.0 | 0.6 | 25.0 | 0.0000 |
| 9.0 | 0.4 | 40.0 | 0.0000 | 6.0 | 0.6 | 25.0 | 0.0000 |
| 6.0 | 0.4 | 25.0 | 0.0000 | 9.0 | 0.6 | 40.0 | 0.0000 |
| 6.0 | 0.4 | 40.0 | 0.0000 | 7.5 | 0.5 | 32.5 | 0.0000 |
| 9.0 | 0.4 | 25.0 | 3.2392 | 7.5 | 0.5 | 32.5 | 0.0000 |

| 9.0 | 0.6 | 25.0 | 0.0000 | 6.0 | 0.6 | 40.0 | 15.4302 |

**Constants:** irradiation time 840 sec; Initial concentration of the contaminant: 0.15 mM. The pH values will be controlled with buffer solutions; Lamps: UV

The table 13 shows the ANOVA test, where the variable for pH, temperature and concentration of the photosensitize and its interactions, have a high level of significance reflected in the results of the p-values. When analyzing the $R^2$ statistic, it is evident that it represents 87% of the variability of the experiment, which can be refined with an optimization method.

As explained in previous experiments, Bisphenol A by having two OH groups in the structure can favor oxidation reactions thanks to the effects of protonation, therefore, at acidic pH the reactions are favored (Gerdes et al., 1997)(Alnaizy & Akgerman, 2000). Secondly, with regard to the concentration of the photosensitizer, as there is an environment rich in this compound, it can favor the yields obtained; finally with respect to the temperature, due to the characteristics of the reaction and taking into account that at this temperature, the compound does not suffer any affectation, it may be that it is an endothermic reaction, that is to say, that having a medium with saturation of the species radical, the temperature increases this speed, but not significantly so that it avoids the ISC favoring the photodegradation reaction, these results are shown in  Figure 54 and 55.

**Table 13.** ANOVA of design for $ZnCl_2(6OMeQ)_2$ and BPA

| Source | sum of squares | DF | mean square | F-reason | P- value |
|---|---|---|---|---|---|
| A: pH | 55.6724 | 1 | 55.6724 | 14.31 | 0.0011 |
| B: Photosensitizer | 55.6724 | 1 | 55.6724 | 14.31 | 0.0011 |
| C: temperature | 55.6724 | 1 | 55.6724 | 14.31 | 0.0011 |
| AB | 129.846 | 1 | 129.846 | 33.37 | 00000 |
| AC | 129.846 | 1 | 129.846 | 33.37 | 0.0000 |
| BC | 129.846 | 1 | 129.846 | 33.37 | 0.0000 |
| block | 0.00646 | 2 | 0.00323 | 0.00 | 0.9992 |
| Total error | 81.7166 | 21 | 3.89127 | | |
| Total (corr.) | 638.277 | 29 | | | |

R-square = 87.20 percent
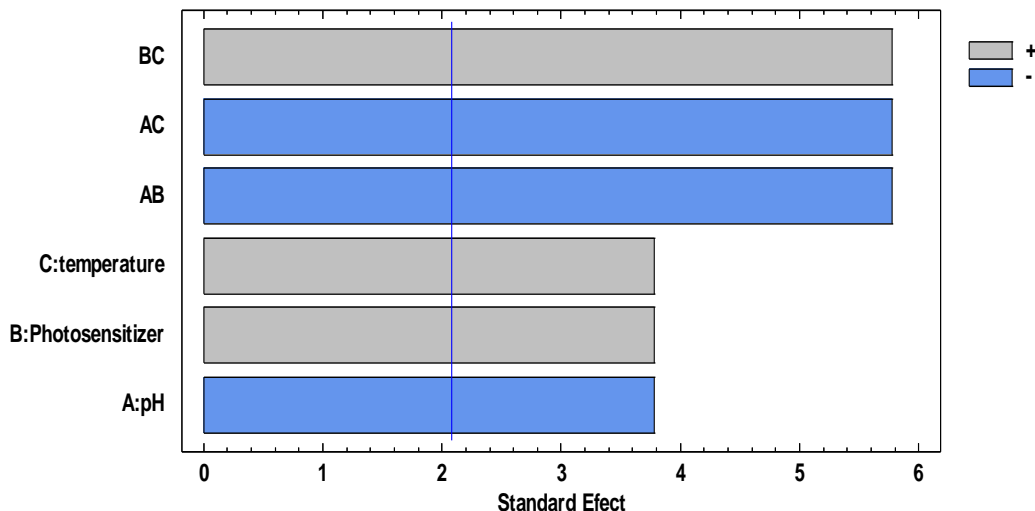
**Figure 54.** Pareto diagram of the process of photodegradation of BPA and the ZnCl$_2$(6OMeQ)$_2$ as a photosensitizer
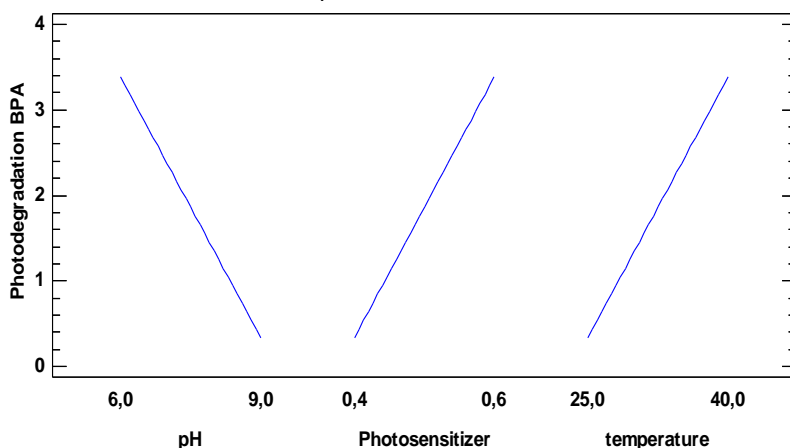


**Figure 55.** Graph of main effects in the process of photodegradation of BPA and the ZnCl$_2$(6OMeQ)$_2$ as a photosensitizer

Subsequently, the optimization analysis was used for the concentration of photosensitizer in a range 0.00089 mM (0.6Abs) - 0.00119 mM(0.8Abs) and pH (5-6), in the case of the temperature it was constant, although the study temperature does not affect the composition of the ZnCl$_2$ (6OMeQ)$_2$ (Villa-Pérez et al., 2018b). For operational purposes the modification of the afore mentioned variables was proposed. These results were in average around 26%, which is shown in the table 14. For this result, the combination of an acidic pH and a high concentration of the photosensitizer continue to be one of the most predominant reasons in the results obtained, since thanks to protonation, oxidation is favored added with a suitable medium so that there is an abundance of the species derived from a high concentration of the photosensitizer which are significant factors for this type of reaction.

**Table 14.** Response Surface Method (RSM) for $ZnCl_2(6OMeQ)_2$ and BPA

| pH | Abs Photosensitizer | (%) Phot. | pH | Abs Photosensitizer | (%) Phot. |
|-----|-----|-----|-----|-----|-----|
| 6.0 | 0.7 | 12.6623 | 5.0 | 0.8 | 26.4352 |
| 6.0 | 0.7 | 12.7056 | 5.0 | 0.7 | 20.7365 |
| 5.5 | 0.6 | 15.3268 | 5.0 | 0.6 | 16.5576 |
| 6.0 | 0.8 | 15.2731 | 5.5 | 0.7 | 18.8641 |
| 5.5 | 0.6 | 15.4125 | 5.0 | 0.6 | 16.5089 |
| 5.5 | 0.8 | 24.9922 | 6.0 | 0.6 | 14.8711 |
| 6.0 | 0.8 | 15.4523 | 5.0 | 0.8 | 26.7183 |
| 6.0 | 0.6 | 14.9617 | 5.0 | 0.7 | 20.7733 |

Lamp: UV, distance: 7 cm height: 21.5 cm, constant:0.6 ppm TCS temperature:$40^0C$

In the ANOVA test, as shown in the table 15, the variables chosen that have a high significance through a statistical test was 95.31% in comparation with the screening experiment (87.19%), although the optimization was not achieved, it was sought to maintain the conditions of pH that adjusted to the reality of natural waters.

The Eq 16 explained the model: Photodegradation = -317,847 + 109,714*pH + 121.823*Abs – 7.54315*pH^2 – 47.986*pH*Abs + 124.234*Abs^2. The Response surface is shown in the figure 56.

**Table 15.** ANOVA of Optimization design for $ZnCl_2(6OMeQ)_2$ and BPA

| Source | sum of squares | DF | mean square | F-reason | P- value |
|-----|-----|-----|-----|-----|-----|
| A: pH | 124.407 | 1 | 124.407 | 74.63 | 0.0000 |
| B: Photosensitizer | 107.403 | 1 | 107.403 | 64.43 | 0.0000 |
| AA | 11.1879 | 1 | 11.1879 | 6.71 | 0.0292 |
| AB | 46.0531 | 1 | 46.0531 | 27.63 | 0.0005 |
| BB | 4.85564 | 1 | 4.85564 | 2.91 | 0.1221 |
| block | 093769 | 1 | 0.93769 | 0.56 | 0.4724 |
| Total error | 15.0023 | 9 | 1.66692 | | |
| Total (corr.) | 319.589 | 15 | | | |

R-square = 95.31 percent
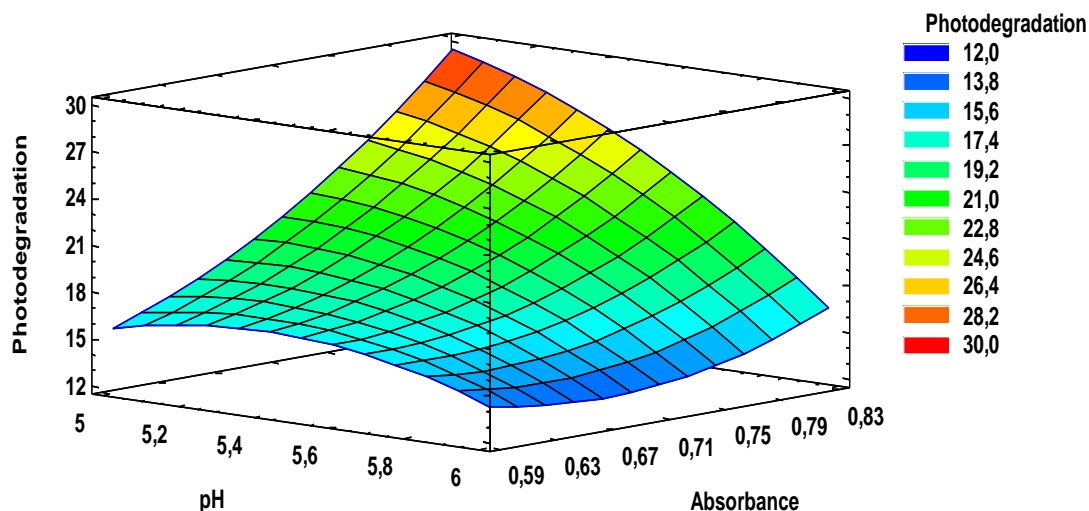
**Figure 56.** Response surface estimated of the optimized model of $ZnCl_2(6OMeQ)_2$ and BPA

In general, when comparing the degradation results of eosin with respect to $ZnCl_2(6OMeQ)_2$, it is evident that the results are quite competitive among them, since for EO yielded it was a value of around 20% and with $ZnCl_2(6OMeQ)_2$ was 26%; however, among the benefits of the latter, its low susceptibility to photobleaching and its susceptibility to temperature stand out.

### 5.3.4 Experimental Design and Optimization for the Triclosan and $ZnCl_2(6OMeQ)_2$

The results screening design for the triclosan are shown in the table 16 where better results are evidenced at pH 6 and photosensitizer concentration of 0.00059 mM (0.4 Abs) with a percentage of around 11%, preliminary. In these experiments, it is possible to demonstrate that the pH is a significantly variable, which is favored by acidic medium because the phenolic compounds, such as triclosan, are generally more reactive upon deprotonation, this effect occurs because O- from phenolate triclosan is better at activating the aromatic ring toward substitution reactions than OH from triclosan(Rule et al., 2005). Then, the temperature contributes in the photo-transformation reactions taking into account the previous studies reported relate to triclosan. Finally, with the initial concentration of the photosensitizer, it is evident that the higher its concentration, the effectiveness decreases, and it is possible that a reaction between the triclosan and the photosensitizer occurs (Gallard & von Gunten, 2002). The conclusions were obtained from of the Figure 57 and 58.

**Table 16.** Screening design for $ZnCl_2(6OMeQ)_2$ and Triclosan

| pH | mM Photosensitizers | (°C) Temperature | (%) Phot. | pH | mM Photosensitizers | (°C) Temperature | (%) Phot. |
|---|---|---|---|---|---|---|---|
| 9.0 | 0.4 | 40.0 | 0.0000 | 6.0 | 0.6 | 25.0 | 0.0000 |

| | | | | | | | |
|---|---|---|---|---|---|---|---|
| 6.0 | 0.4 | 25.0 | 7.3982 | 9.0 | 0.6 | 40.0 | 0.0000 |
| 6.0 | 0.4 | 40.0 | 11.2322 | 7.5 | 0.5 | 32.5 | 0.0000 |
| 9.0 | 0.4 | 25.0 | 0.0000 | 7.5 | 0.5 | 32.5 | 0.0000 |
| 9.0 | 0.6 | 25.0 | 0.0000 | 6.0 | 0.6 | 40.0 | 4.2707 |
| 6.0 | 0.6 | 25.0 | 0.0000 | 9.0 | 0.4 | 40.0 | 0.0000 |
| 9.0 | 0.6 | 40.0 | 0.0000 | 6.0 | 0.4 | 25.0 | 7.5954 |
| 7.5 | 0.5 | 32.5 | 0.0000 | 6.0 | 0.4 | 40.0 | 11.1817 |
| 7.5 | 0.5 | 32.5 | 0.0000 | 9.0 | 0.4 | 25.0 | 0.0000 |
| 6.0 | 0.6 | 40.0 | 4.2363 | 9.0 | 0.6 | 25.0 | 0.0000 |
| 9.0 | 0.4 | 40.0 | 0.0000 | 6.0 | 0.6 | 25.0 | 0.0000 |
| 6.0 | 0.4 | 25.0 | 7.8182 | 9.0 | 0.6 | 40.0 | 0.0000 |
| 6.0 | 0.4 | 40.0 | 11.2109 | 7.5 | 0.5 | 32.5 | 0.0000 |
| 9.0 | 0.4 | 25.0 | 0.0000 | 7.5 | 0.5 | 32.5 | 0.0000 |
| 9.0 | 0.6 | 25.0 | 0.0000 | 6.0 | 0.6 | 40.0 | 4.5429 |

**Constants:** irradiation time 840 sec; Initial concentration of the contaminant: 0.15 mM. The pH values will be controlled with buffer solutions; Lamps: UV
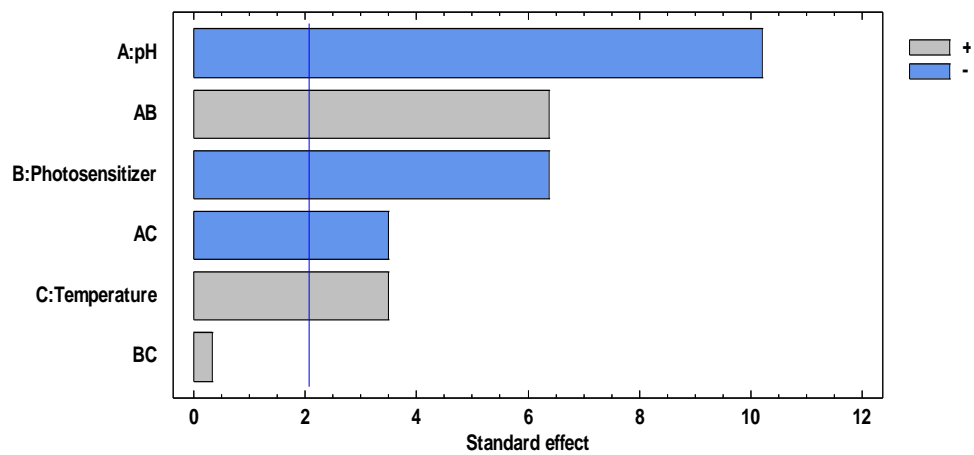


**Figure 57.** Pareto diagram of the photodegradation process of Triclosan and the $ZnCl_2(6OMeQ)_2$ as a photosensitizer
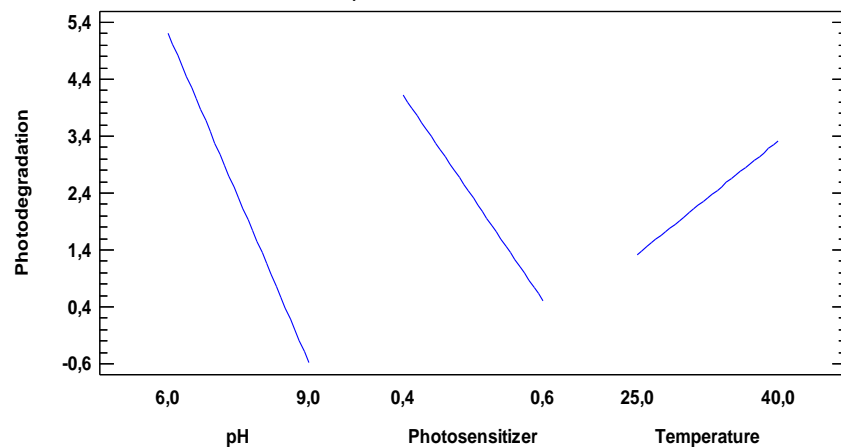


**Figure 58.** Graph of main effects in the photodegradation process of Triclosan and the $ZnCl_2(6OMeQ)_2$ as a photosensitizer

In the ANOVA variance analysis of the experiment shown in the table 17, it is evident that both study variables have high significance and its interactions. In relation to the statistics,

the model represents 90.9% of the variability, which allows us to affirm that an optimization model could be necessary to find the best photodegradation conditions.

**Table 17.** ANOVA of design for $ZnCl_2(6OMeQ)_2$ and Triclosan

| Source | sum of squares | DF | mean square | F-reason | P- value |
|---|---|---|---|---|---|
| A: pH | 201.182 | 1 | 201.182 | 104.12 | 0.0000 |
| B: Photosensitizer | 78.4336 | 1 | 78.4336 | 40.59 | 0.0000 |
| C: temperature | 23.7266 | 1 | 23.7266 | 12.28 | 0.0021 |
| AB | 78.4336 | 1 | 78.4336 | 40.59 | 0.0000 |
| AC | 23.7266 | 1 | 23.7266 | 12.28 | 0.0021 |
| BC | 0208488 | 1 | 0.20849 | 0.11 | 0.7458 |
| block | 0.01311 | 2 | 0.00656 | 0.00 | 0.9966 |
| Total error | 40.5778 | 21 | 1.93228 | | |
| Total (corr.) | 446.302 | 29 | | | |

R-square = 90.908 percent

For the optimization, the range of PH (5-6) was proposed and the temperature between (40 ⁰C - 50 ⁰C) and initial concentration of the photosensitizer of 0.00059 mM (0.4 Abs) were used as constant. Preliminarily, these results, shown in the table 18, are coherent with the EO results since the higher value may involve other reactions that are not necessarily caused by oxidation; in this case, it is better to check the intermediary's products.

**Table 18.** Response Surface Method (RSM) by $ZnCl_2(6OMeQ)_2$ and Triclosan

| Temperature (°C) | pH | (%) Phot. | Temperature (°C) | pH | (%) Phot. |
|---|---|---|---|---|---|
| 40 | 5.00 | 46.4690 | 40 | 5.50 | 0.0000 |
| 45 | 5.50 | 20.9047 | 50 | 5.00 | 52.6805 |
| 40 | 6.00 | 0.0000 | 45 | 5.50 | 20.8333 |
| 45 | 6.00 | 0.0000 | 40 | 5.50 | 0.1810 |
| 45 | 5.00 | 16.6868 | 40 | 5.00 | 46.0485 |
| 50 | 6.00 | 0.0000 | 45 | 5.50 | 20.9780 |
| 50 | 5.50 | 16.0841 | 50 | 6.00 | 52.3613 |
| 45 | 5.50 | 20.9585 | 45 | 6.00 | 0.0000 |

Lamp: UV without filter, distance 7 cm height 21.5 cm, fixed variable: 0.6 ppm TCS

The ANOVA shown in the table 19 demonstrates that, for this optimization, it is less than the screening tests, because the statistic test is lesser (before 90.90% adjusted and later 78.96%). For future research projects, it is possible to put a constant temperature and change the pH and initial concentration of the photosensitizer. However, for this model, the pH had a significant effect in the reaction.

For this proposed model of optimization proposal in the Eq 17 is: $Removal_{283}$= 962.305 – 0.45459*temperature – 306.57*pH + 0.0265181*temperature^2 – 0.169903*temperature*pH + 24.7249*pH^2 shown in the Figure 59.

**Table 19.** ANOVA of Optimization design for eosin Y and Triclosan

| Source | sum of squares | DF | mean square | F-reason | P- value |
|---|---|---|---|---|---|
| A: temperature | 197.414 | 1 | 197.414 | 1.42 | 0.2640 |

| | | | | | |
|---|---|---|---|---|---|
| B: pH | 3716.48 | 1 | 3716.48 | 26.72 | 0.0006 |
| AA | 1.69285 | 1 | 1.69285 | 0.01 | 0.9146 |
| AB | 0.93633 | 1 | 0.93633 | 0.01 | 0.9364 |
| BB | 141.927 | 1 | 141.927 | 1.02 | 0.3388 |
| bloques | 24.6489 | 1 | 24.6489 | 0.18 | 0.6837 |
| Error total | 1251.99 | 9 | 139.11 | | |
| Total (corr.) | 5951.65 | 15 | | | |

**R-square =** 78.96 percent
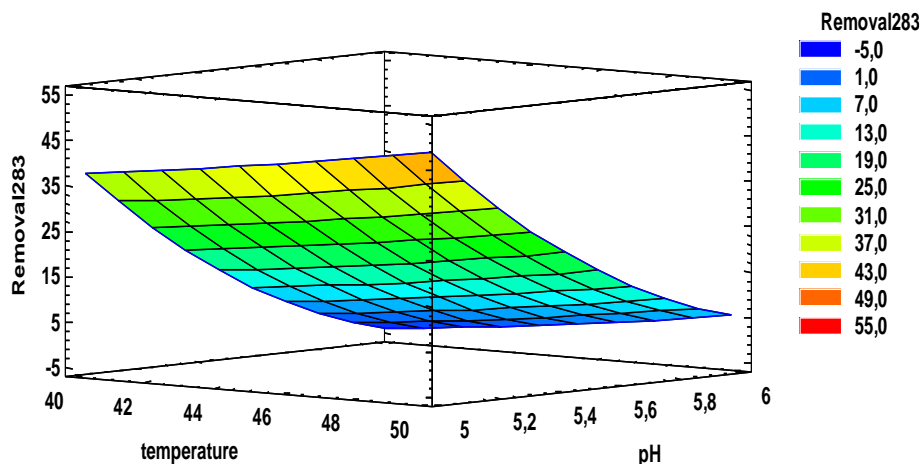


**Figure 59.** Response surface estimated of the optimized model of $ZnCl_2$ (6OMeQ) – Triclosan

## 5.3.2 Experimental Design of Persulfate and Triclosan/Bisphenol A

With the persulfate oxidation method, a comparative methodology was considered necessary. The analysis was based on the assumption that the initial concentration is not a significant variable in the photodegradation process.

In Table 20 of the experimental design of the photodegradation of BPA in the presence of persulfate, it is evidenced that, at basic pH (~ 9), a temperature of 25°C and a concentration of 20 mM, it is possible to reach a photodegradation of around 5%. At pH < 7 sulfate radicals are the dominant reactive species, however, hydroxyl and sulfate radicals participate equally in reactions at neutral pHs, the reaction that happen are shown in the equation 18 and 19 (Matzek & Carter, 2016):

$$SO_4^{\cdot-} + H_2O \rightarrow SO_4^{2-} + OH^\cdot + H^+ \text{ **Eq 18**}$$

$$SO_4^{\cdot-} + OH^- \rightarrow SO_4^{2-} + OH^\cdot \text{ **Eq 19**}$$
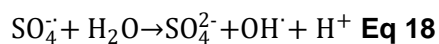
So, for this reason, the reaction was promoted, because the hydroxyl radical was formed at this pH. Other variable is the persulfate concentration, the higher $S_2O_8^{2-}$ concentration to generate more specie $SO_4^{\cdot-}$ and better photodegradation(X. Jiang et al., 2013). Finally, at

this temperature is not thermal activate for the species $S_2O_8^{2-}$, near 40ºC, only 20% of BPA could be susceptible by transformation (Olmez-Hanci et al., 2013).However, the combination of these three variables are important in the photodegradation process, such as those shown in the Figure 60 and 61.

**Table 20.** Screening design for persulfate and BPA

| pH | mM Persulfate | (°C) Temperature | (%) Phot. | pH | mM Persulfate | (°C) Temperature | (%) Phot. |
|---|---|---|---|---|---|---|---|
| 9.0 | 20.0 | 40.0 | 0.0000 | 9.0 | 20.0 | 25.0 | 4.9455 |
| 6.0 | 20.0 | 40.0 | 0.0000 | 6.0 | 5.0 | 40.0 | 0.0000 |
| 6.0 | 5.0 | 25.0 | 0.0000 | 9.0 | 5.0 | 40.0 | 0.0000 |
| 7.5 | 12.5 | 32.5 | 0.2868 | 7.5 | 12.5 | 32.5 | 0.3542 |
| 6.0 | 20.0 | 25.0 | 0.0000 | 9.0 | 5.0 | 25.0 | 0.0000 |
| 9.0 | 20.0 | 25.0 | 4.8379 | 9.0 | 20.0 | 40.0 | 0.0000 |
| 6.0 | 5.0 | 40.0 | 0.0000 | 6.0 | 20.0 | 40.0 | 0.0000 |
| 9.0 | 5.0 | 40.0 | 0.0000 | 6.0 | 5.0 | 25.0 | 0.0000 |
| 7.5 | 12.5 | 32.5 | 0.3475 | 7.5 | 12.5 | 32.5 | 0.3137 |
| 9.0 | 5.0 | 25.0 | 0.0000 | 6.0 | 20.0 | 25.0 | 0.0000 |
| 9.0 | 20.0 | 40.0 | 0.0000 | 9.0 | 20.0 | 25.0 | 4.8442 |
| 6.0 | 20.0 | 40.0 | 0.0000 | 6.0 | 5.0 | 40.0 | 0.0000 |
| 6.0 | 5.0 | 25.0 | 0.0000 | 9.0 | 5.0 | 40.0 | 0.0000 |
| 7.5 | 12.5 | 32.5 | 0.3280 | 7.5 | 12.5 | 32.5 | 0.3130 |
| 6.0 | 20.0 | 25.0 | 0.0000 | 9.0 | 5.0 | 25.0 | 0.0000 |

**Constants:** irradiation time 840 sec; Initial concentration of BPA: 0.15mM; the pH values will be controlled with buffer solutions; Lamp: germicidal with filter glass; distance:7 cm

The results of the ANOVA shown in the table 21 of this analysis reflect the behavior of the variables within the experimental design. Both the individual variables and their interactions are evident, in the statistical test, it is the 85.16%, so, it is important to choose the variables in order to proceed to the optimization.

**Table 21.** ANOVA of design for persulfate and BPA

| Source | sum of squares | mean square | F-reason | P- value |
|---|---|---|---|---|
| A: pH | 8.91528 | 8.91528 | 20.10 | 0,0002 |
| B: Conc. persulfate | 8.91528 | 8.91528 | 20.10 | 0,0002 |
| C: temperature | 8.91528 | 8.91528 | 20.10 | 0,0002 |
| AB | 8.91528 | 8.91528 | 20.10 | 0,0002 |
| AC | 8.91528 | 8.91528 | 20.10 | 0,0002 |
| BC | 8.91528 | 8.91528 | 20.10 | 0,0002 |
| block | 0.00162 | 0.00082 | 0.00 | 0.9982 |
| Total error | 9.31561 | 0.44360 | | |
| Total (corr.) | 62.8089 | | | |

R-square = 85,16 percent
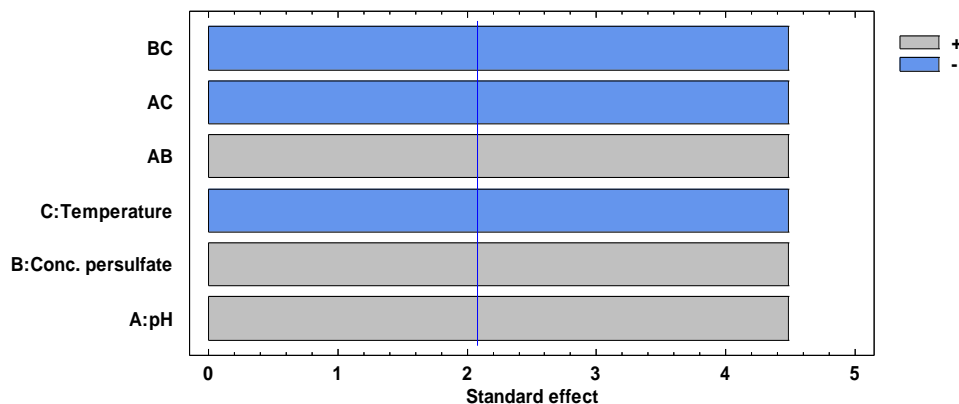
**Figure 60.** Pareto diagram of the photodegradation process of BPA and persulfate as oxidant
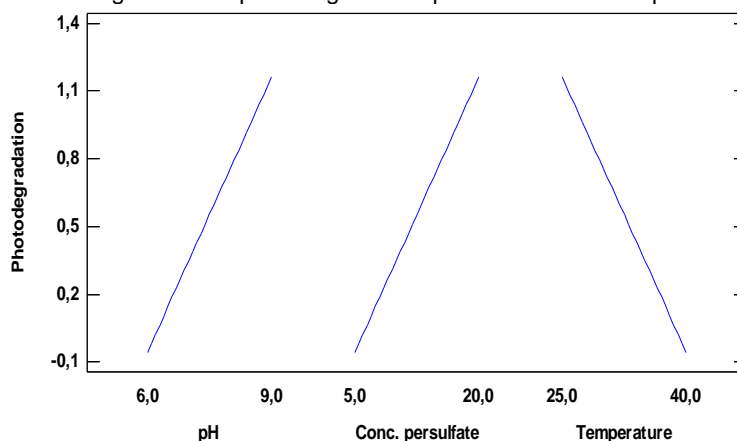


**Figure 61.** Graph of main effects in the oxidation process of BPA and persulfate as oxidant

For the screening design for the Triclosan, the condition reported in the methodology was taken. These results were reported in the table 22. For the triclosan, and according to studies reported, the photodegradation at acidic pH is more effective because: First, to promote the interaction, $SO_4^{-}$ is less reactive but mainly through electron transfers; but the hydroxyl radical abstracting H from C-H, N-H or O-H bonds and adds to C=C double bonds or aromatic rings that could be other products and influence in the photodegradation. the other reason is that it is higher than 7.6, the ionized form of TCS and formed other microspecies (L. Chen et al., 2019). These effects are shown in the Figure 62 and 63.

**Table 22.** Screening design for persulfate and TCS

| pH | mM Persulfate | (°C) Temperature | (%) Phot. | pH | mM Persulfate | (°C) Temperature | (%) Phot. |
|---|---|---|---|---|---|---|---|
| 9.0 | 20.0 | 40.0 | 2.4787 | 9.0 | 20.0 | 25.0 | 1.2077 |
| 6.0 | 20.0 | 40.0 | 2.7444 | 6.0 | 5.0 | 40.0 | 2.7723 |
| 6.0 | 5.0 | 25.0 | 0.0000 | 9.0 | 5.0 | 40.0 | 1.1012 |
| 7.5 | 12.5 | 32.5 | 0.0000 | 7.5 | 12.5 | 32.5 | 0.0000 |
| 6.0 | 20.0 | 25.0 | 2.6553 | 9.0 | 5.0 | 25.0 | 1.1002 |
| 9.0 | 20.0 | 25.0 | 1.2447 | 9.0 | 20.0 | 40.0 | 2.4741 |
| 6.0 | 5.0 | 40.0 | 2.7717 | 6.0 | 20.0 | 40.0 | 2.7865 |

| | | | | | | | |
|---|---|---|---|---|---|---|---|
| 9.0 | 5.0 | 40.0 | 1.1506 | 6.0 | 5.0 | 25.0 | 0.0000 |
| 7.5 | 12.5 | 32.5 | 0.0000 | 7.5 | 12.5 | 32.5 | 0.0000 |
| 9.0 | 5.0 | 25.0 | 1.1362 | 6.0 | 20.0 | 25.0 | 2.6543 |
| 9.0 | 20.0 | 40.0 | 2.4751 | 9.0 | 20.0 | 25.0 | 1.2281 |
| 6.0 | 20.0 | 40.0 | 2.7767 | 6.0 | 5.0 | 40.0 | 2.7758 |
| 6.0 | 5.0 | 25.0 | 0.0000 | 9.0 | 5.0 | 40.0 | 1.1586 |
| 7.5 | 12.5 | 32.5 | 0.0000 | 7.5 | 12.5 | 32.5 | 0.0000 |
| 6.0 | 20.0 | 25.0 | 2.6525 | 9.0 | 5.0 | 25.0 | 1.1038 |

**Constants:** irradiation time 840 sec; Initial concentration of TCS: 0.15mM; the pH values will be controlled with buffer solutions; Lamp: germicidal with filter glass; distance:7 cm

The ANOVA results shown in table 23 are clear with the comparison between the graphical analyses, because, for the experiment of persulfate with triclosan, the most influence is for the concentration of the persulfate and the temperature, in this case the statistical test was 45%, so, the optimization is necessary.

**Table 23.** ANOVA of design for persulfate and TCS

| Source | sum of squares | DF | mean square | F-reason | P- value |
|---|---|---|---|---|---|
| A: pH | 1.8875 | 1 | 1.88748 | 1.92 | 0.1807 |
| B: Conc. persulfate | 6.3116 | 1 | 6.3116 | 6.41 | 0.0194 |
| C: temperature | 6.4926 | 1 | 6.4926 | 6.59 | 0.0179 |
| AB | 0.5376 | 1 | 0.5376 | 0.55 | 0.4681 |
| AC | 0.9791 | 1 | 0.9792 | 0.99 | 0.3300 |
| BC | 0.7694 | 1 | 0.7694 | 0.78 | 0.3867 |
| block | 0.0006 | 2 | 0.0003 | 0.00 | 0.9997 |
| Total error | 20.676 | 21 | 0.9846 | | |
| Total (corr.) | 37.6545 | 29 | | | |

R-square = 45.09 percent
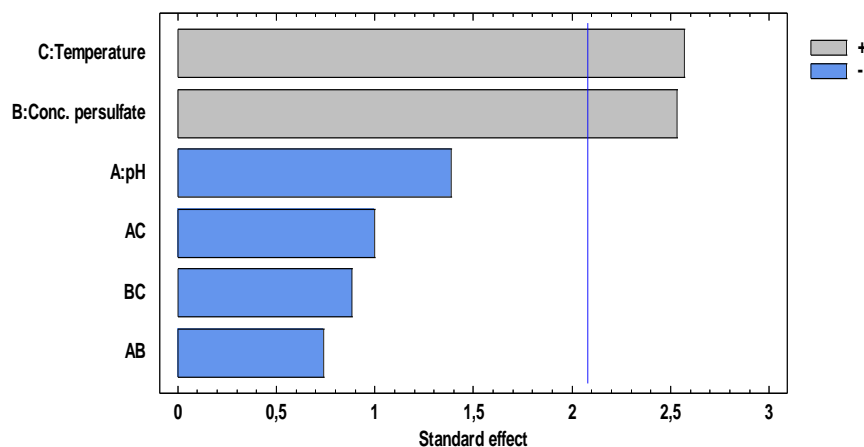


**Figure 62.** Pareto diagram of the process of photodegradation of BPA and persulfate as oxidant
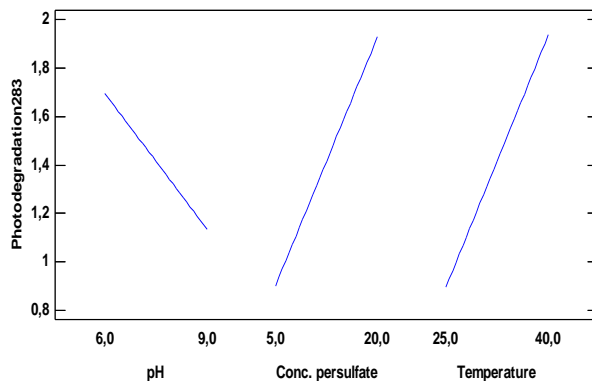
**Figure 63** Graph of main effects in the oxidation process of BPA and persulfate as oxidant

Consequently, in the optimization phase, it was not possible to establish the effect of degradation, since when analyzing the initial concentration, the reaction occurred. It could be determined that the concentrations of work carried out in other investigations were in the range of around 50 ppm for triclosan (L. Chen et al., 2019) and for BPA of 20 ppm (Olmez-Hanci et al., 2013). These concentrations are well above the scope of this research (0.1 ppm-1 ppm); therefore, they cannot be considered this comparable method.

## 5.4 Degradation Byproducts and Mineralization of the Process Photosensitization for The Bisphenol A and Triclosan using the ZnCl$_2$(6OMeQ)$_2$

Applying the methodology mentioned in the section 4.2, and understanding the methodological limitations, it was possible to obtain the degradation of some products for bisphenol A such those shown in the Figure 64 allusive to 4-isopropenylphenol as hydroxylation sub product of BPA (T. Zhang et al., 2015). In the figure 65 shown the photodegradation of the BPA for oxidation is shown.
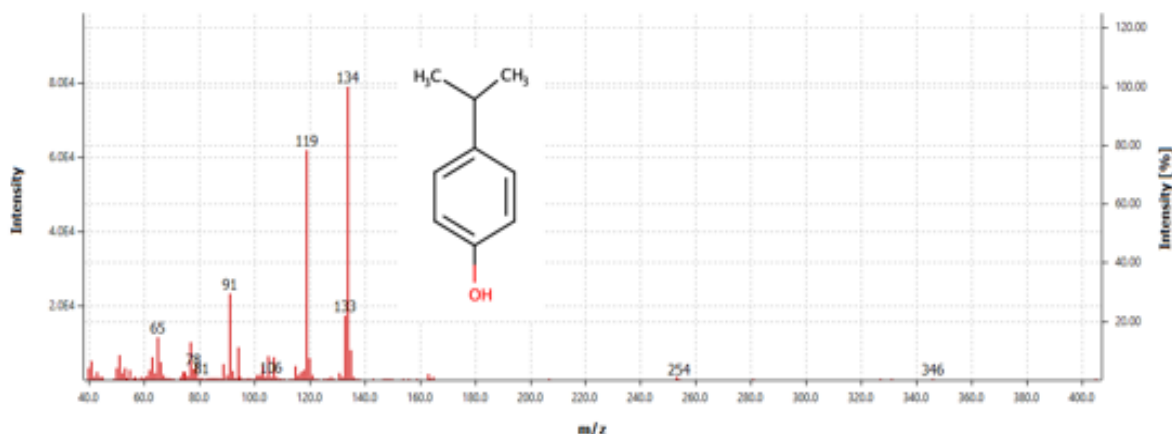


**Figure 64.** Mass spectrum 4-isopropenylphenol
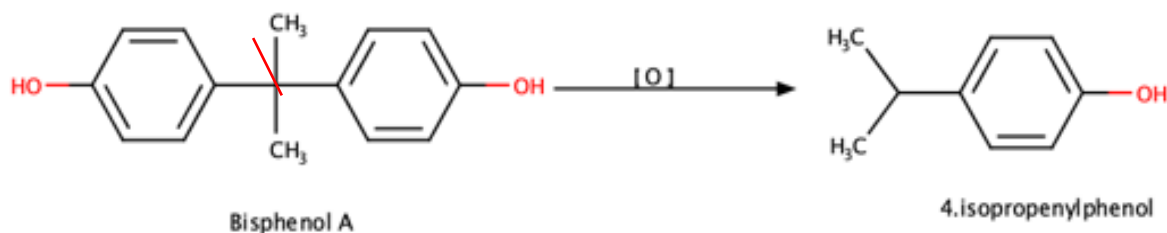
**Figure 65.** Mechanism of degradation of Bisphenol A

The other by-products found in the GC/MS analysis were diethyl phthalate and dibutyl phthalate, shown in the figure 66 and 67, which propose a possible radical route for the degradation. Firstly, the radicals attack the aromatic ring, and phenoxyl BPA is produced; then it forms the phenoxyl and isopropenylphenol radicals. Later, it is transformed into its quinone, to shape intermediate aromatics that are formed through oxidative skeletal rearrangement, hydroxylation, dehydration and ring cleavage products (S. Yang et al., 2018)
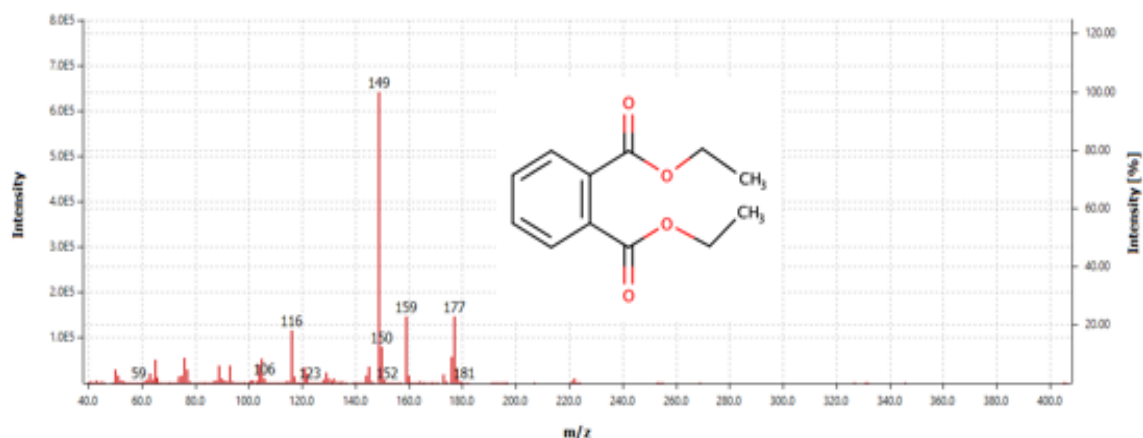


**Figure 66.** Mass spectrum of Diethyl phthalate
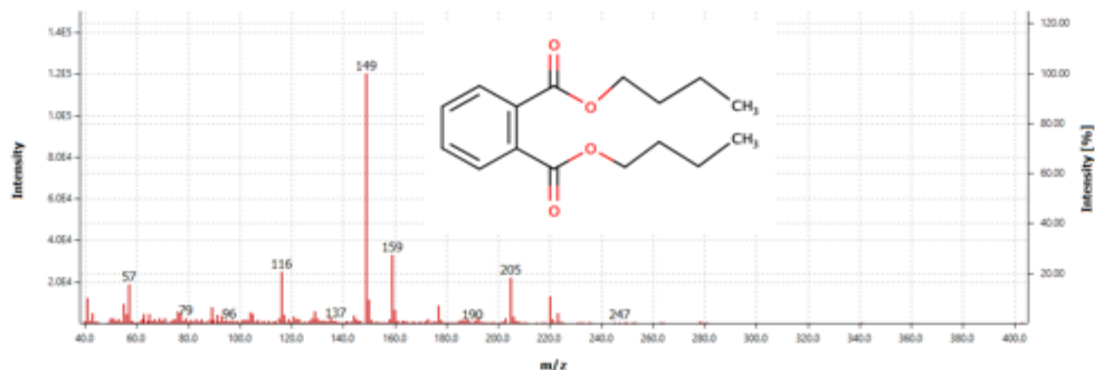


**Figure 67.** Mass spectrum of dibutyl phthalate

Finally, regarding the degradation of triclosan, the transformation was evidenced by the formation of a quinoline derivative shown in figure 68 (B. Yang et al., 2011). However, the losses of chlorines in the structure make triclosan a more oxidizable molecule and consequently with a greater probability of photodegradability.
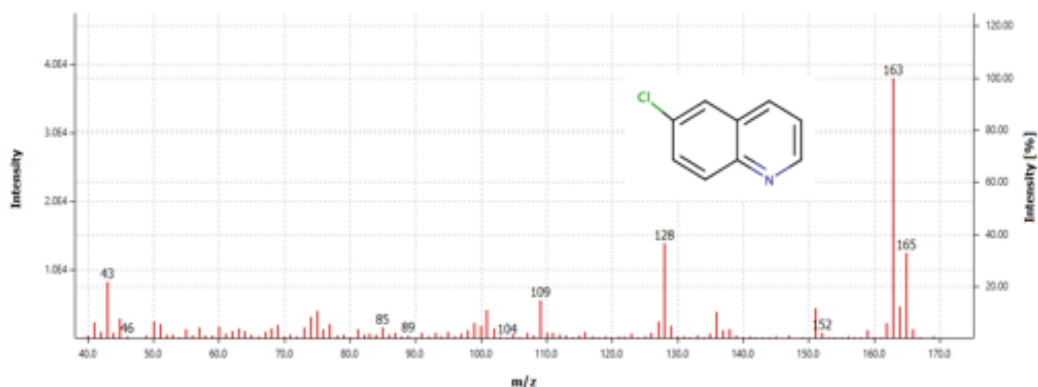


**Figure 68.** Mass spectrum of 6-cloroquinoline

## 6. Conclusions

The synthesis products exceeded the expectation valued in the research, given that three new compounds were obtained, two of which could be established by characterization analysis that were synthesized in a satisfactory manner, because, for the characterization technical and the change respect at the reactants and products. Specifically, in the case of the manganese complex, it was considered amorphous, and that the thermal stability of the manganese complex is too low, so, when placed in severe conditions of pH and temperature, it cannot be considered a good photosensitizer in a specific condition.

In the case of the gold complex, AuCl(6OMeQ)$_3$, it is considered one of the main novelties of this research, given that the complex showed in the STEM analysis that it has a crystalline phase, and it was possible to demonstrate the formation of nanoparticles, a great gain of this compound, given that this confers characteristics of insolubility (aspect that was evident in the determination of quantum yield). Having this great feature means it can be fixed in polymers for the immobilization of this, which increases the interest in its use for scaling. With respect at the photosensitizing capacity, was possible to demonstrated that the reaction in the second order, own speeds bimolecular reactions.

In the evaluation of the best condition in the photodegradation process, it was possible to establish parameters in similar condition at natural water; in the case of the Bisphenol A treated with EO, the parameters were: at pH 5 and initial concentration of 0.00104 mM and

constant temperature (25 ºC); in the case of using $ZnCl_2(6OMeQ)_2$ with BPA  were pH 5.0 and Initial concentration of the photosensitizer of 0.00119 mM(0.8 Abs) at constant temperature (40 ºC); in the case of Triclosan with EO were pH 5 and temperature of 50 ºC at initial concentration of photosensitizer of 0.0054 mM; in the case of triclosan with $ZnCl_2(6OMeQ)_2$ were 50 ºC and a pH of 6.0 and initial concentration of the photosensitizer of 0.00059 mM (0.4Abs) as constant; in the case of the persulfate for the Bisphenol A and Triclosan, it was not possible to establish the best condition because the reaction occurred so fast that it could not be monitored, taking into account that the concentration was very low; therefore, in relation to efficiency, undoubtedly persulfate has better characteristics in With respect to the percentage of the photodegradation for the BPA with EO, it was around 20% and with respect to $ZnCl_2(6OMeQ)_2$ the percentage of the photodegradation it was 26%; in the case of Triclosan with EO it was around 56%; and for $ZnCl_2(6OMeQ)_2$ it was around 52%. In both cases, the percentage was similar and competitive. Regarding $ZnCl_2(6OMeQ)_2$, there is an advantage because photobleaching rate is low as it is not susceptible to temperature or changes in pH and the light, which makes difficult coloring. For the mineralization, it was not possible to make complex mixes between the photosensitizer, pollutants and buffers; therefore, to determine these values, it is suggested that heterogeneous systems or other complementary techniques be made that are not affected by the matrix effect.

Then, for the intermediary byproducts, it could be demonstrated that 4-isopropenylphenol was obtained as product of the oxidation. The other products were possibly obtained from the radical reactions obtained.

Finally, as a recommendation, it is important to continue investigating the synthesized complexes and their potential applications in the case of the gold compound, since its bactericidal application is known. With the photodegradation conditions, trying several variables such as pH may improve optimization. In relation to persulfate, working at such low concentrations of pollutants should be considered, making sure to use measurements over time that allow more information about the photodegradation process.

## 7. Related Academic Productivity

- Financed project: Degradación fotosensibilizada del Bisfenol A usando complejos de coordinación con el ligando 6-metoxiquinolina, en solución e inmovilizados. Universidad Nacional de Colombia – Medellín campus, 2016.

- Financed project: Síntesis y caracterización de compuesto de coordinación de un metal de transición con el ligando 6-metoxiquinolina y evaluación de su capacidad fotosensibilizadora con potencial aplicación para el tratamiento y desinfección de aguas. Fundación para la Promoción de la Ciencia y la Tecnologia, 2017.

- Speaker in 67th Canadian Chemical Engineering Conference, 2017.

- Speaker in 3rd Iberoamerican Conference on Advanced Oxidation Technologies (III CIPOA) and 2nd Colombian Conference on Advanced Oxidation Processes (II CCPAOX), 2017.

- 4-nonylphenol: effects, quantification and methods of removal in superficial and drinking water. Revista de Investigación Agraria y Ambiental, 2020.

- Spectrophotometric Determination Profile of Bisphenol A in The Photodegradation Process with Singlet Molecular Oxygen. Revista Ciencia en Desarrollo, 2020.

## 8. References

Abdelrazek, E. M., Elashmawi, I. S., Hezma, A., & Rajeh, A. (2012). The Accessibility of Change of the Structural, Morphological and Thermal Properties by Intermolecular Hydrogen Bonding in PEO/PVA Blend Containing MnCl 2. *International Journal of Modern Applied Physics International Journal of Modern Applied Physics Journalaspx Int. J. Modern App. Physics*, *1*(12), 83–96.

Alessio, E. (2004). Synthesis and Reactivity of Ru-, Os-, Rh-, and Ir-Halide−Sulfoxide Complexes †. *Chemical Reviews*, *104*(9), 4203–4242. https://doi.org/10.1021/cr0307291

Alessio, E., Balducci, G., Calligaris, M., Costa, G., Attia, W. M., & Mestroni, G. (1991). Synthesis , Molecular Structure , and Chemical Behavior of Hydrogen trans - Bis(dimethyl sulfoxide) tetrachlororuthenate(III) and mer-Trichlorotris(dimethyl sulfoxide) ruthenium(III): The First Fully Characterized Chloride-Dimethyl Sulfoxide-Ruthenium. *Inorganic Chemistry, 30*, 609–618. https://doi.org/10.1021/ic00004a005

Alessio, E., Mestroni, G., Nardin, G., Attia, W. M., Calligaris, M., Sava, G., & Zorzets, S. (1988). Cis- and trans-dihalotetrakis(dimethyl sulfoxide)ruthenium(II) complexes:

synthesis, structure and Antitumor Activity. *Inorganic Chemistry*, *27*(d), 4099–4106. https://doi.org/10.1021/ic00296a006

Allan, J. R., & Dahyrnple, J. (1991). Thermal , spectral and magnetic studies of cobalt ( II ), copper ( II ) and zinc ( II ) complexes of 5 , 6-benzoquinoline and 6-methoxyquinoline. *Thermochimica Acta*, *191*, 223–230.

Alnaizy, R., & Akgerman, A. (2000). Advanced oxidation of phenolic compounds. *Advances in Environmental Research*, *4*(3), 233–244. https://doi.org/10.1016/S1093-0191(00)00024-1

Andreozzi, R. (1999). Advanced oxidation processes (AOP) for water purification and recovery. *Catalysis Today*, *53*(1), 51–59. https://doi.org/10.1016/S0920-5861(99)00102-9

Aranami, K., & Readman, J. W. (2007). Photolytic degradation of triclosan in freshwater and seawater. *Chemosphere*, *66*(6), 1052–1056. https://doi.org/10.1016/j.chemosphere.2006.07.010

Benesi, H., & Hildebrand, J. H. (1949). *A Spectrophotometric Investigation of the Interaction of Iodine with Aromatic Hydrocarbons. 2832*(1948).

Bodhipaksha, L. C., Sharpless, C. M., Chin, Y.-P., Sander, M., Langston, W. K., & MacKay, A. A. (2015). Triplet photochemistry of effluent and natural organic matter in whole water and isolates from effluent-receiving rivers. *Environmental Science & Technology*, *49*(6), 3453–3463. https://doi.org/10.1021/es505081w

Bolong, N., Ismail, a. F., Salim, M. R., & Matsuura, T. (2009). A review of the effects of emerging contaminants in wastewater and options for their removal. *Desalination*, *238*(1–3), 229–246. https://doi.org/10.1016/j.desal.2008.03.020

Bower, J. P., & Anastasio, C. (2013). Measuring a 10,000-fold enhancement of singlet molecular oxygen (1O2*) concentration on illuminated ice relative to the corresponding liquid solution. *Atmospheric Environment*, *75*, 188–195. https://doi.org/10.1016/j.atmosenv.2013.04.054

Brastos, I., Alessio, E., Ringenberg, M. E., & Rauchfuss, T. B. (2010). Ruthenium Complexes 35. Rutheniu(II)-Chlorido Complexes of Dimethylsulfoxide. In T. B. Rauchfuss (Ed.), *Inorganic Syntheses* (Vol. 35, Issue Ii, pp. 148–163). John Wiley

&Sons Inc. https://doi.org/10.1002/9780470651568.ch8

Buchalska, M., Kras, G., Oszajca, M., Łasocha, W., & MacYk, W. (2010). Singlet oxygen generation in the presence of titanium dioxide materials used as sunscreens in suntan lotions. *Journal of Photochemistry and Photobiology A: Chemistry*, *213*(2–3), 158–163. https://doi.org/10.1016/j.jphotochem.2010.05.019

Burns, J. M., Cooper, W. J., Ferry, J. L., King, D. W., DiMento, B. P., McNeill, K., Miller, C. J., Miller, W. L., Peake, B. M., Rusak, S. A., Rose, A. L., & Waite, T. D. (2012). Methods for reactive oxygen species (ROS) detection in aqueous environments. *Aquatic Sciences*, *74*(4), 683–734. https://doi.org/10.1007/s00027-012-0251-x

Careghini, A., Mastorgio, A. F., Saponaro, S., & Sezenna, E. (2014). Bisphenol A, nonylphenols, benzophenones, and benzotriazoles in soils, groundwater, surface water, sediments, and food: a review. *Environmental Science and Pollution Research*, 5711–5741. https://doi.org/10.1007/s11356-014-3974-5

Chang, C., Yang, H., Mu, W., Cai, Y., Wang, L., Yang, L., & Qin, H. (2019). In situ fabrication of bismuth oxyiodide (Bi7O9I3/Bi5O7I) n-n heterojunction for enhanced degradation of triclosan (TCS) under simulated solar light irradiation. *Applied Catalysis B: Environmental*, *254*, 647–658. https://doi.org/10.1016/j.apcatb.2019.05.030

Chen, D., Kannan, K., Tan, H., Zheng, Z., Feng, Y. L., Wu, Y., & Widelka, M. (2016). Bisphenol Analogues Other Than BPA: Environmental Occurrence, Human Exposure, and Toxicity - A Review. In *Environmental Science and Technology* (Vol. 50, Issue 11, pp. 5438–5453). https://doi.org/10.1021/acs.est.5b05387

Chen, L., Hu, X., Cai, T., Yang, Y., Zhao, R., Liu, C., Li, A., & Jiang, C. (2019). Degradation of Triclosan in soils by thermally activated persulfate under conditions representative of in situ chemical oxidation (ISCO). *Chemical Engineering Journal*, *369*(February), 344–352. https://doi.org/10.1016/j.cej.2019.03.084

Chiu, Y. C., Ho, K. Y., Chen, I. C., Hua, S. A., Cheng, M. C., & Peng, S. M. (2014). IR, Raman, and surface-enhanced Raman spectroscopic study on triruthenium dipyridylamide diruthenium nickel dipyridylamide family: Metal-metal bonding and structures. *Journal of the Chinese Chemical Society*, *61*(12), 1289–1296. https://doi.org/10.1002/jccs.201400220

Cho, C. S., Kim, B. T., Kim, T. J., & Chul Shim, S. (2002). Ruthenium-catalyzed regioselective ??-alkylation of ketones with primary alcohols. *Tetrahedron Letters*, *43*(44), 7987–7989. https://doi.org/10.1016/S0040-4039(02)01625-8

Colborn, T., Vom Saal, F. S., & Soto, A. M. (1993). Developmental effects of endocrine-disrupting chemicals in wildlife and humans. In *Environmental Health Perspectives* (Vol. 101, Issue 5, pp. 378–384). https://doi.org/10.1289/ehp.93101378

D.García-Fresnadillo,Y.Georgiadou,G.Orellana,A.M.Braun, E. O. (1996). Singlet-Oxygen(1g)Production by ruthenium(II) Complexes Containing poli¡yazaheterocyclic Ligand in methanol and in water. *Helvetica Chemica Acta*, *79*, 1232–1238.

Daughton, C. G., & Ternes, T. a. (1999). *Personal Care Products in the Environment : by Pharmaceuticals and Personal Care Products in the Environment : Agents of Subtle Change ?* http://epa.gov/esd/bios/daughton.htm

De Frémont, P., Scott, N. M., Stevens, E. D., & Nolan, S. P. (2005). Synthesis and structural characterization of N-heterocyclic carbene gold(I) complexes. *Organometallics*, *24*(10), 2411–2418. https://doi.org/10.1021/om050111c

De la Cruz, N., Esquius, L., Grandjean, D., Magnet, a., Tungler, a., de Alencastro, L. F., & Pulgarín, C. (2013). Degradation of emergent contaminants by UV, UV/H2O2 and neutral photo-Fenton at pilot scale in a domestic wastewater treatment plant. *Water Research*, *47*(15), 5836–5845. https://doi.org/10.1016/j.watres.2013.07.005

Deborde, M., Rabouan, S., Mazellier, P., Duguet, J. P., & Legube, B. (2008). Oxidation of bisphenol A by ozone in aqueous solution. *Water Research*, *42*(16), 4299–4308. https://doi.org/10.1016/j.watres.2008.07.015

DeRosa, M. C., & Crutchley, R. J. (2002). Photosensitized singlet oxygen and its applications.pdf. *Coordination Chemistry Reviews*, *234*, 351–371.

Díez-Mato, E., Cortezón-Tamarit, F. C., Bogialli, S., García-Fresnadillo, D., & Marazuela, M. D. (2014). Phototransformation of model micropollutants in water samples by photocatalytic singlet oxygen production in heterogeneous medium. *Applied Catalysis B: Environmental*, *160–161*, 445–455.

Dimmer, J., Cabral, F. V., Sabino, C. P., Silva, C. R., Núñez-Montoya, S. C., Cabrera, J. L., & Ribeiro, M. S. (2019). Natural anthraquinones as novel photosentizers for

antiparasitic photodynamic inactivation. *Phytomedicine*, *61*, 152894. https://doi.org/10.1016/j.phymed.2019.152894

Douglas, S., James, H., & Nieman Timothy. (2001). *Principios de Análisis Instrumental* (M. G. Hill (ed.); 5th editio).

Evans, P., Spencer, A., & Wilkinson, G. (1973). Dichlorotetrakis(dimethyl sulphoxide)ruthenium(ii) and its Use as a Source Material for Some New Ruthenium(II) Complexes. *Journal Chemistry Society*, *204*, 204–209.

Fernandez, J. M., Bilgin, M. D., & Grossweiner, L. I. (1997). Singlet oxygen generation by photodynamic agents. *Journal of Photochemistry and Photobiology B: Biology*, *37*(1–2), 131–140. https://doi.org/10.1016/S1011-1344(96)07349-6

Ferreira, L. T., Alarcon, R. T., Perpétuo, G. L., & Bannach, G. (2019). Investigation and characterization by TG/DTG–DTA and DSC of the fusion of Riboflavin, and its interaction with the antibiotic norfloxacin in the screening of cocrystal. *Journal of Thermal Analysis and Calorimetry*, *136*(2), 581–588. https://doi.org/10.1007/s10973-018-7696-7

Frost, B. J., Bautista, C. M., Huang, R., & Shearer, J. (2006). Manganese complexes of 1,3,5-triaza-7-phosphaadamantane (PTA): The first nitrogen-bound transition-metal complex of PTA. *Inorganic Chemistry*, *45*(9), 3481–3483. https://doi.org/10.1021/ic060322p

Fuller, Z. J., Bare, W. D., Kneas, K. a, Xu, W., Demas, J. N., & Degraff, B. a. (2003). Photostability of Luminescent Ruthenium ( II ) Complexes in Polymers and in Solution Photostability of Luminescent Ruthenium ( II ). *Society*, *75*(Ii), 4803–4810. https://doi.org/10.1021/ac0261707

Gallard, H., & von Gunten, U. (2002). Chlorination of phenols: Kinetics and formation of chloroform. *Environmental Science and Technology*, *36*(5), 884–890. https://doi.org/10.1021/es010076a

Gao, H., Chen, J., Zhang, Y., & Zhou, X. (2016). Sulfate radicals induced degradation of Triclosan in thermally activated persulfate system. *Chemical Engineering Journal*, *306*, 522–530. https://doi.org/10.1016/j.cej.2016.07.080

Gao, Y., Ji, Y., Li, G., & An, T. (2014). Mechanism, kinetics and toxicity assessment of OH-

initiated transformation of triclosan in aquatic environments. *Water Research*, *49*, 360–370. https://doi.org/10.1016/j.watres.2013.10.027

Garcia-Fresnadillo. (2002). Fotosensibilización y el sensibilizador : síntesis , propiedades y limitaciones. In *Solar safe water* (pp. 227–242).

García-Fresnadillo, D. (2001). Desinfección mediante fotosensibilizadores : principios básicos. In *Solar safe water* (Issue sección 4, pp. 243–258).

Garoma, T., & Matsumoto, S. (2009). Ozonation of aqueous solution containing bisphenol A: Effect of operational parameters. *Journal of Hazardous Materials*, *167*(1–3), 1185–1191. https://doi.org/10.1016/j.jhazmat.2009.01.133

Geissen, V., Mol, H., Klumpp, E., Umlauf, G., Nadal, M., van der Ploeg, M., van de Zee, S. E. a. T. M., Ritsema, C. J., Jiang, J. Q., Zhou, Z., & Sharma, V. K. (2015). Emerging pollutants in the environment: A challenge for water resource management. *Microchemical Journal, 3*(1), 57–65. https://doi.org/10.1016/j.microc.2013.04.014

Gerdes, R., Whrle, D., Spiller, W., Schneider, G., Schnurpfeil, G., & Schulz-ekloff, G. (1997). Photo-oxidation of phenol and monochlorophenols in oxygen-saturated aqueous solutions by different photosensitizers. *Journal of Photochemistry and Photobiology A: Chemistry*, *111*(4), 65–74.

Gil, J., Soto, M., Usma, J., & Gutiérrez, O. (2012). Contaminantes emergentes en aguas, efectos y posibles tratamientos. *Producción Más Limpia*, *7*(2), 52–73.

Gogate, P. R., & Pandit, A. B. (2004). A review of imperative technologies for wastewater treatment I: Oxidation technologies at ambient conditions. *Advances in Environmental Research*, *8*(3–4), 501–551. https://doi.org/10.1016/S1093-0191(03)00032-7

Granados Cristancho, Y. A. (2015). *Importancia De Los Ensayos TGA y DSC en el Estudio de las Propiedades Térmicas de Mezclas Asfálticas*. https://doi.org/10.1117/12.771970

Gross, R., & Kaim, W. (1987). Deprotonated p -Phenylenediamines as Noninnocent Ligands. Metal-to-Ligand Spin Transfer in the Ground State and Ligand-to-Metal Charge Transfer in the Lowest Excited State of Low-Spin Manganese(II) Complexes. *Inorganic Chemistry*, *26*(21), 3596–3600. https://doi.org/10.1021/ic00268a035

Gryglik, D., Miller, J. S., & Ledakowicz, S. (2007). Singlet molecular oxygen application for 2-chlorophenol removal. *Journal of Hazardous Materials*, *146*(3), 502–507.

https://doi.org/10.1016/j.jhazmat.2007.04.048

Gürol, I., Durmuş, M., Ahsen, V., & Nyokong, T. (2007). Synthesis, photophysical and photochemical properties of substituted zinc phthalocyanines. *Journal of the Chemical Society. Dalton Transactions*, *34*, 3782–3791. https://doi.org/10.1039/b704345g

Gutierrez, H., & De la vara, R. (2012). *Analisis y diseño de experimentos.*

Gutierrez, M., Martinez, C., Fresnadillo, D., Castro, A. M., Orellana, G., Braun, M., & Oliveros, E. (2003). Singlet Oxygen (1△g ) Production by Ruthenium ( II ) Complexes in. *J.Phys. Chem*, *107*(II), 3397–3403.

Haag, W R, & Hoigne, J. (1986). Singlet oxygen in surface waters. 3. Photochemical formation and steady-state concentrations in various types of waters. *Environmental Science & Technology*, *20*(4), 341–348. https://doi.org/10.1021/es00146a005

Haag, Werner R., Hoigne´, J., Gassman, E., & Braun, A. (1984). Singlet oxygen in surface waters — Part I: Furfuryl alcohol as a trapping agent. *Chemosphere*, *13*(5–6), 631–640. https://doi.org/10.1016/0045-6535(84)90199-1

Heidt, L. J. (1942). The photolysis of persulfate. *The Journal of Chemical Physics*, *10*(5), 297–302. https://doi.org/10.1063/1.1723724

Herculano, L. S., Malacarne, L. C., Zanuto, V. S., Lukasievicz, G. V. B., Capeloto, O. A., & Astrath, N. G. C. (2013). Investigation of the photobleaching process of eosin y in aqueous solution by thermal lens spectroscopy. *Journal of Physical Chemistry B*, *117*(6), 1932–1937. https://doi.org/10.1021/jp3119296

Hughes, S., & Denver, J. (2006). *Environmental Emergence of Triclosan. January*, 1–11.

Lu, K.-K., & Ogilby, P. R. (1987). A time- resolved study of singlet molecular Oxigen formation in a solution- phase photosensitized reaction: a new experimental technique to examine the dynamics of quenching by Oxigen. *Journal Physic Chemistry*, *91*(20), 1611–1617.

Jeong, H. G., & Choi, M. S. (2016). Design and Properties of Porphyrin-based Singlet Oxygen Generator. *Israel Journal of Chemistry*, *56*(2–3), 110–118. https://doi.org/10.1002/ijch.201500026

Jiang, J. Q., Zhou, Z., & Sharma, V. K. (2013). Occurrence, transportation, monitoring and

treatment of emerging micro-pollutants in waste water - A review from global views. *Microchemical Journal*, *110*, 292–300. https://doi.org/10.1016/j.microc.2013.04.014

Jiang, X., Wu, Y., Wang, P., Li, H., & Dong, W. (2013). Degradation of bisphenol A in aqueous solution by persulfate activated with ferrous ion. *Environmental Science and Pollution Research*, *20*(7), 4947–4953. https://doi.org/10.1007/s11356-013-1468-5

Karlsson, E. A., Lee, B. L., Åkermark, T., Johnston, E. V., Kärkäs, M. D., Sun, J., Hansson, Ö., Bäckvall, J. E., & Åkermark, B. (2011). Photosensitized water oxidation by use of a bioinspired manganese catalyst. *Angewandte Chemie - International Edition*, *50*(49), 11715–11718. https://doi.org/10.1002/anie.201104355

Katsumata, H., Kawabe, S., Kaneco, S., Suzuki, T., & Ohta, K. (2004). Degradation of bisphenol A in water by the photo-Fenton reaction. *Journal of Photochemistry and Photobiology A: Chemistry*, *162*(2–3), 297–305.

Kira, A., Ikeda, Y., & Koizumi, M. (1966). Reactive Species in the Photochemical Hydrogenation of Acridine in Ethanol. *Bulletin of the Chemical Society of Japan*, *39*(8), 1673–1678. https://doi.org/10.1246/bcsj.39.1673

Kitajima, N., Umehara, Y., Son, A., Kondo, T., & Tanabe, K. (2018). Confinement of Singlet Oxygen Generated from Ruthenium Complex-Based Oxygen Sensor in the Pores of Mesoporous Silica Nanoparticles. *Bioconjugate Chemistry*, *29*(12), 4168–4175. https://doi.org/10.1021/acs.bioconjchem.8b00811

Kolthoff, I. M., & Miller, I. K. (1951). The Chemistry of Persulfate. I. The Kinetics and Mechanism of the Decomposition of the Persulfate Ion in Aqueous Medium. *Journal of the American Chemical Society*, *73*(7), 3055–3059. https://doi.org/10.1021/ja01151a024

Komiya, S. (1997). Synthesis of Organometallic Compounds: A Practical Guide. In *J. Wiley & Sons Ltd.*

Koppenol, W. H., & Butler, J. (1985). Energetics of interconversion reactions of oxyradicals. *Advances in Free Radical Biology and Medicine*, *1*(1), 91–131. https://doi.org/10.1016/8755-9668(85)90005-5

Larson, R. A., & Marley, K. A. (1999). Singlet oxygen in the environment. *Environmental Photochemistry*, *2*, 123–136. https://doi.org/10.1007/978-3-540-69044-3_5

Latch, D. E., Packer, J. L., Arnold, W. a., & McNeill, K. (2003). Photochemical conversion of triclosan to 2,8-dichlorodibenzo-p-dioxin in aqueous solution. *Journal of Photochemistry and Photobiology A: Chemistry*, *158*(1), 63–66. https://doi.org/10.1016/S1010-6030(03)00103-5

Legeay, S., & Faure, S. (2017). Is bisphenol A an environmental obesogen? *Fundamental and Clinical Pharmacology*, *31*(6), 594–609. https://doi.org/10.1111/fcp.12300

Lin, H., Wu, J., & Zhang, H. (2013). Degradation of bisphenol A in aqueous solution by a novel electro/Fe 3+/peroxydisulfate process. *Separation and Purification Technology*, *117*, 18–23. https://doi.org/10.1016/j.seppur.2013.04.026

Loffredo, E., Traversa, A., & Senesi, N. (2012). Biodecontamination of water from bisphenol A using ligninolytic fungi and the modulation role of humic acids. *Ecotoxicology and Environmental Safety*, *79*, 288–293. https://doi.org/10.1016/j.ecoenv.2012.01.013

Londoño, Y. A., & Peñuela, G. A. (2015). Anaerobic biological treatment of methylparaben in an expanded granular sludge bed (EGSB). *Water Science & Technology*, *71*(11), 1604. https://doi.org/10.2166/wst.2015.118

Manikandan, T. S., Ramesh, R., & Semeril, D. (2016). Synthesis and characterisation of cycloruthenated benzhydrazone complexes: Catalytic application to selective oxidative cleavage of olefins to aldehydes. *RSC Advances*, *6*(99), 97107–97115. https://doi.org/10.1039/c6ra19044h

Maroto, A., Kissingou, P., Diascorn, A., Benmansour, B., Deschamps, L., Stephan, L., Cabon, J. Y., & Giamarchi, P. (2011). Direct laser photo-induced fluorescence determination of bisphenol A. *Analytical and Bioanalytical Chemistry*, *401*(9), 3011–3017. https://doi.org/10.1007/s00216-011-5375-7

Martínez-Zapata, M., Aristizábal, C., & Peñuela, G. (2013). Photodegradation of the endocrine-disrupting chemicals 4n-nonylphenol and triclosan by simulated solar UV irradiation in aqueous solutions with Fe(III) and in the absence/presence of humic acids. *Journal of Photochemistry and Photobiology A: Chemistry*, *251*, 41–49. https://doi.org/10.1016/j.jphotochem.2012.10.009

Martínez, R., Brand, G. J., Ramón, D. J., & Yus, M. (2005). [Ru(DMSO)4] Cl2 catalyzes the α-alkylation of ketones by alcohols. *Tetrahedron Letters*, *46*(21), 3683–3686.

https://doi.org/10.1016/j.tetlet.2005.03.158

Matzek, L. W., & Carter, K. E. (2016). Activated persulfate for organic chemical degradation: A review. *Chemosphere*, *151*, 178–188. https://doi.org/10.1016/j.chemosphere.2016.02.055

Meallier, P., Guittonneau, S., Emmelin, C., & Konstantinova, T. (1999). Photochemistry of fluorescein and eosin derivatives. *Dyes and Pigments*, *40*(2–3), 95–98. https://doi.org/10.1016/s0143-7208(98)00040-0

Michałowicz, J. (2014). Bisphenol A - Sources, toxicity and biotransformation. *Environmental Toxicology and Pharmacology*, *37*(2), 738–758. https://doi.org/10.1016/j.etap.2014.02.003

Miyoshi, N., Ueda, M., Fuke, K., Tanimoto, Y., Itoh, M., & Tomita, G. (1982). *Lifetime of Singlet Oxygen and Quenching by NaN 3 in Mixed Solvents*. 7–10. https://doi.org/10.1515/znb-1982-0520

Moldovan, Z. (2006). Occurrences of pharmaceutical and personal care products as micropollutants in rivers from Romania. *Chemosphere*, *64*(11), 1808–1817. https://doi.org/10.1016/j.chemosphere.2006.02.003

Molkenthin, M., Olmez-Hanci, T., Jekel, M. R., & Arslan-Alaton, I. (2013). Photo-Fenton-like treatment of BPA: Effect of UV light source and water matrix on toxicity and transformation products. *Water Research*, *47*(14), 5052–5064. https://doi.org/10.1016/j.watres.2013.05.051

Momzikoff, A., Santus, R., & Giraud, M. (1983). A study of the photosensitizing properties of seawater. *Marine Chemistry*, *12*(1), 1–14. https://doi.org/10.1016/0304-4203(83)90024-5

Moussavi, G., Pourakbar, M., Shekoohiyan, S., & Satari, M. (2018). The photochemical decomposition and detoxification of bisphenol A in the VUV/H2O2 process: Degradation, mineralization, and cytotoxicity assessment. *Chemical Engineering Journal*, *331*, 755–764. https://doi.org/10.1016/j.cej.2017.09.009

Nakamoto, K. (2006). Infrared and Raman Spectra of Inorganic and Coordination Compounds. Handbook of Vibrational Spectroscopy. In *Handbook of Vibrational Spectroscopy* (pp. 1872–1892). https://doi.org/10.1002/9780470027325.s4104

Nfodzo, P., & Choi, H. (2011). Triclosan decomposition by sulfate radicals: Effects of oxidant and metal doses. *Chemical Engineering Journal*, *174*(2–3), 629–634. https://doi.org/10.1016/j.cej.2011.09.076

Noguera-Oviedo, K., & Aga, D. S. (2016). Lessons Learned from more than Two Decades of Research on Emerging Contaminants in the Environment. *Journal of Hazardous Materials.* https://doi.org/10.1016/j.jhazmat.2016.04.058

Nolan, S. P. (2011). The development and catalytic uses of N-heterocyclic carbene gold complexes. *Accounts of Chemical Research*, *44*(2), 91–100. https://doi.org/10.1021/ar1000764

Oller, I., Malato, S., & Sánchez-Pérez, J. a. (2011). Combination of Advanced Oxidation Processes and biological treatments for wastewater decontamination-A review. *Science of the Total Environment*, *409*(20), 4141–4166. https://doi.org/10.1016/j.scitotenv.2010.08.061

Olmez-Hanci, T., Arslan-Alaton, I., & Genc, B. (2013). Bisphenol A treatment by the hot persulfate process: Oxidation products and acute toxicity. *Journal of Hazardous Materials*, *263*, 283–290. https://doi.org/10.1016/j.jhazmat.2013.01.032

Orellana Moraleda, G., Jiménez Hernández, M. E. y, & García Fresnadillo, D. (2006). *2 226 576 21*.

Otto, K., Oja Acik, I., Krunks, M., Tõnsuaadu, K., & Mere, A. (2014). Thermal decomposition study of HAuCl4·3H2O and AgNO3 as precursors for plasmonic metal nanoparticles. *Journal of Thermal Analysis and Calorimetry*, *118*(2), 1065–1072. https://doi.org/10.1007/s10973-014-3814-3

Pal, A., Gin, K. Y. H., Lin, A. Y. C., Reinhard, M., Gabet-Giraud, V., Miège, C., Choubert, J. M., Ruel, S. M., & Coquery, M. (2010). Impacts of emerging organic contaminants on freshwater resources: Review of recent occurrences, sources, fate and effects. *Science of the Total Environment*, *408*(24), 6062–6069. https://doi.org/10.1016/j.scitotenv.2010.09.026

Paul, A., Hackbarth, S., Vogt, R. D., Röder, B., Burnison, B. K., & Steinberg, C. E. W. (2004). Photogeneration of singlet oxygen by humic substances: Comparison of humic substances of aquatic and terrestrial origin. *Photochemical and Photobiological*

*Sciences*, *3*(3), 273–280. https://doi.org/10.1039/b312146a

Payán Aristizábal, A. (2015). *Síntesis y caracterización estructural de un compuesto de coordinación con el ligando 6-metoxiquinolina y evaluación del carácter fotosensibilizador de oxígeno molecular singulete*. Universidad del Quindio.

Pedersen, S. K., Holmehave, J., Blaikie, F. H., Gollmer, A., Breitenbach, T., Jensen, H. H., & Ogilby, P. R. (2014). Aarhus sensor green: A fluorescent probe for singlet oxygen. *Journal of Organic Chemistry*, *79*(7), 3079–3087. https://doi.org/10.1021/jo500219y

Peters, J. W., Bekowies, P. J., Winer, A. M., & Pitts, J. N. (1976). Additions and Corrections: An Investigation of Potassium Perchromate as a Source of Singlet Oxygen. *Journal of the American Chemical Society*, *98*(8), 2371. https://doi.org/10.1021/ja00424a602

Pibiri, I., Buscemi, S., Palumbo Piccionello, A., & Pace, A. (2018). Photochemically Produced Singlet Oxygen: Applications and Perspectives. *ChemPhotoChem*, *2*(7), 535–547. https://doi.org/10.1002/cptc.201800076

Piwowar, K., Blacha-Grzechnik, A., Bernas, P., & Zak, J. (2015). Phenol degradation in heterogeneous system generating singlet oxygen employing light activated electropolymerized phenothiazines. *Applied Surface Science*, *359*, 426–431. https://doi.org/10.1016/j.apsusc.2015.10.103

Poerschmann, J., Trommler, U., & Górecki, T. (2010). Aromatic intermediate formation during oxidative degradation of Bisphenol A by homogeneous sub-stoichiometric Fenton reaction. *Chemosphere*, *79*(10), 975–986. https://doi.org/10.1016/j.chemosphere.2010.03.030

Porras, J., Bedoya, C., Silva-Agredo, J., Santamaría, A., Fernández, J. J., & Torres-Palma, R. A. (2016). Role of humic substances in the degradation pathways and residual antibacterial activity during the photodecomposition of the antibiotic ciprofloxacin in water. *Water Research*, *94*, 1–9. https://doi.org/10.1016/j.watres.2016.02.024

Pospíšil, J., Nešpůrek, S., & Pilař, J. (2008). Impact of photosensitized oxidation and singlet oxygen on degradation of stabilized polymers. *Polymer Degradation and Stability*, *93*(9), 1681–1688. https://doi.org/10.1016/j.polymdegradstab.2008.06.004

Prakash, G., & Viswanathamurthi, P. (2014). New ruthenium(II) carbonyl complexes bearing disulfide Schiff base ligands and their applications as catalyst for some organic

transformations. *Spectrochimica Acta. Part A, Molecular and Biomolecular Spectroscopy*, *129C*(Ii), 352–358. https://doi.org/10.1016/j.saa.2014.03.086

Puntoriero, F., Sartorel, A., Orlandi, M., La Ganga, G., Serroni, S., Bonchio, M., Scandola, F., & Campagna, S. (2011). Photoinduced water oxidation using dendrimeric Ru(II) complexes as photosensitizers. *Coordination Chemistry Reviews*, *255*(21–22), 2594–2601. https://doi.org/10.1016/j.ccr.2011.01.026

Rigo, P., Baratta, W., Siega, K., Chelucci, G. A., Ballico, M. Y., & Magnolia, S. (2014). *2 452 352*.

Rodríguez, E. M., Fernández, G., Klamerth, N., Maldonado, M. I., Álvarez, P. M., & Malato, S. (2010). Efficiency of different solar advanced oxidation processes on the oxidation of bisphenol A in water. *Applied Catalysis B: Environmental*, *95*(3–4), 228–237.

Rozas, O., Baeza, C., Núñez, K., Rossner, A., Urrutia, R., & Mansilla, H. D. (2017). Organic micropollutants (OMPs) oxidation by ozone: Effect of activated carbon on toxicity abatement. *Science of the Total Environment*, *590–591*, 430–439. https://doi.org/10.1016/j.scitotenv.2016.12.120

Rule, K. L., Ebbett, V. R., & Vikesland, P. J. (2005). Formation of chloroform and chlorinated organics by free-chlorine-mediated oxidation of triclosan. *Environmental Science and Technology*, *39*(9), 3176–3185. https://doi.org/10.1021/es048943+

Seneviratne, D. S., Uddin, M. J., Swayambunathan, V., Schlegel, H. B., & Endicott, J. F. (2002). Characteristics and properties of metal-to-ligand charge-transfer excited states in 2,3-bis(2-pyridyl)pyrazine and 2,2′-bypyridine ruthenium complexes. Perturbation-theory-based correlations of optical absorption and emission parameters with electrochemis. *Inorganic Chemistry*, *41*(6), 1502–1517. https://doi.org/10.1021/ic010172c

Shibata, N., Kohno, Y., Findlay, S. D., Sawada, H., Kondo, Y., & Ikuhara, Y. (2010). New area detector for atomic-resolution scanning transmission electron microscopy. *Journal of Electron Microscopy*, *59*(6), 473–479. https://doi.org/10.1093/jmicro/dfq014

Smith, E. R., & Matheson, H. (1938). Boiling points of benzene, ethylene chloride, n-heptane, and 2,2,4-trimethylpentane over the range 660- to 860-mm pressure. *Journal of Research of the National Bureau of Standards*, *20*(5), 641.

https://doi.org/10.6028/jres.020.011

Staples, C. a, Dom, P. B., Klecka, G. M., Sandra, T. O., & Harris, L. R. (1998). A review of the environmental fate, effects, and exposures of Bisphenol A. *Chemosphere*, *36*(10), 2149–2173. https://doi.org/10.1016/S0045-6535(97)10133-3

Tan, X., Wan, Y., Huang, Y., He, C., Zhang, Z., He, Z., Hu, L., Zeng, J., & Shu, D. (2017). Three-dimensional MnO2 porous hollow microspheres for enhanced activity as ozonation catalysts in degradation of bisphenol A. *Journal of Hazardous Materials*, *321*, 162–172. http://linkinghub.elsevier.com/retrieve/pii/S0304389416308160

Teixeira, R. I., De Lucas, N. C., Garden, S. J., Lanterna, A. E., & Scaiano, J. C. (2020). Glass wool supported ruthenium complexes: Versatile, recyclable heterogeneous photoredox catalysts. *Catalysis Science and Technology*, *10*(5), 1273–1280. https://doi.org/10.1039/c9cy02479d

Torres, R. a., Abdelmalek, F., Combet, E., Pétrier, C., & Pulgarin, C. (2007). A comparative study of ultrasonic cavitation and Fenton's reagent for bisphenol A degradation in deionised and natural waters. *Journal of Hazardous Materials*, *146*(3), 546–551. https://doi.org/10.1016/j.jhazmat.2007.04.056

Varin, R. A., Mattar, D. K., Bidabadi, A. S., & Polanski, M. (2017). Synthesis of amorphous manganese borohydride in the (NaBH4–MnCl2) system, its hydrogen generation properties and crystalline transformation during solvent extraction. *Journal of Energy Chemistry*, *26*(1), 24–34. https://doi.org/10.1016/j.jechem.2016.08.011

Villa-Pérez, C., Ortega, I. C., Vélez-Macías, A., Payán, A. M., Echeverría, G. A., Soria, D. B., & Valencia-Uribe, G. C. (2018a). Crystal structure, physicochemical properties, Hirshfeld surface analysis and antibacterial activity assays of transition metal complexes of 6-methoxyquinoline. *New Journal of Chemistry*, *42*(9), 7166–7176. https://doi.org/10.1039/c8nj00661j

Villa-Pérez, C., Ortega, I. C., Vélez-Macías, A., Payán, A. M., Echeverría, G. A., Soria, D. B., & Valencia-Uribe, G. C. (2018b). Crystal structure, physicochemical properties, Hirshfeld surface analysis and antibacterial activity assays of transition metal complexes of 6-methoxyquinoline. *New Journal of Chemistry*, *42*(9), 7166–7176. https://doi.org/10.1039/c8nj00661j

Villa-Pérez, Cristian, Ortega, I. C., Payán-Aristizábal, A. M., Echeverría, G., Valencia-Uribe, G. C., & Soria, D. B. (2015). Synthesis, crystal structure and physicochemical characterization of a Hg(II) complex with 6-methoxyquinoline as ligand. *Zeitschrift Für Naturforschung B*, *70*(10), 719–725. https://doi.org/10.1515/znb-2015-0069

Villén, L., Manjón, F., García-Fresnadillo, D., & Orellana, G. (2006). Solar water disinfection by photocatalytic singlet oxygen production in heterogeneous medium. *Applied Catalysis B: Environmental*, *69*(1–2), 1–9.

Wang, J., Liu, Y., Li, Y., Xia, L., Jiang, M., & Wu, P. (2018). Highly Efficient Visible-Light-Driven H2 Production via an Eosin Y-Based Metal-Organic Framework [Rapid-communication]. *Inorganic Chemistry*, *57*(13), 7495–7498. https://doi.org/10.1021/acs.inorgchem.8b00718

Wang, S., Gao, R., Zhou, F., & Selke, M. (2004). Nanomaterials and singlet oxygen photosensitizers: Potential applications in photodynamic therapy. *Journal of Materials Chemistry*, *14*, 487–493. https://doi.org/10.1039/b311429e

Wilkinson, F., Helman, W. P., & Ross, A. B. (1993). Quantum Yields for the Photosensitized Formation of the Lowest Electronically Excited Singlet State of Molecular Oxygen in Solution. *Journal of Physical and Chemical Reference Data*, *22*(1993), 113. https://doi.org/10.1063/1.555934

Williams, D., & Carter, B. (2013). *Transmission electron microscopy assay Transmission electron microscopy assay* (Spinger (ed.)).

Wolff, C. J. M., Halmans, M. T. H., & Heijde, H. B. Van Der. (1981). The Formation of Singlet Oxygen in Surface Waters. *Chemosphere*, *10*, 59–62. https://doi.org/Doi 10.1016/0045-6535(81)90159-4

Xue, L.-X., Meng, T.-T., Yang, W., Wang, K.-Z., & Wanga, K.-Z. (2015). Recent advances in ruthenium complex-based light-driven water oxidation catalysts. *Journal of Photochemistry and Photobiology B: Biology*, 12–18. https://doi.org/10.1016/j.jphotobiol.2015.07.005

Yamamoto, T., Yasuhara, A., Shiraishi, H., & Nakasugi, O. (2001). Bisphenol A in hazardous waste landfill leachates. *Chemosphere*, *42*(4), 415–418. https://doi.org/10.1016/S0045-6535(00)00079-5

Yang, B., Ying, G. G., Zhao, J. L., Zhang, L. J., Fang, Y. X., & Nghiem, L. D. (2011). Oxidation of triclosan by ferrate: Reaction kinetics, products identification and toxicity evaluation. *Journal of Hazardous Materials*, *186*(1), 227–235. https://doi.org/10.1016/j.jhazmat.2010.10.106

Yang, S., Qiu, X., Jin, P., Dzakpasu, M., Wang, X. C., Zhang, Q., zhang, L., Yang, L., Ding, D., Wang, W., & Wu, K. (2018). MOF-templated synthesis of CoFe2O4 nanocrystals and its coupling with peroxymonosulfate for degradation of bisphenol A. *Chemical Engineering Journal*, *353*(March), 329–339. https://doi.org/10.1016/j.cej.2018.07.105

Yang, X., Sun, J., Fu, W., Shang, C., Li, Y., Chen, Y., Gan, W., & Fang, J. (2016). PPCP degradation by UV/chlorine treatment and its impact on DBP formation potential in real waters. In *Water Research* (Vol. 98). Elsevier Ltd. https://doi.org/10.1016/j.watres.2016.04.011

Ye, C., Hu, K., Niu, Z., Lu, Y., Zhang, L., & Yan, K. (2019). Controllable synthesis of rhombohedral α-Fe2O3 efficient for photocatalytic degradation of bisphenol A. *Journal of Water Process Engineering*, *27*(October 2018), 205–210. https://doi.org/10.1016/j.jwpe.2018.12.008

Yin, H. J., Liu, Y. J., Gao, J., & Wang, K. Z. (2017). A highly sensitive and selective visible-light excitable luminescent probe for singlet oxygen based on a dinuclear ruthenium complex. *Dalton Transactions*, *46*(10), 3325–3331. https://doi.org/10.1039/c6dt04813g

Ying, G. G., & Kookana, R. S. (2007). Triclosan in wastewaters and biosolids from Australian wastewater treatment plants. *Environment International*, *33*(2), 199–205. https://doi.org/10.1016/j.envint.2006.09.008

Zafiriou, O. C., Hole, W., Joussot-dubien, J., Zepp, R. G., & Zika, R. G. (1984). Photochemistry of natural waters. *Environmental Science & Technology*, *18*(12), 358A-371A.

Zapata, J. M. M., & Gustavo Antonio Peñuela Mesa. (2012). *Evaluación de los contaminantes emergentes triclosan y nononilfenol en los embalses de Riogrande II y la Fe*. Universidad de Antioquia.

Zepp, R., Lee Wolfe, N., Baughman, G. L., & Hollis, R. (1977). Singlet oxygen in natural water. *Nature*, *267*, 421–423.

https://www.nature.com/nature/journal/v269/n5629/pdf/269585a0.pdf

Zhang, T., Ding, Y., & Tang, H. (2015). Generation of singlet oxygen over Bi(V)/Bi(III) composite and its use for oxidative degradation of organic pollutants. *Chemical Engineering Journal*, *264*, 681–689. https://doi.org/10.1016/j.cej.2014.12.014

Zhang, X. F., & Li, X. (2011). The photostability and fluorescence properties of diphenylisobenzofuran. *Journal of Luminescence*, *131*(11), 2263–2266. https://doi.org/10.1016/j.jlumin.2011.05.048

Zúñiga-benítez, H., Aristizábal-ciro, C., & Peñuela, G. A. (2015). Photodegradation of the endocrine-disrupting chemicals benzophenone-3 and methylparaben using Fenton reagent : Optimization of factors and mineralization / biodegradability studies. *Journal of the Taiwan Institute of Chemical Engineers*, *000*, 1–9. https://doi.org/10.1016/j.jtice.2015.09.004

**UNIVERSIDAD DE ANTIOQUIA**

1803

# ENGINEERING

## FACULTY

GDCON Group